GABRIELE CIVILETTO
Matr. N° 760739

OPA1 overexpression as potential therapy in mitochondrial diseases

Coordinator: Prof. Andrea Biondi
Tutor: Prof. Msssimo Zeviani
Co-Tutor: Dr. Carlo Viscomi

Table of Contents

Chapter 1

General introduction

MITOCHONDRIA

Mitochondria are essential organelles found within almost all eukaryotic cells. The most prominent role for mitochondria is to supply the cell with spendable energy in the form of ATP generated by oxidative phosphorylation (OXPHOS). Besides this fundamental role, mitochondria take part in a number of relevant processes for cellular physiology including, among others, apoptosis, detoxification of reactive oxygen species (ROS), intracellular Ca^{2+} regulation, steroid hormone and porphyrin synthesis and lipid metabolism. The term "mitochondrion" originates from the Greek words "mitos," thread, and "chondros," grain, reflecting the typical morphology of distinct structures noted inside of cells coined in1898 by microbiologist Carl Benda (1857-1933). Soon after the discovery of mitochondria, many speculations have been done about their origin. The discovery of mitochondrial DNA (mtDNA)[1,2] and the following evidences about the close genetic relations between mitochondria and the photosynthetic α-proteobacteria[3,4] led to the development of the endosymbiotic hypothesis[5], which has now been widely accepted among the scientific community. The triggering event leading to mitochondrial uptake within a primordial prokaryotic cell, likely a methanogenic archaebacterium[6], has been hypothesized to date back to 2,4 billion years ago. This timescale coincides with the accumulation of oxygen in the Earth's atmosphere, due to cyanobacteria photosynthetic activity, which is supposed to

have driven the host cell to engulf an oxygen tolerant organism. This event has substantially contributed to the overall evolution of the eukaryotic cell, optimizing its energy production[7,8]. A critical step in the evolution of an autonomous endosymbiont organism into the contemporary organelle has been a drastic reduction of its gene subset, most of which is believed to have been transferred to the nucleus or lost because of redundancy with the host-cell genome[9,10]. The first images of the mitochondrial internal structure have been provided in the 1950s thanks to the development of electron microscopy (EM) technologies. The interpretation of ultrastructural details of mitochondria has been a challenging task, in spite of the high resolution of this technique. Several hypothetical models have been proposed, all converging on the resolution of mitochondria into 4 morphologically and functionally distinct compartments: the outer membrane (OM), the inter-membrane space (IMS), the inner membrane (IM) and the matrix (Fig. 1). The OM is freely permeable to ions and small molecules, but not to bigger metabolites and proteins, whose traffic is mediated by specific transporters and channels, such as the voltage dependent anionic channel (VDAC or porin) and TOM, the system carrying out the protein transport across the outer membrane The OM also contains the sorting and assembly machinery (SAM) that is involved in the assembly of mitochondrial β-barrel proteins in the membrane. The IMS plays a pivotal role in the coordination of mitochondrial activities with other cellular processes. These activities include the exchange of proteins, lipids, or metal ions

between the matrix and the cytosol, the initiation of apoptotic cascades, signaling pathways that regulate mitochondrial respiration and other bioenergetics-related metabolic pathways, and the control of mitochondrial morphogenesis. The IM surrounds the matrix, which contains the mtDNA, various proteins involved in a huge number of biochemical pathways, e.g. the tricarboxylic acid cycle (TCA), the genetic and protein synthetic machinery related to mtDNA, catabolic pathways of several aminoacids,, part of the urea cycle, biosynthesis of heme moieties and Fe-S clusters, etc. The transport of ions, metabolites and proteins through the IM depends on several membrane-associated protein systems, including ATP synthase, the transporter of the inner membrane (TIM) complexes, the adenine nucleotide translocator (ANT) and four of the five canonical complexes of the respiratory chain that translocate protons across the IMM. Tight control of IM permeability allows the generation and maintenance of an electrochemical membrane potential ($\Delta pH_m + \Delta\Psi_m$) that is essential for a number of energy-requiring mitochondrial functions, including OXPHOS.

The IM can be further divided in two different compartments: the inner boundary membrane, adjacent to the OM, and the cristae, i.e. invaginations of the inner membrane protruding into the matrix space[11], that have recently shown to harbour the OXPHOS complexes. Accordingly, the cristae area measured in various tissues positively correlates with the amount of ATP produced by OXPHOS [12].

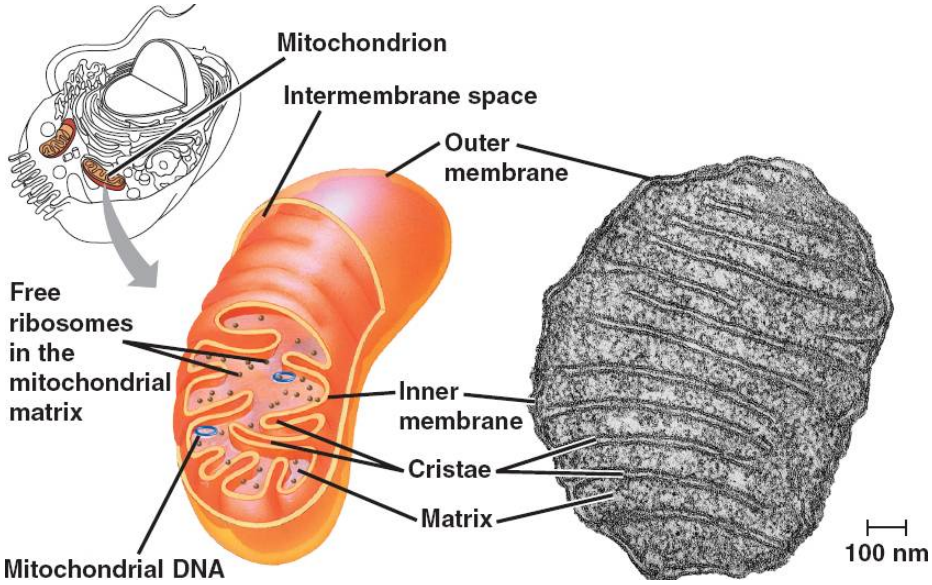

Figure 1. Mitochondrial structure. Schematic representation and ultrastructure of mitochondria

Mitochondrial genetics

The human mitochondrial genome is a circular double stranded DNA molecule (mtDNA) of 16.6 kb encoding 13 proteins, which are all part of four of the five canonical multiheteromeric enzyme complexes constituting the OXPHOS system. In addition, mtDNA contains genes encoding 22 tRNAs, and 12S and 16S rRNAs which are required for mitochondrial protein synthesis[13,14] (Fig. 2). The two mtDNA strands are termed heavy (H) and light (L), because of the dfferent content of purine vs. pyrimidine residues (H>L), reflecting their separation by centrifugation in buoyant density gradients. There are no introns in the mitochondrial genome and all 37 genes are adjacent to each other with few exceptions. An untranslated region of approximately 1 Kb harbours the replication origin for

the H strand synthesis and the promoters for transcription of the H- and L-strands. Both rRNA- and most of the polypeptide-encoding genes are located on the H-strand, except for the ND6 gene, which is located on the L-strand. Nuclear DNA (nDNA) genes encode all the other subunits which take part in the OXPHOS complexes, and also all the proteins required for their assembly, those carrying out the maintenance and expression of mtDNA, the biosynthesis of the respiratory cofactors and prosthetic groups, etc. Thus the mitochondrial proteome includes approximately 1500 nDNA-encoded mitochondrial genes in addition to the 37 mtDNA genes[14]. In sexuate eukaryotes, mtDNA is maternally transmitted through generations, although a single case of paternal inheritance has been reported in a patient affected by a mitochondrial myopathy[15]; despite several studies, additional cases of paternal mtDNA transmission have never been described.

Each human cell has hundreds to several thousands mitochondria and every mitochondrion can carry as many as ten copies of mtDNA packed in histone-like nucleoprotein structures called nucleoid[16]. Cells and tissues with higher ATP demand typically have more mtDNA copies[17]. The mitochondrial genome replicates independently from the cell cycle and at cell division mtDNA copies segregate randomly into daughter cells, according to the statistical distribution of the organelles. Usually, all mtDNA copies are identical, a condition known as homoplasmy. However errors occurring during replication or repair of mtDNA, can lead to the formation of a

mutant mtDNA molecule, which can clonally expand through unknown mechanisms, and eventually fixate in a metastable condition referred to as heteroplasmy, where mutant and wild-type genomes coexist in the same organelles/cells/tissues, in different proportions. Low levels of heteroplasmy have been shown to be present in normal cells, particularly in post-mitotic tissues such as skeletal muscle, or in stem cells of the colonic crypts. However, only when the mutation load of mtDNAs offsets a minimum critical threshold, mitochondrial dysfunction becomes manifest in a particular tissue leading to organ failure and development of a mitochondrial disease in an individual. Generally, the critical threshold for a heteroplasmic mtDNA mutation to become phenotypically relevant ranges from 70 to 90%[18]. However, different tissues exhibit variation in their mutant threshold, with germ cells, for example, having minimal tolerance for the accumulation of mtDNA mutations[19].

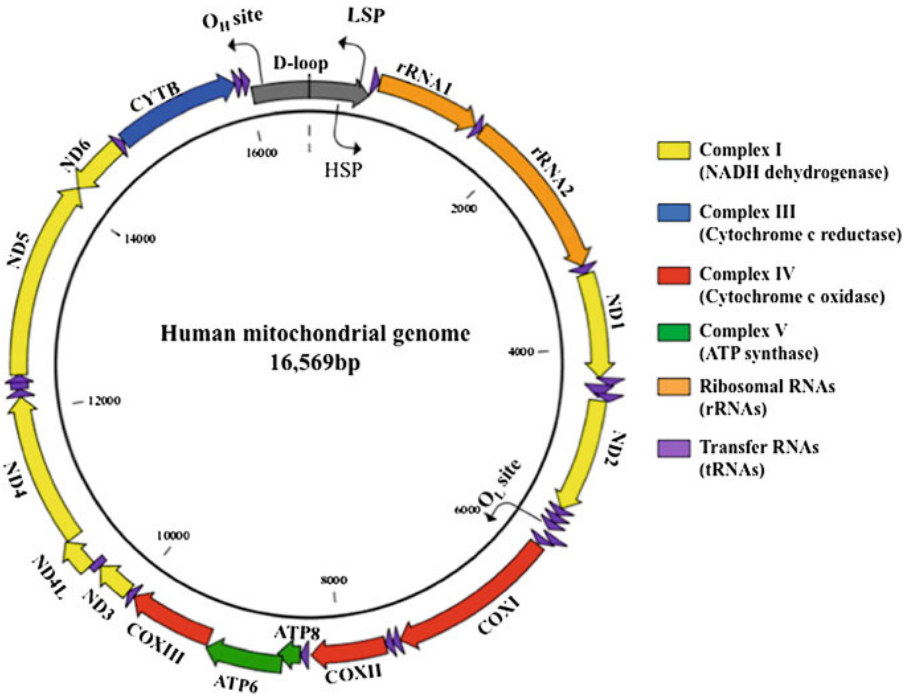

Figure 2. Mitochondrial DNA. The mitochondrial genome encodes 13 polypeptides involved in the electron transport chain: 7 subunits of complex I, 1 subunit of complex III, 3 subunits of complex IV and 2 subunits of complex V.

Energetics in eukaryotes depends on the availability of reducing equivalents (hydrogen atoms), intaken as nutrients, stripped off the carbon backbones of carbohydrates, amino acids and fats, and ultimately reacting with oxygen to generate water through mitochondrial respiration. Anaerobic glycolysis, occurring in the cytosol, produces only 5% of the ATP necessary for the life of cells, through cleavage and partial oxidation of glucose into two molecules of pyruvate, and reduction of two molecules of nicotinamide adenine dinucleotide (NAD^+) into NADH. Pyruvate is further reduced in mitochondria by pyruvate dehydrogenase

and the TCA cycle, which strip all its hydrogens and transferring them to NAD^+, again converting it into NADH. Reducing equivalents are also generated by β-oxidation of fatty acids within mitochondria, generating mitochondrial acetyl-CoA, which feeds the TCA cycle, and $FADH_2$. Electrons from NADH and $FADH_2$ are sequentially transferred to molecular oxygen through the IM-associated electron transport chain (ETC). The ETC is composed of four multiheteromeric complexes (cI-IV), which carry out mitochondrial respiration, and of the ATP synthase (or complex V, cV), which exploits the energy derived from the ETC and stored in the proton gradient across the IM, to convert ADP into ATP (Fig. 3). Since the respiratory complexes are composed of several subunits (as detailed below), a number of assembly factors and chaperones, several of which are still unknown, are involved in the biogenesis of the respiratory chain. In addition, the respiratory complexes interact to each other in different combnations, to form supercomplexes, whose physiological role remains however controversial.

In addition to the respiratory complexes, coenzyme Q (a lipoidal quinone) and cytochrome c are also involved in mitochondrial respiration, serving as 'electron shuttles' between the complexes[20]. The four enzymatic complexes of the respiratory chain use the energy released during the electron flow through the ETC, to pump protons across the IM thus generating a proton electrochemical gradient (ΔΨ) between the matrix and the IMS. The potential energy stored as ΔΨ is then used for multiple purposes: (*a*) to import proteins and Ca2+ into the

mitochondrion, (*b*) to generate heat, and (*c*) to synthesize ATP within the mitochondrial matrix by the ATP synthase (complex V). These energy-requiring processes tend to dissipate the ΔΨ, by promoting the flow of protons through the IM back into the matrix.

Complex I

Complex I (CI), or NADH:ubiquinone oxidoreductase is a main "entry point" of electrons to the ETC. It is the biggest among the ETC complexes with a predicted molecular mass of 969 kDa[21,22] and is composed of 44 polypeptides, 14 of which are essential for its catalytic function[23]. These 14 core subunits consist of seven highly hydrophobic mtDNA-encoded subunits (ND1, ND2, ND3, ND4, ND4L, ND5, and ND6), and seven hydrophilic nDNA-encoded subunits (NDUFV1, NDUFV2, NDUFS1, NDUFS2, NDUFS3, NDUFS7, and NDUFS8). Human CI contains 30 additional (supernumerary) nDNA-encoded subunits that may have alternative functions or be important for assembly, regulation, stability or protection against oxidative stress. Recently the molecular architecture of mammalian CI has been characterized at 5 Å resolution[24]. This is an important progress toward the understanding of the structural and functional role of the CI supernumerary subunits and the structural changes of CI during catalysis. Electron microscopy analysis demonstrates that CI has an L-shaped conformation consisting of a peripheral, matrix-protruding arm and an IM-embedded membrane arm of similar size[25,26]. In the fully

assembled mammalian CI a cofactor, flavin mononucleotide (FMN), in the NDUFV1 subunit accepts electrons from NADH. The electrons are then transported through the hydrophilic arm by eight FeS clusters and are eventually transferred to Coenzyme Q[27,28]. The mechanism that couples CI electron transport to proton pumping in the IMS remains incompletely understood, although the NDUFS2 and ND1 subunits appear to play a crucial role[29].

Complex II

Complex II (CII), or succinate:ubiquinone oxidoreductase, is assembled from four nDNA encoded polypeptides (SDHA, SDHB, SDHC, and SDHD). The catalytic core, which dehydrates succinate to fumarate, is formed by the two bigger hydrophilic subunits, SDHA and SDHB, which also harbour the redox cofactors that participate in electron transfer to coenzyme Q. The cofactor FAD is covalently bound to SDHA, which provides the succinate-binding site, and SDHB has three Fe-S clusters, which mediate the electron transfer to coenzyme Q. The smaller hydrophobic SDHC and SDHD subunits constitute the anchor to the IM and form the CoQ binding site[30,31]. Complex II does not translocate protons, and therefore it only feeds electrons to the electron transport chain[32].

Complex III

Complex III (CIII), or ubiquinol:cytochrome c oxidoreductase, is a homodimeric complex with a mass of approximately 480 kDa,

consisting of 11 subunits for each monomer[33]. The catalytic core is formed by three subunits: (a) the membrane embedded cytochrome b, (b) the Rieske protein carrying one Fe_2S_2 cluster, and (c) cytochrome c_1. Most of the other eight subunits are small proteins that surround the metalloprotein nucleus, but two so-called “core proteins” face the mitochondrial matrix and are homologous to mitochondrial processing peptidases which function in protein import. Thus, CIII may be multifunctional[34]. CIII couples the delivery of electrons from ubiquinol (coenzyme QH_2) to cytochrome c with the generation of a proton gradient across the membrane; this mechanism is known as the “Q cycle”[35]. Cytochrome b provides two quinone-binding sites (Q_o and Q_i), which are located on the opposite sides of the membrane and are linked by a transmembrane electron-transfer pathway. The two electrons from ubiquinol bound to the Q_0 site are not linearly transferred to two cytochrome c molecules, but take two distinct pathways: the first electron is transferred along a high-potential chain to the Rieske protein, and then to cytochrome c1, which delivers it to the soluble cytochrome c. The second electron is transferred to the Q_i site via the hemes bL and bH of the cytochrome b subunit. This creates a proton-motive force that leads to a net translocation of two protons for each electron transferred to cytochrome c. The mechanism responsible for the electron bifurcation in Q_0 is still unknown at the molecular level.

Complex IV

Complex IV (CIV), or cytochrome c oxidase (COX) is the terminal enzyme of the ETC, and catalyzes the electron transfer from reduced cytochrome c to molecular oxygen. According to the structure of the bovine enzyme, mammalian CIV is a heteromeric complex composed of 13 different subunits[36,37], although recent evidence has shown that an additional subunit, previously attributed to CI, is in fact a fourteenth COX subunit[38]. The three largest subunits Cox1, Cox2 and Cox3 are highly hydrophobic transmembrane proteins encoded by mtDNA and form the catalytic core. The ten small subunits (Cox4, Cox5a, Cox5b, Cox6a, Cox6b, Cox6c, Cox7a, Cox7b, Cox7c and Cox8) surrounding the core of the enzyme are encoded in the nuclear genome. They are probably necessary for the regulation of the COX function, its assembly/stability and its dimerization of the catalytically active enzyme[39]. Cox1 contains two heme prosthetic groups (heme a and heme a_3) of cytochrome and a single copper-containing CuB site. A second copper site comprising two copper ions, the CuA site, is present in the Cox2 subunit and is the first site to receive electron from cytochrome c. The electrons from CuA site are transferred to the low-spin cytochrome a in subunit I, and then to the bimetallic cytochrome a_3/CuB active site. Two hydrophilic channels connect the catalytic core to the mitochondrial matrix compartment. These channels are called D and K after a conserved aspartate and lysine, respectively. During the reduction of oxygen, protons that are actively transported enter

through D and K channels[40]. In the catalytic cycle, the transfer of each of the four electrons required for the reduction of an oxygen molecule is accompanied by the translocation of the two protons, of which one is consumed internally in the binuclear center for the chemical reduction of oxygen ("chemical or substrate proton") and the other is pumped across the membrane ("vectorial or pumped proton"). Both chemical and pumped protons are delivered along the D- and K-channels[41].

Complex V

Complex V (CV), or ATP synthase catalyses the synthesis of ATP from ADP and inorganic phosphate (P_i) using the energy provided by the proton electrochemical gradient[42]. The structure and, intriguingly, the oligomerization of complex V determine its function, the former by the so-called "rotary catalysis"[43] and the latter by influencing mitochondrial and cristae morphology[44], as discussed below. ATP synthase consists of two well-defined protein entities: the F_1 sector, a soluble portion situated in the mitochondrial matrix, and the F_o sector, bound to the inner mitochondrial membrane. F_1 is composed of three copies of each of subunits α and β, and one each of subunits γ, δ and ε. F_1 subunits γ, δ and ε constitute the central stalk of complex V. F_o consists of a subunit c-ring and one copy each of subunits a, b, d, F6 and the oligomycin sensitivity-conferring protein (OSCP). Subunits b, d, F6 and OSCP form the peripheral stalk which lies to one side of the complex. A number of additional subunits (e, f, g, and A6L), all spanning the membrane, are

associated with F_o[45]. Two of the F_o subunits, subunit *a* and A6L, are encoded by the mtDNA ATP6 and ATP8 genes, respectively[13]. During ATP synthesis, the proton flow from the IMS into the matrix, causes rotation of the c-ring in F_o along with subunits γ, δ and ε in F_1. Each site switches cooperatively through conformations in which ADP and Pi bind, ATP is formed, and then released[46]. The $\alpha_3\beta_3$ hexamer must remain fixed relative to subunit a during catalysis; this occurs through the peripheral stalk (also called the stator). ETC activity is thus tightly coupled to Complex V activity by the transmembrane potential, so that mitochondrial oxygen consumption rate is regulated by both matrix ADP concentration and Complex V activity. When ATP is high and ADP low, oxygen consumption rate is low and it is regulated by proton leakage across the inner membrane; this condition is known as *state 4* of respiration. When ADP increases due to high ATP breakdown, protons start to flow through F_0 of Complex V and the inner membrane becomes depolarized. This activates in turn the electron flow through the respiratory chain in order to restore membrane potential, determining a shift towards the so-called *state 3* of respiration. Uncoupling drugs such as DNP (2,4-dinitrophenol) or proteins as UCP1, 2 or 3 (uncoupling proteins) dissipate the proton gradient, and thus the membrane potential, uncoupling electron transport from ATP synthesis. In this condition the ETC works at its maximum rate determining an increase in oxygen consumption (uncoupled respiration).

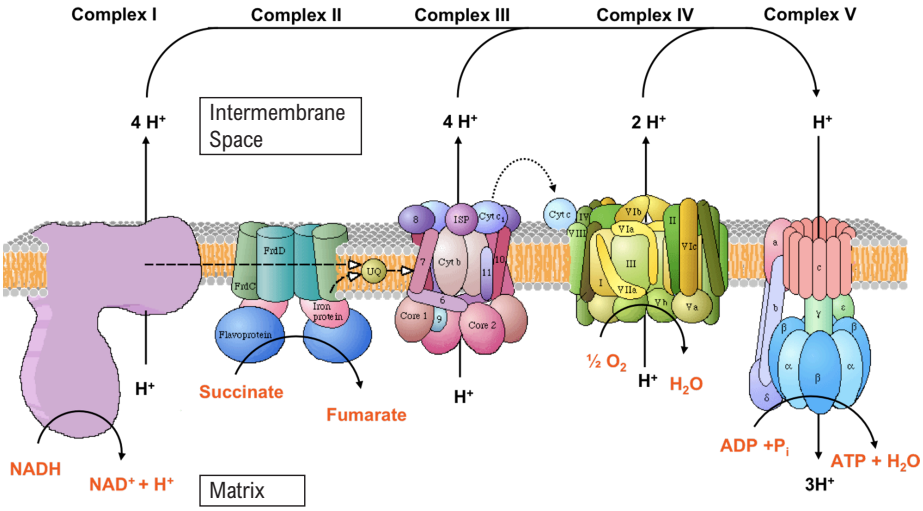

Figure 3. **Mitochondrial OXPHOS system**. Representation of the electron transfer and proton pumping in the mitochondrial respiratory chain

Respiratory Chain Supercomplexes (RCS)

The structural and functional organization of the RC has been a matter of debate for more than 50 years. Two models of organization have been hypothesized so far (Fig. 4). The "fluid" model proposes that OXPHOS complexes diffuse freely in the IM and electron transport occurs when the complexes randomly collide[47]. Conversely, the "solid" model proposes that OXPHOS complexes are organized within the IM in supramolecular structures known as supercomplexes or respirasomes[48,49]. This structural arrangement may offer functional advantages such as the enhancement of electron transport efficiency and substrate channeling, or the decrease of electron or proton leakages [50]. It is currently accepted that both organizations likely coexist, giving rise to the ''dynamic aggregate'' or ''plasticity'' model.

This model suggests that OXPHOS complexes switch from freely moving to fixed structures in order to adapt to changes in cellular metabolism[51]. The development of the Blue Native Polyacrylamide Gel Electrophoresis (BN-PAGE) technology has been important to investigating the interactions between the different complexes[52]. In these studies, supercomplexes of various stoichiometries have been detected, such as assemblies of CI+CIII+CIV together with CIII dimers and CIV oligomers[53,54]. Conversely, the association of CII and CV with supercomplexes remains controversial[55].

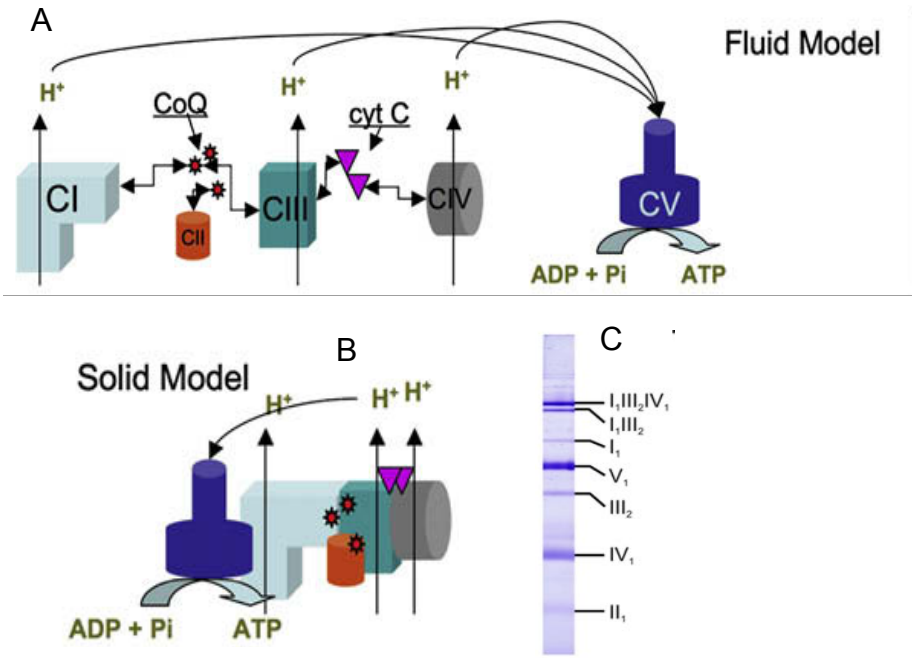

Figure 4. Models of mitochondrial OXPHOS organization. Schematic representation of the fluid (A) and solid (B) models for the organization of the OXPHOS system. (C) Blue native gel electrophoresis (BNGE) and Coomassie staining on isolated mitochondria for the identification of the supercomplex components. From *Acìn-Pèrez et al. Molecular Cell 2008*

Regulation of mitochondrial biogenesis

Mitochondria are under the double genetic control of mtDNA and nDNA, and a finely tuned genetic network has evolved in order to connect the two genomes[56].

Pathways controlling mitochondrial biogenesis have been intensively investigated and characterized in skeletal muscle and brown adipose tissue (Fig. 5). These pathways are centred on the activity of the PPARγ coactivators (PGC) α and β, which interact with drive the activity of several OXPHOS-related transcription factors, including the Nuclear Respiratory Factors (NRF1 and 2), and the Peroxisomal Proliferator Activator receptors (PPAR α, β, and γ) among others. NRFs and PPARs in turn increase the transcription of OXPHOS and fatty acid oxidation (FAO) related genes. They also regulate the expression of mitochondrial transcription factor A (TFAM), which is an indispensable component of the mitochondrial transcription and replication systems[57]. PGC1α is the best characterized member of this family, its activity being regulated by acetylation, which is dependent on the activities of the acetylase GCN5 and of the deacetylase SIRT1, and by phosphorylation, regulated by several kinases, including p38 MAPKp38 MAPK, glycogen synthase kinase 3b (GSK3b) and AMP-dependent kinase (AMPK)[58,59].

The intricate molecular machinery involved in the maintenance, transcription and translation of mtDNA includes several nDNA-encoded proteins. Transcription and replication are jointly initiated by TFAM and mitochondrial transcription factor B2

(TFB2M), which generate a DNA/RNA hybrid primer in the presence of mitochondrial RNA polymerase[60]. TFB2M represents one of two mitochondrial coactivator transcription factors, with TFB2M being more active relative to its counterpart mitochondrial transcription factor B1 (TFB1M)[61]. The DNA/RNA hybrid that is produced is utilized by the catalytic subunit of the polymerase γ A (POLGA) to replicate the mtDNA template[62]. POLGA is assisted in this process by its accessory subunits, POLGB that promotes DNA binding and processivity of the enzyme complex[63]. Other factors include the mtDNA helicase, TWINKLE and the mtDNA specific single stranded binding protein (mtSSB), which together allow for efficient replication of mtDNA[64]. Two mechanisms of mtDNA replication have been proposed, the asynchronous-displacement mechanism[65] and the coupled leading and lagging strand mechanism[66]. The asynchronous-displacement mechanism describes the binding of POLG to the transcribed RNA primer, thereby allowing heavy strand replication to begin from O_H in the D-loop. After replication of approximately two thirds of the genome, the formation of the new heavy strand exposes the origin of light strand replication (O_L) on the parent heavy strand. Light strand replication is then able to commence in the opposite direction[65]. The more recently proposed coupled leading and lagging strand mechanism describes the replication of both mtDNA strands at the same time from the same replication origin in the D-loop. It has been hypothesised that the choice of replication mechanism may be influenced by variations in TFAM or

POLGB binding or the number of dNTPs present within mitochondria in different cell types and that the asynchronous-displacement mechanism was responsible for the maintenance of mtDNA, whilst the coupled leading and lagging strand mechanism occurs primarily when mtDNA amplification is required[66].

Transcription of mtDNA occurs following interaction between nuclear-encoded regulatory proteins and regions within the D-loop of mtDNA. TFAM binds to a region 10 to 40bp upstream of the promoter region within the D-loop, which separates the two strands of DNA, allowing access for mtRNAPol and TFB1M or TFB2M for initiation of transcription. Once initiated, transcription generates a polycistronic precursor RNA transcript, allowing co-ordinated transcription of all genes on the same strand. Excision of the polycistronic precursor by endonucleases produces precursor rRNAs and tRNAs which are then processed further to allow translation of the precursor mRNAs.

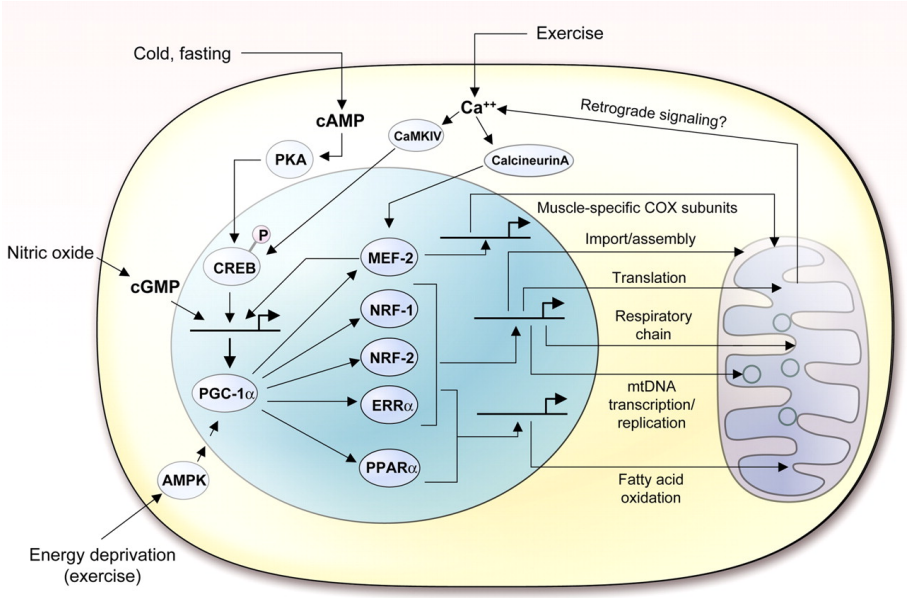

Figure 5. Mitochondrial biogenesis pathways. Illustration summarizing PGC-1 α -mediated pathways governing mitochondrial biogenesis and function. From *Scarpulla 2008. Physiological reviews*

MITOCHONDRIAL DYNAMICS, AUTOPHAGY AND APOPTOSIS

In spite of the static morphology often represented in textbooks, mitochondria are highly dynamic organelles that fuse and divide continuously and adapt their shape and structure to meet the metabolic requirements of the cell. Thereby, many factors regulate mitochondrial shape and their network in the cytoplasm.

OPA1 and regulation of cristae shape

The first evidence of these phenomena has been provided by microtomographic experiments showing that cristae folding is tightly linked to the metabolic state of isolated mitochondria[67].

This ultrastructural flexibility is characterized by a change of matrix configuration from an orthodox state, when respiration is not stimulated, to a condensed state reached after ADP addition; of note, the volume of isolated mitochondria is not changing during this transition. Moreover the cristae are connected to the inner boundary membrane by small tubular structures, called cristae junctions, which play a crucial role in establishing IM topology and matrix configuration[68]. Cristae size and number may change in response to metabolic requirements optimizing diffusion of metabolites and proteins such as Cytochrome c[69].

Cardiolipin (CL), a phospholipid almost exclusively found in mitochondrial membranes[70], has an exquisite capacity to specifically interact with respiratory chain complexes, both participating in the proton conduction through the IM and maintaining inner membrane fluidity and osmotic stability[71]. In addition to its role in mitochondrial bioenergetics, CL electrostatically anchors cytochrome *c* to the inner mitochondrial membrane and regulates its release, which triggers the downstream events of apoptosis[72]. Mitochondria of patients suffering from Barth syndrome, caused by mutations of tafazzin, a cardiolipin-specific phospholipid-lysophospholipid transacylase, exhibit 80% reduction in cardiolipin content, which is accompanied by severe ultrastructural changes of the mitochondrial inner membrane topology[73].

Mitochondrial cristae structure is also regulated by Prohibitin-1 (PHB1) and the closely related protein Prohibitin-2 (PHB2). As

implied by their name, prohibitins were originally thought to have a central role in the inhibition of cell-cycle progression, by interacting with retinoblastoma tumor suppressor protein (Rb) and p53[74,75]. On the other hand recent studies suggest that prohibitins are assembled into large ring complexes in the IM, where they are deemed to play a variety of functions, such as protein and lipid scaffolds[76]. Furthermore, they affect cell proliferation and apoptosis by regulating the processing of the dynamin-like GTPase OPA1 (described below), thus controlling the morphogenesis of the mitochondrial cristae[77].

The mitochondrial contact site and cristae organizing system (MICOS) complex[78], is required for maintenance of the characteristic architecture of the IM and forms contact sites with the OM[79]. These contact sites allow import of proteins, metabolite channeling, lipid transport, and membrane dynamics[80]. MICOS consists of six subunits (Mic10, Mic12, Mic19, Mic26, Mic27, and Mic60) that are all inner membrane proteins exposed to the IMS. Two core proteins, Mic10 and Mic60, are essential for keeping the cristae membranes attached to the inner boundary membrane; the other subunits contribute to complex integrity and cristae folding. In addition to its role in inner membrane architecture, MICOS was found to interact with protein complexes of the outer mitochondrial membrane, including the TOM transport[81] and the SAM machinery[82].

Besides its role in ATP production, it has been proposed that ATP synthase takes part in the establishment of cristae structure. Interaction between ATP synthase monomers leads to dimerization or oligomerization of the enzyme[83]. Factors such as the inhibitor peptide IF1 and the subunit s (also called factor B) promote the organization of these supramolecular forms of the enzyme[84]. Allen et al. proposed that the arrangement of the ATP synthase in dimers serves as a protein backbone, plying and stabilizing the tubular cristae structures[85]. Experiments in yeast have shown that the ablation of either subunits *e* or *g*, located in the F_0 domain and involved in ATP synthase dimerization, leads to misfolded cristae structure that convert into concentric circles resembling an onion-like structure[86]. It is now widely accepted that the oligomerization of the cone-shaped ATP synthase would be responsible for the IM curvature leading to the formation of cristae[44].

The studies addressing the molecular mechanisms that govern mitochondrial morphology and cristae remodeling have identified Optic Atrophy 1 (OPA1) protein as a central regulator of these pathways. OPA1 is the only dynamin-like protein found in the IMS being specifically localised to cristae[87,88]. OPA1 shares three domains conserved within the dynamin-protein family: a GTPase domain, a middle domain and a GTPase effector region containing a coiled-coil domain (CC2). Other two coiled-coil domains (CC0 and CC1) are located along the structure of the protein and are involved in the assembly of functionally active OPA1 oligomers[89]. Electron microscopy

analyses showed that mitochondria from OPA1-depleted cells have an altered cristae structure[90]. As a consequence, its function has been related to the maintenance of IM dynamic architecture and to its effects on mitochondrial physiology like respiration, coordinated OM and IM fusion (discussed below) and apoptosis. Human OPA1 ORF is built from 31 exons, 3 of which (4, 4b and 5b) are alternatively spliced leading to 8 mRNA variants (Fig. 6A)[91]. The eight precursors of OPA1 are targeted to mitochondria via a common mitochondrial targeting sequence (MTS), which is removed in the matrix by the mitochondrial processing peptidase (MPP). This process leads to the formation of the mature long OPA1 isoforms, collectively termed l-OPA1. Each l-OPA1 isoform might be further processed from proteolytic enzymes cleaving them in either S1 or S2 sites. This further post-translational processing results in the accumulation of five short isoforms called s-OPA1[92,93]. Both short and long isoforms of OPA1 are localized across the IMS, are produced in equal amount in normal conditions and are required for mitochondrial fusion (Fig. 6B)[94]. Recent evidences suggest that the accumulation of s-OPA1 stimulate mitochondrial fission[95].

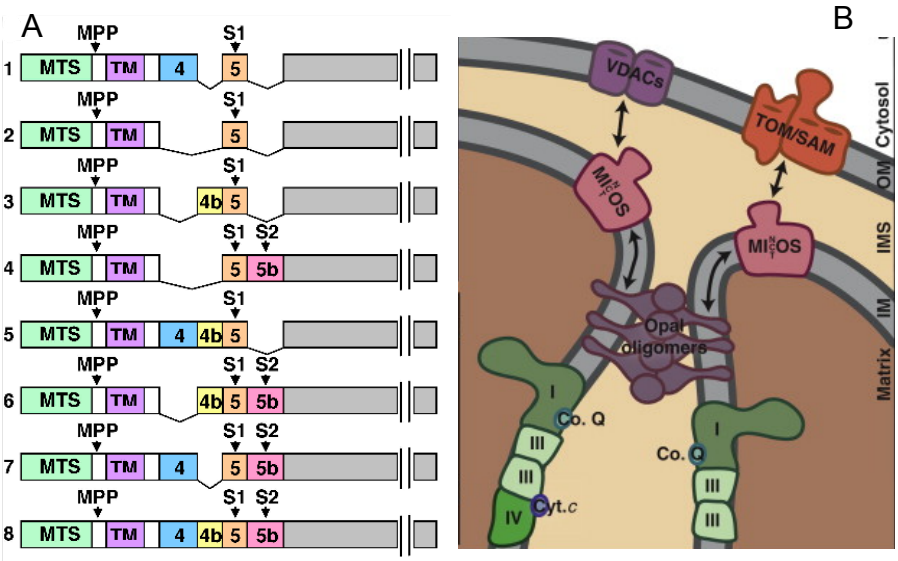

Figure 6. OPA1 splice isoforms and its schematic localization (A) Schematic representation of the eight *OPA1* mRNA splice forms. The mRNA splice forms differ by the presence or absence of exons 4, 4b, and 5b. Cleavage of the mitochondrial targeting sequence (MTS) by MPP leads to the long isoforms. Additional cleavage at sites S1 (exon 5) or S2 (exon 5b) leads to the short isoforms. TM, transmembrane domain. (B) Respiratory chain complexes involved in maintenance of cristae morphology. Double-ended arrows indicate potential interaction partners involved in cristae structure. OM, outer membrane; IM, inner membrane; Cyt. *c*, Cytochrome *c*; Co. Q, Coenzyme Q. From *Stroud et al. 2013 Current Biology*

L-OPA1 is anchored to the IM whereas s-OPA1 is peripherally attached to the IM and a fraction of it may diffuse in the IMS and become associated with the OM[88,90,92]. Various stress conditions, including mitochondrial respiratory chain impairment, low mitochondrial ATP levels, dissipation of the membrane potential across the IM, or apoptotic stimuli, can trigger OPA1 cleavage, resulting in the loss of long isoforms[92,96,97] (Fig. 7). The IMS i-AAA (ATPase associated with diverse cellular activities) protease YME1L1 mediates OPA1 cleavage at S2, found only in some of OPA1 variants[94,98]. In the

last years various proteases have been associated to the processing of OPA1 at S1 site, present in all forms of OPA1, raising a debate on this matter. Both the rhomboid protease PARL (presenilin-associated rhomboid-like protein) and the matrix AAA (*m*-AAA) protease AFG3L2, an oligomeric ATP-dependent metallopeptidase in the inner membrane, have been proposed to be involved in OPA1 processing[92,99]. However it has been observed that mouse embryonic fibroblast lacking PARL or AFG3L2 processed OPA1 properly, casting doubt about the role of both proteases in OPA1 processing[100]. Recent evidence has revealed that the zinc metalloprotease Oma1 is indeed responsible for S1 cleavage, which occurs at basal levels but can be dramatically induced by depolarization of mitochondria[95,101,102]. Additional recent data suggest that prohibitins control OPA1 processing by inhibiting m-AAA proteases, thus defining a functional link between the energy-sensitive processing of OPA1 and the maintenance of intra-mitochondrial structure[77].

By controlling cristae shaping Opa1 also impact apoptosis (discussed below).

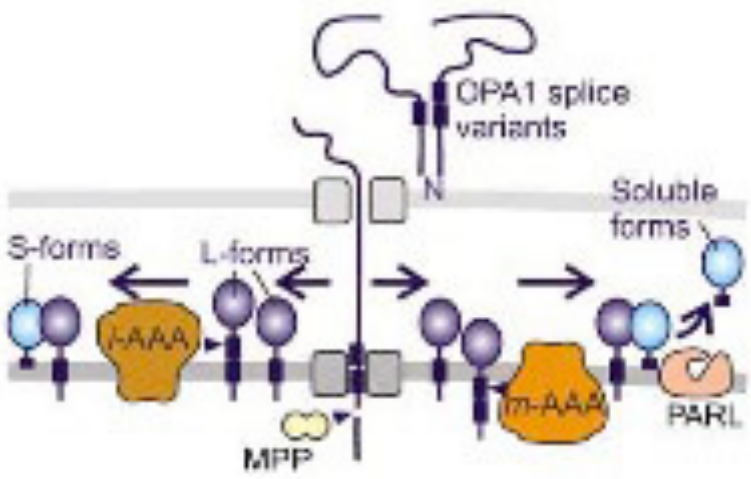

Figure 7. Model for the processing of OPA1 in mammalian mitochondria. After processing of newly imported OPA1 by MPP, long and short isoforms of OPA1 are generated by constitutive (left pathway) and inducible (right pathway) cleavage at sites 2 and site 1, respectively. m- and i-AAA proteases and PARL have been linked to OPA1 processing, but the exact proteolytic pathways remained speculative. From *Tatsuta 2008 The EMBO Journal*

Mitochondrial fusion and fission

In addition to their complex internal structure, mitochondria exhibit a dynamic organization within the cell, finely tuned by the opposing processes of fusion and fission[103,104] (Fig. 8). These conserved activities are coordinately regulated and fully integrated with cellular physiology to meet the needs of the cell. For instance, mitochondria become elongated during the G1/S transition, fragmented at the onset of mitosis and apoptosis, and hyperfused in response to nutrient starvation and oxidative stress[105-107]. Mitodynamics transactions provide an important quality control mechanism, since fusion contributes to mitochondrial maintenance and fission allows the segregation

of dysfunctional mitochondria[108,109]. Mitofusin (MFN) 1 and 2 are two dynamin-related GTPases inserted in the OM through two transmembrane domains, which may form homo- and hetero-dimers. Mfn1 and 2 undergo conformational changes upon GTP hydrolysis in order to promote OM fusion[110,111]. Although each Mfn appears to possess specific and non-redundant roles, the presence of both Mfn1 and Mfn2 is imperative for the maintenance of normal rates of mitochondrial fusion[112]. Although under certain conditions the OM can fuse without subsequent fusion of the IM, these events are usually synchronized[113]. Fusion of the OM allows spatial contact between the inner membranes, which subsequently fuse through the action of OPA1. By analogy with dynamin structure, OPA1 is proposed to be surrounded by the membrane and therefore constitute a scaffold on which the IM is dynamically wrapped. The GTPase domain drives the fusion process providing biochemical energy required to the energetic barrier that must be overcome to promote lipid bilayer mixing. Mitochondrial fusion is thought to depend on the presence of L- and S-OPA1[94], which assemble into oligomeric complexes maintaining cristae structure[114,115]. Various stress conditions including apoptotic stimulation disrupt these complexes and trigger the complete cleavage of L-OPA1 into S-OPA1, thus inhibiting mitochondrial fusion[94]. OMA1 is required for the stress induced processing of OPA1 and causes fragmentation of the mitochondrial network, revealing a role of S-OPA1 in promoting mitochondrial fission[95]. In addition, elimination of dysfunctional

mitochondria depends on local activation of mitochondrial fission, which allows the isolation of aberrant mitochondria from the mitonetwork bulk. Isolated dysfunctional mitochondria are then targeted for autophagic degradation[108,109].

In contrast to mitochondrial fusion, mitochondrial fission is mediated by the cytosolic soluble dynamin-related protein 1 (DRP1)[116]. DRP1 contains a N-terminal GTPase, a middle domain and a C-terminal GTPase effector domain that is involved in self-assembly. Normally a major cellular fraction of Drp1 localizes to the cytosol, and the translocation of Drp1 to the OM, followed by interactions with docking adaptors (FIS1, MFF, and MiD49/51), is needed to initiate mitochondrial division[117]. DRP1 oligomerises and forms spiral filaments that drive mitochondrial constriction and fragmentation. DRP1 activity is regulated by post-translational modifications, such as phosphorylation, ubiquitination, small ubiquitin-like modifier (SUMO)-ylation, and S-nitrosylation[118], which activate or inhibit its function favoring mitochondrial fragmentation or elongation respectively.

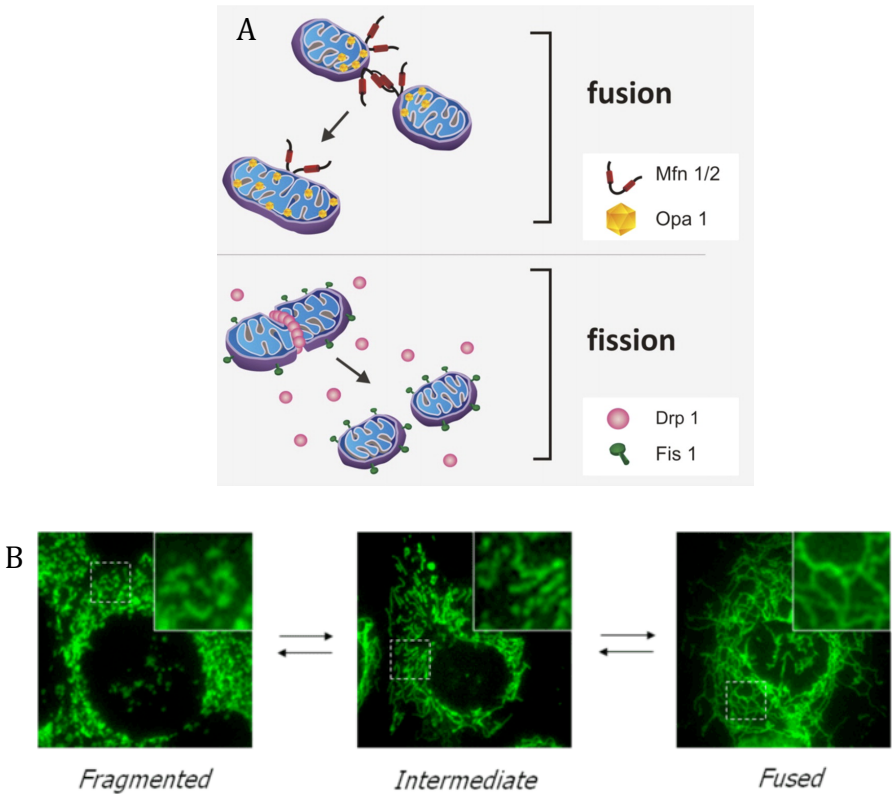

Figure 8. Mitochondrial fusion and fission. (A) Overview of mitochondrial fusion and fission. (B) Live cells are treated with MitoTracker®, which selectively labels mitochondria. Different mitochondrial networks are shown.

A link between mitochondrial dynamics, apoptosis and autophagy

Mitochondria are involved in the so-called intrinsic pathway of apoptosis where they release soluble proteins, including cytochrome c, from the IMS to initiate caspase activation in the cytosol[119,120]. Once in the cytosol, cytochrome c interacts with its adaptors, mainly Apaf1, to form the apoptosome, which in turn activates the caspase cascade, the principal executors of

apoptosis[121,122]. During apoptosis, mitochondria become highly fragmented, as a consequence of increased recruitment of DRP1 onto the OM. This event is key for the positive regulatory role that DRP1 plays in the Bax/Bak-mediated mitochondrial outer-membrane permeabilization (MOMP)[123,124]. In contrast, mitochondrial fusion protects cells from apoptotic cell death, and activation of apoptosis coordinately inhibits fusion activity[125]. Recent converging data suggest that some OPA1 isoforms could form the cristae junction bottleneck and act as a "cork" that restraints most of cytochrome c in the cristae volume, suggesting an anti-apoptotic function of OPA1[114]. Cristae junctions are the target of pro-apoptotic BH3-only pro-apoptotic proteins, like tBid[126] , that do disassemble peculiar forms of OPA1, inducing subtle cristae remodeling, and full release of cytochrome c. Furthermore, the processed short forms of OPA1 are substrates for PARL protease. PARL produces a quantitatively small, IMS soluble fraction of OPA1 that does not participate in fusion, but regulates cristae morphology and apoptosis[99]. Downregulation of OPA1 induces cristae disorganization, cytochrome c release and caspase-dependent nuclear events[127]. Conversely its overexpression protects cells from apoptosis by counteracting cristae remodeling and by stabilizing mitochondrial bioenergetics function[114,128].

Mitochondrial dynamics are also closely integrated with the mitophagy quality control pathway[108,129,130] (Fig. 9). It has been proposed that hyperfusion observed during nutrient starvation

protects mitochondria from autophagic degradation (mitophagy) through steric hindrance[106,131]. The hyperfusion response, however, is transient and thus cannot buffer long-term defects in electron transport chain activity. A further, terminal response to mitochondrial dysfunction is mitophagy, which is also triggered by a decrease in membrane-potential-driven protein import. In this pathway, the kinase PINK1 is imported into healthy mitochondria and constitutively degraded. A decrease in import triggered by mitochondrial dysfunction causes PINK1 to accumulate on the outer membrane, where it recruits the E3 ligase Parkin[132,133]. Parkin ubiquitinates a specific subset of OM proteins including Mitofusins, and promotes their proteasomal degradation [134-136]. The Parkin-dependent degradation of factors involved in mitochondrial motility and fusion enhances the selectivity of removing defective mitochondria by autophagy. In addition to specifying defective mitochondria for degradation, an *in vivo* study in Drosophila suggests that the PINK1–Parkin pathway is also capable of selectively targeting respiratory complexes for degradation[137]. In support of this idea, selective targeting of complex I for degradation has been described in cell culture models[138], but the mechanisms underlying this phenomenon are currently unknown.

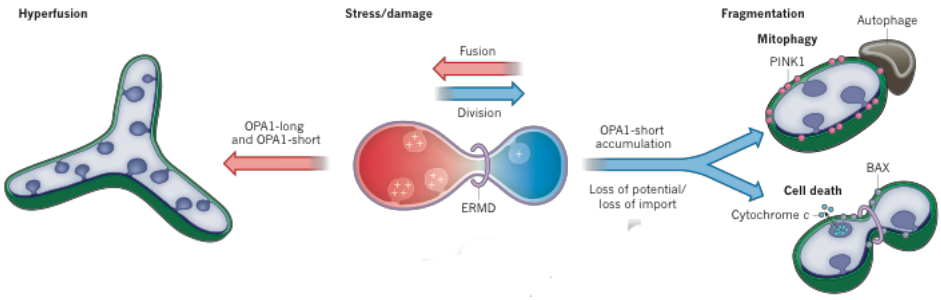

Figure 9. Integration of mitochondrial stress response pathways and their coordination with mitochondrial shape. Several different mitochondrial pathways respond to stress or damage and are coordinated with mitochondrial dynamics.

Other mitochondrial metabolic and biosynthetic pathways

Besides their major role in energy production, carried out through the oxidation of metabolites, mitochondria are deeply integrated in the overall biology of the cell, contributing in many biosynthetic and homeostatic pathways (Fig. 10). These activities are closely interconnected and depend upon the energetic function of mitochondria. The membrane potential, for instance, is harnessed for other essential mitochondrial functions, such as mitochondrial protein import[139].

A crucial role of mitochondria in amino acid and nitrogen metabolism is the participation in the urea cycle. The cycle operates the fixation of nitrogen contained e.g. in amino acids, to urea, a soluble, virtually inert moiety which is excreted in the urine of many terrestrial animals. Only the initial reactions of the cycle take place in mitochondria, whereas the remaining ones are carried out in the cytosol. In all cell types mitochondria harbour a set of enzymes involved in pyrimidine and lipid biosynthesis. Even if some lipids like cardiolipin are totally

synthesized in mitochondria, they depend at the same time on the transfer and assembly of lipids mainly formed in the endoplasmatic reticulum[140]. Moreover, cholesterol is delivered to mitochondria where specialized matrix enzymes participate in the synthesis of steroidal hormones[141]. Mitochondria also act as a Ca^{2+} buffer to prevent cytosolic overload upon release from the endoplasmatic reticulum. Ca^{2+} uptake into the mitochondrial matrix occurs predominantly through the IMM via the mitochondrial Ca^{2+} uniporter (MCU) that rapidly imports Ca^{2+} against a steep electrochemical gradient[142,143]. In neurons, the ability of mitochondria to modulate Ca^{2+} flux is essential for controlling neurotransmitter release, neurogenesis, and neuronal plasticity. In addition, mitochondria supply copious amounts of ATP as well as the TCA intermediates that serve as the building blocks for synthesis of GABA and glutamate neurotransmitters[144,145].

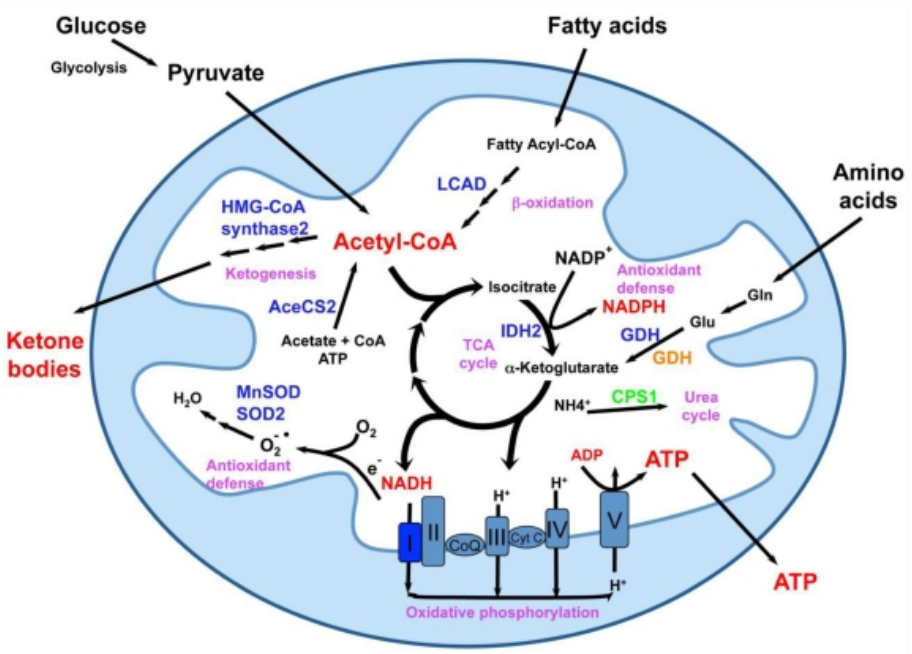

Figure 10. **Mitochondrial metabolism**. Schematic overview of biochemical pathways inside mitochondria. From *Li et al. 2011 Int J Biol Sci*

Mitochondria play a central role in metal metabolism, as the biosynthesis of heme and Fe-S clusters takes place in the mitochondrial matrix. Heme are essential components of the major oxygen carrier, hemoglobin, and cytochromes, whereas Fe-S clusters are essential redox centers of numerous enzymes, mitochondrial, cytosolic, and nuclear[28]. *Heme* is a metal-containing prosthetic group of several proteins, and consists of an iron atom embedded in a porphyrin ring coordinated by four nitrogen atoms. The unique properties of heme, an iron molecule coordinated within a tetrapyrrole, allows it to function both as an electron carrier and a catalyst for redox reactions. The biosynthesis of *heme* is a multistep process that

starts with the formation of a porphyrin ring from succinyl-CoA and glycine. A highly conserved pathway involving both cytosolic and mitochondrial compartments is utilized to generate protoheme IX (heme b); however the final step is catalysed by ferrochelatase, an enzyme that resides in the mitochondrial matrix[146].

There are three biologically important forms of heme (types a, b, and c), all synthesized in mitochondria, which differ by modifications of the porphyrin ring. The most common type is heme b, which is the prosthetic group of hemoglobin and myoglobin, as well as cytochrome b of the mitochondrial CIII. Specific heme lyases are required for heme c synthesis, which unlike heme b is covalently bound to its apoprotein partner[147]. Heme a derives from heme b and is only contained in mitochondrial complex IV. The conversion of heme b into heme a involves two membrane bound enzymes. Cox10 is the heme *o* synthase that transfers a farnesyl diphosphate to heme b. Heme *o* is subsequently oxidized by Cox15 to form heme *a*. In this reaction, a methyl group of the pyrrole ring is oxidized to a formyl group[148] (Fig.11). Both enzymatic functions are conserved from yeast to humans, and defects in both enzymes lead to severe human disorders with cytochrome *c* oxidase deficiency[149-152].

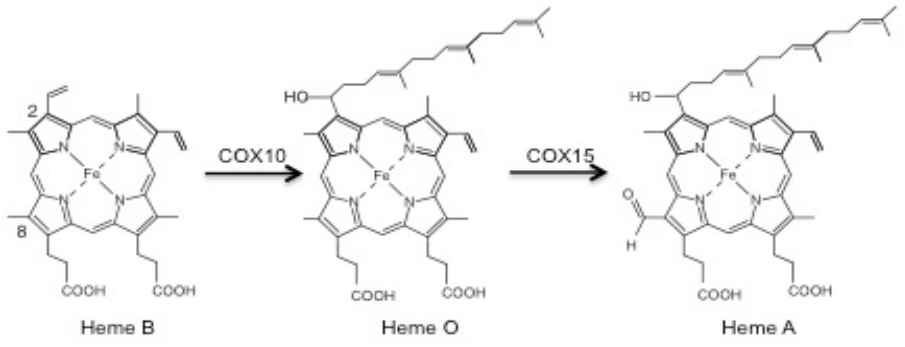

Figure 11. Heme A biosynthetic pathway. COX10 and COX15 are two enzymes involved in the terminal steps of the heme A biosynthetic pathway

MITOCHONDRIAL DISEASES

Mitochondrial diseases are a group of inherited disorders of energy metabolism caused by malfunctioning of the OXPHOS system. They are the most common inborn errors of metabolism in humans, with a minimum estimated prevalence of at least 1 in 5000[153]. They are both genetically and clinically very heterogeneous. From the genetic point of view, they exhibit any kind of possible transmission, including maternal, autosomal dominant, autosomal recessive and X-linked modes of inheritance. Whilst different gene mutations can give rise to a similar range of phenotypes, mutations in the same gene can often lead to a variety of different clinical entities. In addition, different levels of heteroplasmy of the same mtDNA mutation can result in a wide spectrum of phenotypes[154]. From the clinical point of view, mitochondrial diseases are typically characterized by a vast range of symptoms, severity, age of onset and outcome. Being OXPHOS the main source of cellular energy, any organ or tissue may be involved in mitochondrial

diseases but generally involvement of tissues with higher energy demand, such as brain, skeletal and cardiac muscle, kidney and endocrine systems predominates[155]. Clinical features range from lesions in single tissues, such as the optic nerve, the heart or the liver, to complex multisystem syndromes. However, patients with a mitochondrial disease display a number of canonical biochemical and morphological features. Firstly, often defects in one or more OXPHOS complexes are usually detected by enzymatic assays on muscle biopsies or cultured cells (fibroblasts or myoblasts). Increase of lactic acid levels in blood and/or cerebrospinal fluid reflects a block in the import of pyruvate across impaired mitochondria and of NADH accumulating during glycolysis and usually reoxydized by cytosol-mitochondrial shuttles (manly the glycerol-3-phosphate shuttle). If pyruvate cannot be metabolized through the bioenergetics pathways of mitochondria, and cytosolic NADH cannot be reoxydized by transferring reducing equivalents to the respiratory chain, then pyruvate, a chetoacid, is reduced into its homologous hydroxyacid, lactate, which is eventually released into body fluids. One of the best-known morphological alterations of mitochondrial disorders is the “ragged-red” transformation of scattered muscle fibres (ragged-red fibers, RRF) due to the accumulation of abnormal mitochondria under the sarcolemmal membrane[156]. Additional clinical signatures of mitochondrial disorders include skeletal myopathy, deafness, blindness, intestinal dysmotility, subacute neurodegeneration and

peripheral neuropathy; the use of imaging (RMN, PET) and electrophysiology (EMG) tests help in the correct definition of the disease. Patients with late-onset mitochondrial disease usually show signs of myopathy associated with variable involvement of the central nervous system (CNS), although some of them complain only of muscle weakness with or without muscle wasting with exercise intolerance[157]. In early childhood, the most common clinical and neuropathological presentation is Leigh syndrome (LS) characterized by severe psychomotor delay, cerebellar and pyramidal signs, dystonia, seizures, respiratory abnormalities, incoordination of ocular movements and recurrent vomiting[158]. LS can be caused by defects in structural subunits (either mtDNA or nDNA encoded) or assembly factors of mitochondrial OXPHOS complexes, but also, for example, by disturbances in CoQ10 metabolism or dysregulation in RNA/DNA maintenance. The genetic classification of the primary mitochondrial diseases distinguishes disorders due to defects in mtDNA, which are inherited according to the rules of mitochondrial genetics, from those due to defects in nDNA, which are transmitted by mendelian inheritance.

Mutations in mtDNA

In healthy individuals, somatic mtDNA mutations accumulate over time thus correlating with the aging process. For individuals born with partial mitochondrial dysfunction, the time-dependent accumulation of mtDNA mutations and mitochondrial

damage can account for the delayed onset and progressive course of their diseases. The stochastic nature of this process could also explain variable expressivity and/or penetrance of disease. The first evidence of a pathology linked to a mutation in mtDNA dates back to 1988 when Wallace and coworkers found a point mutation in the gene encoding subunit 4 of Complex I in a family with Leber's hereditary optic neuropathy (LHON)[159]. Since then, numerous mtDNA mutations have been associated to several disorders. These alterations, which are distributed throughout the mitochondrial genome (Fig. 12), account for 10-20% of all mitochondrial diseases[160]. Hundreds of pathogenic mtDNA mutations have now been documented (MITO-MAP 2012)[161], which can affect virtually every tissue in the body, leading to different phenotypes depending on their intrinsic severity, targeted gene, and heteroplasmy levels. Since mtDNA contains only 13 structural genes all encoding subunits of the respiratory chain and 24 RNA genes required for synthesis of the corresponding proteins, pathologies caused by mtDNA genetic defects share the common characteristics of defective OXPHOS, and massive mitochondrial proliferation in muscle (resulting in ragged-red fibers). In muscle-biopsy specimens, the mutant mtDNAs accumulate preferentially in ragged-red fibers, which are typically negative for cytochrome *c* oxidase activity. Although defective OXPHOS is a common signature, clinical variability is huge.

Clinically relevant mtDNA variants fall into three classes:

- Recent deleterious mutations that result in maternally transmitted disease;
- Ancient adaptive variants that predispose individuals to disease in different environments;
- Age-related accumulation of somatic mtDNA mutations that may erode function and provide the aging clock. However, the contribution of mtDNA mutations to the aging process is controversial[154].

Mutations in mtDNA can affect specific proteins of the respiratory chain or the synthesis of mitochondrial proteins as a whole (mutations in tRNA or rRNA genes, or giant deletions) and can be in turn divided into large-scale rearrangements (i.e. partial deletions or duplications) and inherited point mutations. Both groups have been associated with well-defined clinical syndromes. While large-scale rearrangements are usually sporadic, point mutations are usually maternally inherited. Large-scale rearrangements include several genes and are invariably heteroplasmic. In contrast, point mutations may be heteroplasmic or homoplasmic[157].

Large-scale rearrangements of mtDNA

mtDNA-rearrangement syndromes are invariably heteroplasmic and can result in a range of clinical manifestations and a wide spectrum of severity. The size of deletions can vary from few bases to several kilobases; they are located within the major arc of the mtDNA between the two origins of replication (according to the leading strand replication model) , and several

genes are usually involved. The syndromes associated with rearrangement of mtDNA range from maternally inherited type 2 diabetes and deafness, due to an mtDNA-duplication mutation, to chronic progressive external ophthalmoplegia (PEO) and the Kearns-Sayre syndrome (KSS). PEO is characterized by a progressive paralysis of the eye muscles leading to impaired eye movement and ptosis. Ptosis is frequently the presenting symptom and may be asymmetrical; however, patients usually progress to bilateral disease. PEO is typically caused by sporadic large-scale single deletions or multiple mtDNA deletions[162]. KSS is characterized by early onset (childhood or young adulthood) of progressive external ophthalmoplegia, ptosis, mitochondrial myopathy with ragged red fibers, CNS involvement (progressive ataxia and cognitive decay), and potentially life-threatening abnormalities of the cardiac rhythm[157,163]. The majority of single large-scale rearrangements of mtDNA are sporadic and are therefore believed to be the result of the clonal amplification of a single mutational event, occurring in the maternal oocyte or early during the development of the embryo[164].

Point mutations of mtDNA

In contrast to large-scale rearrangements, mtDNA point mutations are usually maternally inherited. The following features are frequently present in pathogenic mutations:

- High conservation of the affected nucleotide/amino acid or loss of function of the gene product (e.g. a stop mutation in a mit gene);
- Segregation with phenotype;
- Quantitative correlation between phenotype and heteroplasmy, if present;
- Identification of the mutation in affected families from ethnically distinct human populations[165]

Mutations have been found in all mtDNA-encoded genes. For instance, base-substitution mutations can alter either polypeptide genes or rRNAs and tRNAs resulting in overall mitochondrial impairment of protein synthesis. The most common syndromes are discussed below.

Mitochondrial encephalomyopathy, lactic acidosis and stroke-like episodes (MELAS) is a multisystem disorder that is often fatal in childhood or in young adulthood. The disease principally affects muscle, brain and the endocrine system. Stroke-like episodes are typically occurring before 40 years of age. Most people with MELAS have a buildup of lactic acid in their body fluids. Less commonly, people with MELAS may experience involuntary muscle spasms (myoclonus), impaired muscle coordination (ataxia), hearing loss, heart and kidney problems, diabetes, and hormonal imbalances[166]. Although the most common mutation is the A3243G transition in the mtDNA gene encoding $tRNA^{Leu(UUR)}$, other mutations (in protein coding genes, as well as tRNAs) have been found to be associated with the disease.

Myoclonus epilepsy and ragged red fibres (MERRF) is almost exclusively a result of mutations in the mtDNA gene encoding $tRNA^{Lys}$. MERRF is characterized by muscle twitches, myopathy, and spasticity. Affected individuals sometimes have short stature and heart abnormalities (cardiomyopathy)[167]. Gomori Trichrome staining of skeletal muscle reveals accumulation of Ragged Red Fibers. Clinical manifestations can vary greatly even within the same family. This phenotypic variability is thought to be dependent on the level of heteroplasmy and to the tissue distribution of the mutation.

Mutations in the structural and catalytic subunits of the respiratory chain, leading to a wide spectrum of diseases. For instance, mutations in cI subunits may result in phenotypes as divers as Leigh syndrome, MELAS, LHON, cardiomyopathy etc.

LHON (Leber's hereditary optic neuropathy), the most common mtDNA-related disease, causes severe visual loss in both eyes. LHON, a juvenile onset condition in most of the cases, is typically caused by homoplasmic mutations in one of three CI encoding genes (G11778A in ND4, G3460A in ND1 and T14484C in ND6). A significant percentage of people with a mutation that causes LHON do not develop any feature. Specifically, more than 50 percent of males with a mutation and more than 85 percent of females with a mutation never experience vision loss or related medical problems[168].

Different clinical presentations are also associated with mutations of cIII and cIV mtDNA-encoded subunits. In particular *CYTB* mutations lead to a multisystem disorder characterized

by encephalomyopathy, cardiomyopathy and septo-optic dysplasia[169,170]; whereas mutations in *COX1*, *COX2* and *COX3,* affecting the assembly/stability of cIV, can be associated to several manifestations, including MELAS, encephalomyopathy, and a motor neuron disease-like presentation[171].

Mutations in cV subunits lead **Neurogenic muscle weakness, ataxia, retinitis pigmentosa (NARP),** encephalopathy, LHON etc. NARP can also include, besides the symptoms that give the name to this disorder, epilepsy, and sometimes mental deterioration[172]. Symptoms usually appear in adulthood. Ragged-red fibres are absent in the muscle biopsy. The disease is associated with mutation T8993G in the gene encoding subunit 6 of mitochondrial ATPase (complex V of the respiratory chain). In patients presenting a milder NARP phenotype, a transition T->C in the same position has also been described.

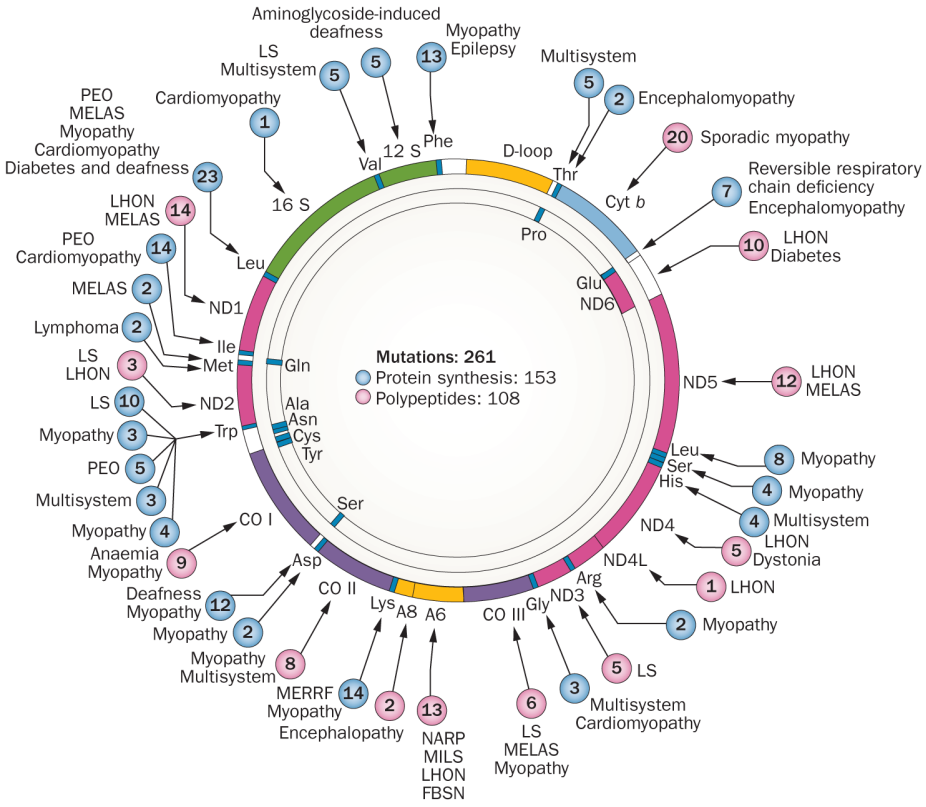

Figure 12. The mitochondrial morbidity map. Human mitochondrial DNA map showing representative pathogenic mutations. From *Di Mauro et al. 2013 Nat. Rev Neurology*

Mutations in nuclear genes

Mutations in nDNA-encoded OXPHOS-related genes have also been linked to a variety of multisystem disorders ranging from fatal infantile Leigh syndrome to predisposition to depression (Fig. 13)[173] . Accordingly, a genetic classification can be proposed for mitochondrial diseases related to nDNA mutations, including:

- Genes encoding structural components of the OXPHOS complexes;

- Genes encoding factors affecting mtDNA maintenance, replication and protein synthesis;
- Genes encoding factors involved in the biosynthesis of lipids and cofactors;
- Genes encoding proteins involved in mitochondrial protein import and dynamics;
- Gene encoding assembly factors of the OXPHOS complexes.

Genes encoding structural subunits of the OXPHOS complexes

Although 72 of the 85 subunits of the OXPHOS system are encoded by nuclear DNA, mutations of these genes have only rarely been described. This could imply that such mutations are highly deleterious and probably embryonic lethal. Accordingly, the reported mutations are usually associated with neonatal or early-onset, although occasional patients with a late onset of disease have been described. However, the screening of nuclear-encoded subunits of the respiratory chain complexes has not always been done systematically. The development of high-throughput technologies for gene screening has in fact been associated with an increased number of mutations in these genes. Mutations identified so far are mainly affecting complex I subunits, found in patients with disease onset in infancy or childhood, Complex I deficiency is the most common cause of respiratory chain disease, accounting for up to 30% of cases in childhood. Most core subunit mutations were reported for NDUFS1 and NDUFS4 but mutations of NDUFV1 and

NDUFS2 have also been reported[174]. The clinical presentation is a progressive neurological disorder, often Leigh syndrome, occasionally complicated by cardiomyopathy, or multisystem involvement.

Mitochondrial disease presentations associated with an isolated deficiency of complex II are rare, estimated to cover only 2% of respiratory chain deficiencies[175]. The majority of reported cases were infantile Leigh syndrome or severe leukodystrophy, with isolated complex II deficiency[176].

Disorders related to mitochondrial CIII deficiency are clinically heterogeneous and relatively rare. Most of the cases are caused by mutations in the mtDNA-encoded subunit cytochrome b. Additional mutations have recently been identified in nuclear structural genes. These include a homozygous deletion of *UQCRB* associated with hepatopathy[177], *UQCRQ*[178], *UQCRC2*[179], and *CYC1*[180] presenting severe neuromuscular syndrome, mental retardation, lactic acidosis and metabolic imbalance.

Few cases of mutations in COX subunits encoded by nDNA have been described recently. The first of them was a COX6B-1 mutation, found in two young brothers and associated to progressive neurological deterioration[181]; COX4-2 mutation has been reported to be associated to congenital exocrine pancreatic insufficiency[182] whereas COX7-B mutations have been associated to Microphthalmia with linear skin lesions (MLS), an unusual X-linked mitochondrial disease characterized by Microphthalmia with linear skin lesions[183].

Until a few years ago no mutations have been reported in nuclear genes encoding for structural subunits of CV. Recently mutations in ATP5E gene[184], encoding for the F_1 subunit ε and in ATP5A1[185] encoding for F_1 subunit α have been found. Both cases presented with neonatal onset and infantile encephalopathy but whilst the former showed a slow progression, the latter was fatal in the first weeks of life.

Genes encoding factors affecting mtDNA maintenance, replication and protein synthesis

MtDNA remains dependent upon nuclear DNA for the production of a range of proteins involved in its replication, transcription, translation, repair, and maintenance. Mutations of these genes can induce multiple mtDNA deletions or depletion of mtDNA. Mitochondria possess a complete DNA replication/maintenance system, including POLG, TWINKLE and other enzymes, requiring a continuous supply of deoxynucleotides. Typically, defects of the DNA-processive enzymes are responsible for qualitative alterations of mtDNA, such as multiple mtDNA deletions. On the contrary, mutations in genes assigned to maintenance of dNTP pools cause quantitative alterations of mtDNA, the so-called mtDNA depletion syndrome (MDS), where there is a reduction of mtDNA copy numbers caused by an alteration of the replication machinery. Qualitative alterations of mtDNA are usually associated with autosomal dominant or recessive forms of PEO and autosomal recessive myoneurogastrointestinal

encephalomyopathy (MNGIE). Causal mutations are documented in 12 nuclear genes. Three of these genes are directly implicated in mtDNA replication: POLG1 and 2 and Twinkle [186-188]. Mutations in these genes are mostly associated with PEO and infantile onset spinocerebellar ataxia (IOSCA) [189]. Seven genes are implicated in regulating mitochondrial deoxynucleotide pools[190,191], and two genes function by unknown mechanisms: MPV17, which causes isolated liver failure[192] and OPA1[193].

Translation and/or stability of the mtDNA encoded transcripts can be affected in recessive mutations of LRPPRC gene causing the French-Canadian variant of Leigh Syndrome (FCLS), a severe unusual form of infantile LS characterized by a profound complex IV deficit in brain and liver[194,195]. The mechanism by which LRPPRC regulates the mtDNA expression is still controversial, however, it has been demonstrated that this protein forms a complex with the stem-loop interacting RNA binding protein (SLIRP), a protein involved in the maintenance of mtRNAs[196].

Genes encoding factors involved in the biosynthesis of lipids and cofactors

Except for cytochrome *c,* which is located in the IMS, all components of the respiratory chain are embedded in the lipid milieu of the IM, which is composed predominantly of cardiolipin. Cardiolipin is not merely a scaffold but is essential for proper functioning of several mitochondrial OXPHOS

complexes and several mitochondrial carrier proteins[197,198]. This is the reason why defects in cardiolipin could cause OXPHOS dysfunction and hence mitochondrial disease. As already mentioned, Barth syndrome (mitochondrial myopathy, cardiomyopathy, growth retardation, and leukopenia)[199] is due to mutations in an X-linked gene, *TAZ* (or *G4.5)*, encoding tafazzin, an acyl–coenzyme A synthetase that plays an important role in cardiolipin synthesis. Cardiolipin concentrations are markedly decreased in skeletal and cardiac muscle and in platelets from affected patients[71]

Also CoQ deficiency is a potentially important cause of recurrent myoglobinuria or ataxia or both. Mutations in the *COQ2*, *PDSS1* and *PDSS2,* encoding for enzymes of CoQ biosynthetic pathway, were reported in patients with severe infantile mitochondrial syndromes and tissue CoQ deficiency[200], whereas the molecular genetic defect of adult-onset CoQ deficiency remains undefined[201].

Genes encoding proteins involved in mitochondrial protein import and dynamics

Cytosolic proteins destined for mitochondria have mitochondrial targeting signals that enable them to be routed to the appropriate compartment within the organelle, where they are then refolded into an active configuration[202] Although a number of mutations in mitochondrial targeting signals have been found, only a few errors in the import machinery itself are known, probably as they are generally incompatible with extrauterine

life[203]. However, at least one such defect has been identified, the deafness–dystonia syndrome (Mohr–Tranebjaerg syndrome), an X-linked recessive disorder characterized by progressive neurosensory deafness, dystonia, cortical blindness, and psychiatric symptoms[204], features that are strikingly similar to those of primary mitochondrial diseases. This disorder is due to mutations in *TIMM8A,* encoding the deafness–dystonia protein (DDP1), a component of the mitochondrial-protein–import machinery in the IMS. According to a recent report, an autosomal dominant form of hereditary spastic paraplegia is associated with mutations in the mitochondrial import chaperonin HSP60[205]. Pathogenic mutations in components regulating mitochondrial dynamics have been found in patients affected by mitochondrial diseases. Mutations in *OPA1* lead to autosomal dominant optic atrophy (ADOA), the most commonly inherited optic neuropathy, characterized by the specific loss of retinal ganglion cells[206]. Moreover, one of the axonal forms of Charcot–Marie–Tooth disease, altogether the most frequent inherited peripheral neuropathy in humans[207], may be caused by mutations in MFN2 and GDAP1 (ganglioside-induced differentiation protein 1) localized in the mitochondrial outer membrane[208,209]. While mutations of MFN2 inhibit fusion, inactivation of GDAP1 promotes fission of mitochondria.

Genes encoding assembly factors of the OXPHOS complexes

Most CI defects remain undefined at the genetic and molecular

levels. Given the complexity of the enzyme, a large number of yet unknown nuclear genes encoding mitochondrially targeted proteins are likely involved in its biogenesis; mutations in any of these factors may, in turn, lead to CI deficiency and disease. ND1, ND4, and ND6 are essential for the assembly of CI, as their mutations are associated with markedly reduced levels of the enzyme[210-212].

Two homozygous missense mutations have been recently found in SDH assembly factor 1 (*SDHAF1*) in two family sets, whose some components were affected by infantile leukoencephalopathy. SDHAF1 contains a LYR tripeptide motif, which is responsible for the insertion or retention of the Fe-S centers within the protein backbones of cI and cII, respectively[213].

More than 20 pathogenic mutations have been reported in the CIII assembly factor BCS1L, a member of the AAA+ family of proteins. BCS1L mutations are associated with a wide variety of phenotypic manifestations: from multivisceral GRACILE syndrome (growth retardation, aminoaciduria, cholestasis, iron overload, lactic acidosis, and early death)[49]; to congenital metabolic acidosis, neonatal proximal tubulopathy, liver failure, and encephalopathy[214]. TTC19 mutations have been described in patients with different clinical features. Whilst the first cases showed early-onset but slowly progressing encephalopathy, in a subsequent patient a late-onset but rapidly progressive neurological failure has been described, always wit complex III deficiency[215].

LYRM7 works as a stabilizing chaperone of the Rieske protein in CIII[216]. A single case of mutation in this assembly factor has been described in a child, which presented at the onset a progressive weakness associated to anemia. The disease developed into a severe encephalopathy and metabolic acidosis leading to death for respiratory failure[217].

In humans, most of the mutations causing CIV deficiency have been found in all mtDNA encoded subunits[218] and in many assembly factors[219]. The first identified COX deficiency with a nuclear origin was associated to SURF-1 mutations[220]. Since then, more than 40 mutations have bee found in the same assembly factor, all causing the same clinical presentation and determining the absence of the corresponding protein. Although the mechanistic function of the SURF1 protein is still unclear, the accumulation of specific subassemblies indicates a role for this protein in the early stages of CIV assembly. Rare mutations have been found in SCO1 and SCO2, two genes involved in copper delivery to COX, cellular copper homeostasis and redox signaling[221,222]. These aberrations have been associated with neonatal hepatopathy and ketoacidotic coma (SCO1) or infantile cardiomyopathy (SCO2), both characterized by profound COX deficiency[223,224]. COX assembly requires the early insertion of heme a groups in order to build the fully assembled holocomplex. In our lab, a mouse model of deficiency of heme a has been created by COX15 gene deletion and it has been employed for most of my *in vivo* work. Defects in the heme a biosynthetic pathway lead to different

clinical presentation, including fatal outcome early in life (from a few months to 2 years of age). The first COX10 mutation reported by Valnot et al. was found in a paediatric patient suffering from ataxia, muscle weakness, hypotonia and pyramidal syndrome, leukodystrophy and proximal tubolopathy accompanied by elevated lactate in both cerebrospinal fluid and blood[152]. Other patients with mutations in COX10 presented with anaemia, sensorineural deafness and hypertrophic cardiomyopathy; with anaemia and Leigh syndrome; and with Leigh-like syndrome. The levels of COX activity in COX10 patients ranged from 5 to 25% of control, depending on the tissues analyzed[149,225]. A few patients with COX15 defects have also been documented. The first patient studied by Antonicka et al. had lactic acidosis, hypotonia and seizures and after developing a massive biventricular cardiomyopathy died before the first month of age (Antonicka et al. 2003). The residual COX activity in this patient ranged from 7 to 25% of control values on the tissues analysed. Another COX15 paediatric patient presented a completely different clinical phenotype. At 7 months of age this second patient had hypotonia, nystagmus, motor regression, retinopathy and microcephaly, increased lactate levels in blood, and cerebrospinal fluid; by 1 year of age he had developed the typical brain lesions of Leigh syndrome. This patient died before the fourth year of age. COX activity in primary cultured fibroblast was undetectable[226]. The third COX15 patient was also diagnosed with Leigh syndrome but with a very slow progression of the disease, dominated by

skeletal muscle and brain involvement. At the time of the report the patient was 16 years old. Initially lactate levels were elevated but they progressively went down to normal range while other features remained unchanged. The COX deficiency in muscle and fibroblast (42 and 22% of control values respectively) was not as severe as in the previous two COX15 patients, accounting for the slow progression of the clinical phenotype[151]. A few cases of complex V deficiency have been attributed to mutations in the assembly factor ATP12. Lactic acidosis was present immediately after birth, together with dysmorphic features, and methyl-glutaconic aciduria[227]. Recently, mutations in another gene, TMEM70, was found in individuals with isolated deficiency of ATP synthase, mostly of Gipsy ethnic origin[228]; the prevalent mutation can result in either severe or milder phenotypes, dominated by hypertrophic cardiomyopathy.

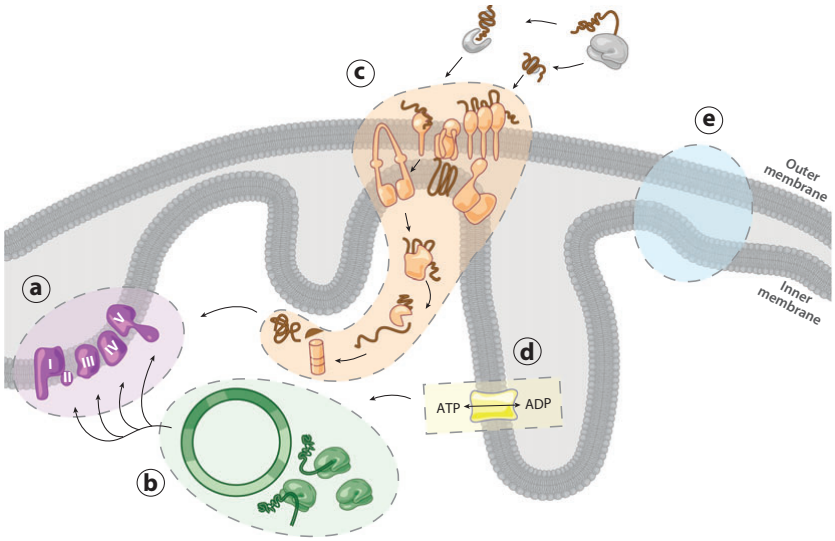

	a	b	c	d	e
	OXPHOS subunits: 34 genes	**mtDNA maintenance/ expression: 14 genes**	**OXPHOS biogenesis/ regulation: 28 genes**	**Nucleotide transport/ synthesis: 8 genes**	**Membrane dynamics/ composition: 8 genes**
Nuclear	I: NDUFV1, NDUFV2, NDUFA1, NDUFA2, NDUFA11, NDUFS1, NDUFS2, NDUFS3, NDUFS4, NDUFS6, NDUFS7, NDUFS8 II: SDHA, SDHB, SDHC, SDHD III: UQCRB, UQCRQ, CYCS IV: COX6B1, COX4I2	POLG, POLG2, C10orf2, MPV17, LRPPRC, MRPS16, MRPS22, GFM1, TSFM, TUFM, DARS2, RARS2, TRMU, PUS1	I: NDUFAF1, NDUFAF2, NDUFAF3, NDUFAF4, C8orf38, C20orf7 II: SDHAF1, SDHAF2 III: BCS1L, HCCS IV: SURF1, SCO1, SCO2, COX10, COX15, TACO1, ETHE1, FASTKD2 V: ATPAF2, TMEM70 Fe/S: FXN, ISCU, ABCB7 Other: TIMM8A, SPG7, HSPD1, DNAJC19, GFER	SLC25A4, SLC25A3, TYMP, DGUOK, TK2, SUCLA2, SUCLG1, RRM2B	COQ2, COQ9, PDSS1, PDSS2, CABC1, TAZ, OPA1, MFN2
mtDNA	I: ND1, ND2, ND3, ND4, ND4L, ND5, ND6 III: CYTB IV: COX1, COX2, COX3 V: ATP6, ATP8				

Figure 13. Biological pathways underlying respiratory chain disease. Bottom panel lists 92 protein-encoding genes that have been shown to cause mitochondrial. From *Calvo et al. 2010 Ann. Rev. Human Genet*.

Treatment of mitochondrial diseases

Given the extreme clinical, biochemical and genetic heterogeneity and the complexity of mitochondrial disease, neither universal nor effective therapy currently exists. However, research progress on the basic and molecular mechanisms of mitochondrial biology leading to disease and increasingly improved understanding on pathomechanisms

allow now to envisage suitable rational therapeutic strategies to treat mitochondrial diseases. These include:

- Increasing mitochondrial biogenesis;
- Stimulating autophagy;
- Heteroplasmy shifting;
- Scavenging toxic compounds;
- Bypassing the electron chain defects
- Targeting fission and fusion

Each of these strategies can be achieved by different approaches, such as pharmacological treatments, gene transfer of the missing or other therapeutic genes, cell therapy.

Increasing mitochondrial biogenesis

Mitochondrial diseases are hallmarked by bioenergetics defects leading to reduced ATP synthesis. Thus, therapeutic interventions aimed at increasing the ATP available may be beneficial to these conditions. Importantly, mitochondrial diseases arise when the residual activity falls below a critical threshold, suggesting that even a partial restoration of the activity may be sufficient to rescue or at least ameliorate the phenotype.

The idea that increasing the amount and/or function of mitochondria could be beneficial in mitochondrial disease, was first introduced by Bastin et al. who used bezafibrate, a pan-PPAR agonist widely used in clinics to treat metabolic syndrome and diabetes, on fibroblasts from patients with

different mitochondrial diseases[58]. They observed an improvement of the defective activities of the respiratory chain complexes by inducing PGC1α expression. These findings were subsequently reinforced by *in vivo* observations reported by Wenz et al[229]. However, these results were not confirmed subsequently. An alternative pathway to induce the PGC1α-dependent mitochondriogenic pathway is centered on the AMP-dependent kinase (AMPK). By using the AMPK agonist 5-aminoimidazole-4-carboxamide ribonucleoside (AICAR) we obtained a clear induction of OXPHOS-related genes and complexes activities in three models of COX deficiency (described in chapter 3) (Fig. 14).

An alternative strategy to activate PGC1α is to stimulate its deacetylation by activating Sirt1. Work carried out in our lab recently showed that increasing NAD^+ by either providing the natural precursor nicotinamide riboside (NR) or inhibiting (by genetic deletion or pharmacological intervention) the activity of Parp1, a poly(ADP) ribosyl-polymerase which is a greedy consumer of NAD^+, leads to the activation of Sirt1 and other sirtuins, thus boosting mitochondrial function by induction of OXPHOS genes and increase of the respiratory chain activities[230].

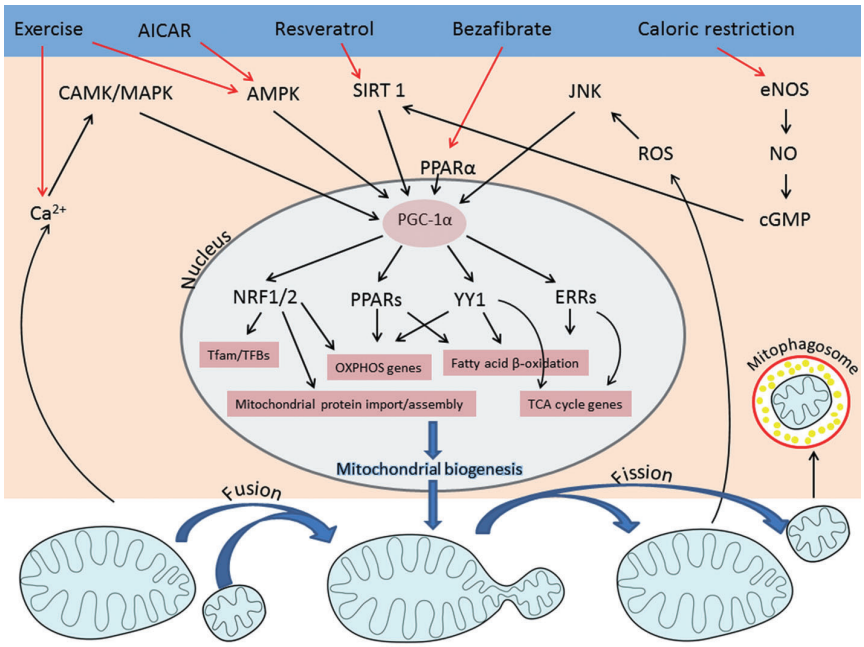

Figure 14. Drugs and external factors regulating mitochondrial biogenesis. In addition to exercise, many pharmaceuticals are available that regulate PGC- 1α and hence mitochondrial biogenesis. From *Jornayvaz et al. 2010 Essays Biochem.*

Stimulating autophagy

Mitophagy targets dysfunctional mitochondria within the cell, by performing a mitochondrial "organelle quality control" [108]. Parkin, an E3 ubiquitin ligase, is selectively recruited to target functionally impaired mitochondria by a PINK1-dependent manner[129], suggesting that autophagy degrades mitochondria carrying mutant mtDNAs, thereby providing a potential therapeutic strategy relying on activation of an intrinsic, physiological cellular pathway. An example of significant success of this strategy in preclinical models has recently been achieved by administering rapamycin, an mTOR inhibitor, to a mouse model of Leigh-like syndrome[231]. Rapamycin

significantly delayed the progression of the disease and significantly prolonged the lifespan of the mutant mice. More investigations are warranted to clarify the underlying mechanism, and to test its efficacy in other models of mitochondrial disease.

Heteroplasmy shifting

When deprived of glucose and treated with ketogenic media supplements, heteroplasmic transmitochondrial cytoplasmic hybrid (cybrid) cells harboring a large partial deletion of mtDNA shifted their heteroplasmy below the critical phenotype threshold and recovered mitochondrial function[232]. Although the mechanism by which this shift occurred is unclear, these results are consistent with the selective degradation of defective mitochondria by either autophagy or mitophagy as the mediator of the shift. Suomalainen and co-workers recently used ketogenic diet to rescue metabolic function in a mouse model of late-onset mitochondrial myopathy due to accumulating deletions of mtDNA but, interestingly, the metabolic improvement was not accompanied by any obvious reduction in the mutation load[233]. Again, this discrepancy may be explained, however, by the possibility that instead of effectively reducing the mutation load, the ketogenic stress ‘‘selected’’ the distribution of the mutation so that cells were favored that contained more mitochondria below the threshold for dysfunction[234]. Ketogenic diet has also been proposed to stimulate OXPHOS activity by increasing mitochondrial

biogenesis in some mitochondrial diseases mouse models[235]. Despite further evidence of beneficial effects of ketogenic diet, some reports show that it can have an opposite, actually detrimental, effect, leading to worsening of the mitochondrial defect in the Mterf2$^{-/-}$ mouse[236] or inducing liver failure in the Mpv17 knockout mouse model (see chapter 4 of this thesis). Heteroplasmic shifting can also be accomplished genetically. Some pathologic mutations create a novel and unique restriction site in human mtDNA. Tanaka et al. demonstrated the feasibility of selectively cleaving mutated mtDNA, targeting an appropriate restriction enzyme to mitochondria by gene therapy[237]. This strategy would only work for mutations that generate a restriction site absent in WT mtDNA but this approach can be generalized by using the recently introduced zinc-finger (ZFs) and TALEN-based technologies, which in principle should by-pass these constraints. ZFs can in fact be modified (for instance by adding a restriction endonuclease) and used as selective DNA-binding and cleaving agents. Although technically challenging, Minzcuk and co-workers recently succeeded to target both a ZF DNA methylase and ZF nucleases (ZFNs) to mitochondria for site specific elimination of pathogenic mtDNA[238,239]. This selective mtDNA targeting approach is strengthened by the recent identification of transcription activator-like (TAL) effector polypeptides in plants that also bind DNA selectively and could also be modified to target mtDNA (MitoTALEN)[240].

Scavenging toxic compounds

Other pharmacological interventions have been used to modify the course of specific mitochondrial diseases in cellular and/animal models. A first example is the use of N-acetylcysteine and metronidazole to correct the increased concentration of H_2S in ethylmalonic encephalopathy (EE), a fatal infant disease due to mutations in ETHE1, a gene encoding a mitochondrial sulfur dioxygenase. Ethe1 is involved in the oxidative disposal of hydrogen sulfide (H_2S), a toxic compound produced by both catabolism of sulfurated aminoacids and metabolism of anaerobes, constituting the colonic bacterial flora[241]. Notably, these compounds significantly ameliorated the clinical conditions of a cohort of EE patients, completely stopping severe diarrhea, microvasculopathy, and epileptic seizures of affected individuals, and ameliorating both alertness and interaction with the environment[242].

Increased ROS production occurs as a consequence of respiratory chain dysfunction due to either aging or OXPHOS defects[243], and may lead to damage of cellular structures, including proteins, lipids and nucleic acids. These observations constitute the rational basis for the use of antioxidants in the therapy of mitochondrial diseases. Cocktails of antioxidant compounds, including lipoic acid, vitamins C and E, CoQ, etc, have been used in the therapy of mitochondrial diseases for a long time, but randomized double blind trials to support their efficacy are still missing[244].

Bypassing the electron chain defects

An emerging concept in mitochondrial medicine is the possibility to by-pass the block of electron transfer through the respiratory chain, by using the "alternative" enzymes NADH DH/CoQ reductase (Ndi1) and CoQ/O2 alternative oxidase (AOX). These are mono-peptide enzymes transferring electrons from and to CoQ, respectively, without pumping protons. NDI1 substitutes complex I in yeast mitochondria complex I and AOX is an alternative electron transport system present in lower eukaryotes, plants and lower animals that can perform the oxidation of CoQH2 instead of complex III and complex IV. These proteins have been shown to be well tolerated in mammalian cells[245] and organisms[246] and they have successfully been exploited to by-pass complex I and complex II-IV defects in cellular[247,248] and Drosophila models of mitochondrial disease[249-251]. The mechanism by which these enzymes are beneficial to mitochondrial defects is based on their capacity to restore electron flux thus preventing accumulation of reduced intermediates and oxidative damage[252]. However, this is not accompanied by restoration of proton translocation across the inner mitochondrial membrane, and does not directly increase ATP production, which may be anyway indirectly achieved by increasing the electronic flux at other proton pumping sites. Although AOX-expressing mice are viable and fertile[246], the capacity of AOX to correct the phenotype of mouse models of complex III or IV deficiencies in vivo has not been assessed.

Gene therapy

Delivery of therapeutic genes as well as replacement of mutated genes with their wild-type species has been investigated for a long time as the definitive cure for genetic diseases. Although we are still far away from achieving this result, several successes have been reported in the last years for a number of genetic diseases in both preclinical models and in some clinical trials on patients. In fact, while the replacement of genes in the whole body is still an unachievable goal, and targeting skeletal muscle seems to be realistic in small rodents but not in humans, targeting specific organs of limited size (e.g. liver) is nowadays feasible. In particular the introduction of Adeno-associated viral (AAVs) vectors has given new stamina to gene therapy. AAVs are parvoviridae not associated to any disease in humans or animals,.AAV DNA remains episomal in host cells for prolonged time, thus reducing the risk of insertional mutagenesis[253]. In addition, several serotypes with different cellular specificity have been identified, allowing specific targeting of several organs and tissues[254].

Targeting fission and fusion

Although alterations of fission and fusion machineries have been shown to cause disease in humans, the possibility for these pathways to play a role as therapeutic targets has remained unexplored so far. Recent observations suggest that the maintenance of physiological balance between fission and fusion processes protects from accumulation of mtDNA mutations through promotion of functional mtDNA

complementation [255]. Two additional observations are relevant in this context. First, it has been recently shown that overexpression of Opa1 increases the respiratory efficiency, possibly by stabilizing the respiratory supercomplexes [128]. Second, some compounds affecting fission and fusion have been identified, such as MDIVI-1, that reduces fission by inhibiting Drp1, and M1-hydrazone, that promotes fusion by an unknown mechanism, whose mechanism of action is abolished by ablation of *OPA1* gene[256,257]. The therapeutic potential of these compounds for mitochondrial diseases has to be tested.

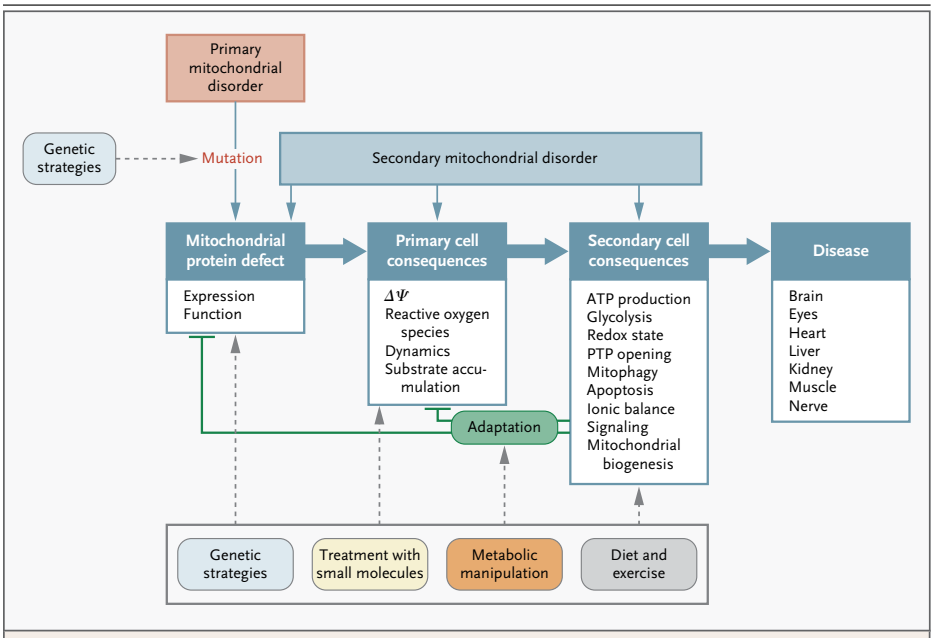

Figure 15. Consequences of mitochondrial dysfunction and potential intervention strategies. Overview of the main therapeutic approaches for mitochondrial diseases.

MOUSE MODELS FOR EXPERIMENTAL THERAPY OF MITOCHONDRIAL DISEASES

The conservation of most mitochondrial pathways in mammals, make recombinant mice an excellent tool to study the molecular basis of mitochondrial diseases. Accordingly several mouse models generated by genetic manipulation show clinical phenotypes similar to the respective human diseases, enabling treatment hypotheses to be tested through preclinical trials (Tab. 1). Informative mouse models have been obtained by the inactivation of OXPHOS related genes encoded by both nDNA and mtDNA even if, in the latter case, the lack of robust technologies to modify the mitochondrial genome has complicated this challenge. The main features of the mouse models used in this project are reported below.

Ndufs4: a model of severe mitochondrial encephalomyopathy

CI deficiency is the most frequent cause of mitochondrial disease in humans. Most of the mutations affect genes encoding structural CI subunits. *Ndufs4* encodes a small protein of about 18 kDa, essential for CI assembly and stability. Ndufs4 is inserted at a late stage during CI biogenesis[22,258] and mutations in this gene are responsible of Leigh syndrome or Leigh-like disease[174,258,259]. The *Ndufs4* knockout (*KO*) mouse has been created by ablating a floxed exon2 of the mouse gene in the germ line[260]. *Ndufs4*$^{-/-}$ mice develop a Leigh-like

phenotype characterized by ataxia, blindness, retarded growth rate and lethargy leading to premature death at about 7 weeks of age. Interestingly, marked differences in CI levels and activity were found in different tissues,. In any case, the defect in the CNS is very profound, which can explain the predominantly neurological phenotype and suggests that neurological impairment is the responsible of early death in this model. To test this hypothesis, a *Ndufs4* KO in neurons and glia, using a *Nestin-Cre* recombinase was generated[261]. The *NesKO* mice developed a phenotype that completely overlapped that of constitutive *Ndufs4*$^{-/-}$ mice and recapitulated several Leigh syndrome hallmarks. *NDUFS4* is considered a mutational "hot spot" for LS and Leigh-like disease in humans. Understanding the pathobiology of the disease is clearly useful for the development of treatment strategies for these devastating conditions that are invariably fatal in infancy or early childhood in humans.

Sco2^{KOKI} and Surf1$^{-/-}$: two models of mild mitochondrial myopathy

SCO2 encodes a mitochondrial chaperone implicated in copper metabolism, required for the proper assembly and function of CIV. The specific function of SCO2 is still not completely clear[221]. In humans, mutations in *SCO2* cause hypertrophic cardiomyopathy, encephalopathy and myopathy soon after birth[223]. The most common mutation found in patients is the c.1541G>A, p.E140K. E140 is close to the copper-binding domain. Patients homozygous for the c.1541G>A mutation

show delayed onset and longer survival compared to compound heterozygotes carrying a null mutation in the second allele[262]. A mouse model has been created harboring a ***Sco2* KO** allele (*Sco2*^{KO}) and a *Sco2* E129K knock-in allele (*Sco2*^{KI}), equivalent to the p.E140K mutation in humans[263]. Whilst the *Sco2*$^{KO/KO}$ mouse is embryonic lethal prior to E8.5, implying a crucial role for this gene in early development, mice homozygous for the knock-in E129K allele, *Sco2*$^{KI/KI}$, and the compound heterozygous *Sco2*$^{KO/KI}$ double mutant are viable. Both genotypes show CIV deficiency in heart, muscle, brain and liver and accumulation of CIV assembly intermediates in brain and liver but the *Sco2*$^{KI/KI}$ has a milder clinical phenotype compared to the *Sco2*$^{KO/KI}$ double mutant model.

Two **Surf1** KO mouse models were generated in our lab. The first model was obtained through gene disruption by targeted insertion of a neomycin cassette and replacement of exons 5 to 7. This genetic lesion caused high embryonic lethality with only a few KO animals surviving. Lethality was attributed to the neomycin insertion rather than to the ablation of *Surf1* gene. In the second constitutive *Surf1*^{KO} mouse model, the neomycin cassette was targeted to *Surf1* exon 7, and then removed by cre technology. As a result of this recombination event, a loxP site is introduced within exon 7, which causes the creation of a premature stop codon interrupting the translation of the protein at approximately 2/3 of its full-length sequence. This second *Surf1*^{KO} mouse model shows a mild CIV deficiency in brain, skeletal muscle, heart and liver (30% - 40% of control values),

the latter been the most affected tissue. This new model also failed to show any overt neurodegenerative phenotype, and unexpectedly, a prolonged lifespan, on average 5 months longer than control liiermates. The reasons for increased longevity remain unexplained although the same phenotype was observed in a CNS specific *Surf1* KO model of *Drosophila melanogaster*[264].

Muscle-specific Cox15 KO: a model of severe mitochondrial myopathy

The *Cox15*^{KO} mouse model is another mouse model of CIV deficit generated in our lab. As extensively discussed above, the enzyme encoded by this gene is involved in heme a biosynthesis and its mutations cause fatal encephalocardiomyopathy with early or late onset Leigh syndrome[150,151,226]. Constitutive *Cox15*^{KO} mice showed a consistent embryonic lethality at E7.5 (Viscomi, 2011). A knock-in mouse with the *Cox15* exons 1-2 flanked by the *loxP* sites was crossed with a transgenic mouse expressing the *Cre* recombinase under the control of the human skeletal muscle-specific alpha-actin (ACTA1) promoter to create the *ACTA-Cox15*$^{-/-}$ mouse, in which ablation of the *Cox15* gene is restricted to skeletal muscle. Albeit born at the expected Mendelian ratio, *ACTA-Cox15*$^{-/-}$ animals were smaller than control littermates at 1 month and had reduced motor performance due to severe mitochondrial myopathy. Histochemical analysis of skeletal muscle confirmed severe reduction of CIV and compensatory proliferation of aberrant

mitochondria (see Chapters 2 and 3 of this thesis).

Mpv17 KO: a model of hepatic mtDNA depletion syndrome

The *Mpv17* gene encodes for a mitochondrial inner membrane protein involved in mtDNA maintenance, although its precise function remains unknown[192]. Mutations in human *MPV17* cause a peculiar form of infantile hepatocerebral mtDNA depletion syndrome, characterized by severe hypoglycemic crises and progressive impairment of hepatic function that ultimately leads to liver cirrhosis. Knockout *Mpv17* mice develop a progressive kidney dysfunction leading to systemic hypertension at 2–3 months after birth[265] Reduction of mtDNA levels is found in multiple tissues, including skeletal muscle, kidney and brain. The tissue displaying the most profound mtDNA depletion is the liver, associated with CI and CIV deficiency. Interestingly, the *Mpv17*^{KO} mice show only a subclinical mitochondrial hepatopathy and myopathy (see chapter 4). Other mice with defects in mtDNA maintenance genes include KO models of *POLG*, *PEO1* (also known as *C10orf2*, encoding the Twinkle helicase), *TK2* and *RRM2B*. Some of these mouse models display embryonic lethality, whereas others show a relatively mild clincial phenotype, but the main biochemical signatures are similar to the corresponding human diseases, thus enabling preclinical trials to be performed.

Gene	Human phenotype	Mouse model	Mouse phenotype	References
ANT1	ADPEO (cardiomyopathy in only recessive case reported)	*Ant1 (–/–)*	Ragged-red fibres, mitochondrial proliferation, cardiomyopathy, very high serum lactate levels.	Graham *et al.*, 1997
POLG	Alpers disease ARPEO ADPEO	*Polg (–/–)* Polg (+/–)	Embryonically lethal. Severe mtDNA depletion. Slight reduction in mtDNA, normal development.	Hance *et al.*, 2005
C10orf2 (PEO1)	ADPEO MDDS (hepatocerebral)	*Twinkle* 'Deletor' mouse	Accumulate multiple mtDNA deletions with progressive COX deficiency and late-onset myopathy.	Tyynismaa *et al.*, 2005
RRM2B	ADPEO MDDS (encephalomyopathic)	*Rrm2b (–/–)*	Normal at birth, at 6 weeks show growth retardation and die prematurely	Kimura *et al.*, 2003
TK2	MDDS (myopathic)	*Tk2 (–/–)* *Tk2* (H126N)	Normal at birth, at 7 days show growth retardation, severe hypothermia, severe mtDNA depletion in muscle, heart, liver and spleen. Death at 30 days. Growth retardation, tremor, ataxic gait and severe weakness on day 10. MtDNA depletion.	Akman *et al.*, 2008; Zhou *et al.*, 2008
MPV17	MDDS (hepatocerebral)	*Mpv17 (–/–)*	Adult mice show nephrotic syndrome and chronic renal failure.	Weiher *et al.*, 1990
TFAM	None reported to date	*Tfam (–/–)*	Embryonically lethal. Severe mtDNA depletion and no detectable OXPHOS.	Larsson *et al.*, 1998
ND6	Leigh syndrome	*Nd6* (P25L)	Optic atrophy, reduced complex I and increased oxidative stress.	Lin *et al.*, 2012
NDUFS4	Leigh syndrome	*Ndufs4 (–/–)*	Encephalomyopathy, ataxia at 5 weeks, death ~7 weeks. Slow growth, lethargy, loss of motor skills, blindness and high serum lactate.	Kruse *et al.*, 2008
NDUFS6	Fatal infantile lactic acidosis	*Ndufs6 (–/–)*	Cardiomyopathy at 4 months (males) and 8 months (females) and death.	Ke *et al.*, 2012
SDHD	Paraganglioma	*Sdhd (–/–)* Sdhd (+/–)	Homozygous KO lethal. Heterozygous KO has a decreased Complex II activity.	Piruat *et al.*, 2004
BCS1L	GRACILE syndrome (cholestasis with iron overload, intrauterine growth restriction, amino aciduria, lactic acidosis and early death), complex III deficiency	*Bcs1l* (S78G)	Failure to thrive, liver steatosis, fibrosis and cirrhosis, tubulopathy, complex III deficiency, premature death.	Leveen *et al.*, 2011
SURF1	COX-deficient Leigh syndrome	*Surf1 (–/–)*	High rates of embryonic lethality. Reduced birth weight, reduced complex IV activity in muscle.	Agostino *et al.*, 2003
SCO2	Cardio-encephalomyopathy	*Sco2 (–/–)* *Sco2* (E140K)	Homozygous KO lethal. Complex IV deficiency, no cardiomyopathy and normal life span.	Yang *et al.*, 2010; 2010
COX10	Encephalomyopathy with renal tubulopathy, Leigh syndrome	*Cox10 (–/–)*	Slowly progressing myopathy at 3 months, severe complex IV deficiency.	Diaz *et al.*, 2005
PDSS2	Encephalomyopathy and nephrotic syndrome, CoQ_{10} deficiency	*Kd/kd (spontaneous mutation)*	Progressive renal failure.	Lyon and Hulse, 1971
COQ9	Fatal multisystem disease with CoQ_{10} deficiency	*Coq9 (R239X/R239X)*	Fatal encephalomyopathy.	Garcia-Corzo *et al.*, 2013
HSP40	None reported to date	*Hsp40 (–/–)*	Dilated cardiomyopathy, RC deficiency and decreased mtDNA levels. Death before 10 weeks.	Hayashi *et al.*, 2006

Table 1. Mitochondrial disease mouse models. Mouse models generated in the last years are listed. From *Kanbus et al. 2014 Bristish journal of Pharmacology*

Scope of the thesis

The purpose of the experimental work that I carried out during my DIMET course has been focused on the evaluation of new therapies aimed to cure mitochondrial diseases. Although relatively rare as individual genetic entities, taken as a group primary mitochondrial diseases are now recognized as one of the major health issue among inborn errors of metabolism, with a prevalence >1 in 5.000. The ever expanding identification of new genes affecting OXPHOS sustains the idea that these disorders are far more common than previously thought. These devastating diseases are complex, with highly variable presentations. Importantly, rational, evidence-based effective treatment is lacking for most of them. In this thesis I have tested three different alternative approaches in vivo using suitable mouse models.

Optimizing the OXPHOS capacity through stimulation of the mitochondrial biogenesis is an emerging strategy that takes advantage from the residual activity, even if minimal, retained by faulty mitochondrial respiratory chain. This approach, discussed in chapter 3, has been accomplished by pharmacological intervention. Two compounds (bezafibrate and AICAR) have been tested on three mouse models of complex IV deficiency in order to stimulate mitochondrial biogenesis through activation of either PPARs- or PGC-1α-regulatory systems and eventually increase ATP production.

Successful pre-clinical trials have been reported in the last few

years using gene replacement therapy for a number of genetic disorders. The most relevant results have been obtained by recombinant Adeno-associated viral (AAVs) vectors carrying a therapeutic gene, specifically targeted to the affected tissues and organs. Whilst replacement of genes through the whole body is still an unachievable goal, and even specific targeting to skeletal muscle is feasible in small rodents but not in humans, gene replacement in smaller-size organs is nowadays feasible. Chapter 4 reports the application of this strategy on a mouse model of severe mtDNA depletion syndrome predominantly affecting the liver.

An alternative, potentially widely applicable approach has drawn my interest in the last stage of my project. Given the importance of mitochondrial ultrastructure and dynamics on cellular physiology and their impact on disease, I wondered if the manipulation of mitochondrial shape was able to restore the energetic deficit in two mouse models of CI and CIV defects. Starting from the assumption that OPA1 is the only known pro-fusion protein also involved in the shaping of the IM and considering that its overexpression protects cells from a number of deleterious triggers and enhance the efficiency of OXPHOS proficiency, I attempted to overexpress the OPA1 gene in two models of severe mitochondrial disease, the *Ndufs4*$^{-/-}$ and the *ACTA-Cox15*$^{-/-}$ mouse models. These two models of disease show different phenotypes, encephalopathy and myopathy, resembling the variability observed in human mitochondrial disorders, thus giving a high translational value to my research.

References

1. Nass S, Nass MM. Intramitochondrial Fibers with DNA Characteristics. Ii. Enzymatic and Other Hydrolytic Treatments. The Journal of cell biology 1963;19:613-29.
2. Luck DJ, Reich E. DNA in Mitochondria of Neurospora Crassa. Proceedings of the National Academy of Sciences of the United States of America 1964;52:931-8.
3. Yang D, Oyaizu Y, Oyaizu H, Olsen GJ, Woese CR. Mitochondrial origins. Proceedings of the National Academy of Sciences of the United States of America 1985;82:4443-7.
4. Cavalier-Smith T. Origin of mitochondria by intracellular enslavement of a photosynthetic purple bacterium. Proceedings Biological sciences / The Royal Society 2006;273:1943-52.
5. Margulis L. Symbiosis and evolution. Scientific American 1971;225:48-57.
6. Martin W, Muller M. The hydrogen hypothesis for the first eukaryote. Nature 1998;392:37-41.
7. Esser C, Ahmadinejad N, Wiegand C, et al. A genome phylogeny for mitochondria among alpha-proteobacteria and a predominantly eubacterial ancestry of yeast nuclear genes. Molecular biology and evolution 2004;21:1643-60.
8. de Duve C. The origin of eukaryotes: a reappraisal. Nature reviews Genetics 2007;8:395-403.
9. Dyall SD, Brown MT, Johnson PJ. Ancient invasions: from endosymbionts to organelles. Science 2004;304:253-7.
10. Esser C, Martin W, Dagan T. The origin of mitochondria in light of a fluid prokaryotic chromosome model. Biology letters 2007;3:180-4.
11. Palade GE. The fine structure of mitochondria. The Anatomical record 1952;114:427-51.
12. Gilkerson RW, Selker JM, Capaldi RA. The cristal membrane of mitochondria is the principal site of oxidative phosphorylation. FEBS letters 2003;546:355-8.
13. Anderson S, Bankier AT, Barrell BG, et al. Sequence and organization of the human mitochondrial genome. Nature 1981;290:457-65.
14. Ruiz-Pesini E, Lott MT, Procaccio V, et al. An enhanced MITOMAP with a global mtDNA mutational phylogeny. Nucleic acids research 2007;35:D823-8.

15. Schwartz M, Vissing J. Paternal inheritance of mitochondrial DNA. The New England journal of medicine 2002;347:576-80.
16. Malka F, Lombes A, Rojo M. Organization, dynamics and transmission of mitochondrial DNA: focus on vertebrate nucleoids. Biochimica et biophysica acta 2006;1763:463-72.
17. St John JC, Ramalho-Santos J, Gray HL, et al. The expression of mitochondrial DNA transcription factors during early cardiomyocyte in vitro differentiation from human embryonic stem cells. Cloning and stem cells 2005;7:141-53.
18. Wong LJ. Diagnostic challenges of mitochondrial DNA disorders. Mitochondrion 2007;7:45-52.
19. Hsieh RH, Tsai NM, Au HK, Chang SJ, Wei YH, Tzeng CR. Multiple rearrangements of mitochondrial DNA in unfertilized human oocytes. Fertility and sterility 2002;77:1012-7.
20. Wallace DC. Mitochondrial diseases in man and mouse. Science 1999;283:1482-8.
21. Dieteren CE, Willems PH, Vogel RO, et al. Subunits of mitochondrial complex I exist as part of matrix- and membrane-associated subcomplexes in living cells. The Journal of biological chemistry 2008;283:34753-61.
22. Lazarou M, McKenzie M, Ohtake A, Thorburn DR, Ryan MT. Analysis of the assembly profiles for mitochondrial- and nuclear-DNA-encoded subunits into complex I. Molecular and cellular biology 2007;27:4228-37.
23. Brandt U. Energy converting NADH:quinone oxidoreductase (complex I). Annual review of biochemistry 2006;75:69-92.
24. Vinothkumar KR, Zhu J, Hirst J. Architecture of mammalian respiratory complex I. Nature 2014;515:80-4.
25. Baradaran R, Berrisford JM, Minhas GS, Sazanov LA. Crystal structure of the entire respiratory complex I. Nature 2013;494:443-8.
26. Friedrich T, Bottcher B. The gross structure of the respiratory complex I: a Lego System. Biochimica et biophysica acta 2004;1608:1-9.
27. Gostimskaya IS, Grivennikova VG, Cecchini G, Vinogradov AD. Reversible dissociation of flavin mononucleotide from the mammalian membrane-bound NADH:

ubiquinone oxidoreductase (complex I). FEBS letters 2007;581:5803-6.
28. Lill R, Muhlenhoff U. Maturation of iron-sulfur proteins in eukaryotes: mechanisms, connected processes, and diseases. Annual review of biochemistry 2008;77:669-700.
29. Murai M, Ishihara A, Nishioka T, Yagi T, Miyoshi H. The ND1 subunit constructs the inhibitor binding domain in bovine heart mitochondrial complex I. Biochemistry 2007;46:6409-16.
30. Sun F, Huo X, Zhai Y, et al. Crystal structure of mitochondrial respiratory membrane protein complex II. Cell 2005;121:1043-57.
31. Yankovskaya V, Horsefield R, Tornroth S, et al. Architecture of succinate dehydrogenase and reactive oxygen species generation. Science 2003;299:700-4.
32. Hagerhall C. Succinate: quinone oxidoreductases. Variations on a conserved theme. Biochimica et biophysica acta 1997;1320:107-41.
33. Meunier B, Fisher N, Ransac S, Mazat JP, Brasseur G. Respiratory complex III dysfunction in humans and the use of yeast as a model organism to study mitochondrial myopathy and associated diseases. Biochimica et biophysica acta 2013;1827:1346-61.
34. Dibrova DV, Cherepanov DA, Galperin MY, Skulachev VP, Mulkidjanian AY. Evolution of cytochrome bc complexes: from membrane-anchored dehydrogenases of ancient bacteria to triggers of apoptosis in vertebrates. Biochimica et biophysica acta 2013;1827:1407-27.
35. Mitchell P. Possible molecular mechanisms of the protonmotive function of cytochrome systems. Journal of theoretical biology 1976;62:327-67.
36. Tsukihara T, Aoyama H, Yamashita E, et al. The whole structure of the 13-subunit oxidized cytochrome c oxidase at 2.8 A. Science 1996;272:1136-44.
37. Yoshikawa S, Shinzawa-Itoh K, Tsukihara T. Crystal structure of bovine heart cytochrome c oxidase at 2.8 A resolution. Journal of bioenergetics and biomembranes 1998;30:7-14.
38. Balsa E, Marco R, Perales-Clemente E, et al. NDUFA4 is a subunit of complex IV of the mammalian electron transport chain. Cell metabolism 2012;16:378-86.

39. Fernandez-Vizarra E, Tiranti V, Zeviani M. Assembly of the oxidative phosphorylation system in humans: what we have learned by studying its defects. Biochimica et biophysica acta 2009;1793:200-11.
40. Wikstrom M. Cytochrome oxidase: structure and mechanism. Foreword. Journal of bioenergetics and biomembranes 1998;30:3-5.
41. Zaslavsky D, Gennis RB. Proton pumping by cytochrome oxidase: progress, problems and postulates. Biochimica et biophysica acta 2000;1458:164-79.
42. Capaldi RA, Aggeler R, Turina P, Wilkens S. Coupling between catalytic sites and the proton channel in F1F0-type ATPases. Trends in biochemical sciences 1994;19:284-9.
43. Devenish RJ, Prescott M, Rodgers AJ. The structure and function of mitochondrial F1F0-ATP synthases. International review of cell and molecular biology 2008;267:1-58.
44. Strauss M, Hofhaus G, Schroder RR, Kuhlbrandt W. Dimer ribbons of ATP synthase shape the inner mitochondrial membrane. The EMBO journal 2008;27:1154-60.
45. Walker JE, Dickson VK. The peripheral stalk of the mitochondrial ATP synthase. Biochimica et biophysica acta 2006;1757:286-96.
46. Boyer PD. A model for conformational coupling of membrane potential and proton translocation to ATP synthesis and to active transport. FEBS letters 1975;58:1-6.
47. Hackenbrock CR, Chazotte B, Gupte SS. The random collision model and a critical assessment of diffusion and collision in mitochondrial electron transport. Journal of bioenergetics and biomembranes 1986;18:331-68.
48. Lenaz G, Genova ML. Kinetics of integrated electron transfer in the mitochondrial respiratory chain: random collisions vs. solid state electron channeling. American journal of physiology Cell physiology 2007;292:C1221-39.
49. Schagger H, Pfeiffer K. Supercomplexes in the respiratory chains of yeast and mammalian mitochondria. The EMBO journal 2000;19:1777-83.
50. Lenaz G, Genova ML. Structure and organization of mitochondrial respiratory complexes: a new understanding of an old subject. Antioxidants & redox signaling 2010;12:961-1008.

51. Acin-Perez R, Fernandez-Silva P, Peleato ML, Perez-Martos A, Enriquez JA. Respiratory active mitochondrial supercomplexes. Molecular cell 2008;32:529-39.
52. Cruciat CM, Brunner S, Baumann F, Neupert W, Stuart RA. The cytochrome bc1 and cytochrome c oxidase complexes associate to form a single supracomplex in yeast mitochondria. The Journal of biological chemistry 2000;275:18093-8.
53. Althoff T, Mills DJ, Popot JL, Kuhlbrandt W. Arrangement of electron transport chain components in bovine mitochondrial supercomplex I1III2IV1. The EMBO journal 2011;30:4652-64.
54. Dudkina NV, Kudryashev M, Stahlberg H, Boekema EJ. Interaction of complexes I, III, and IV within the bovine respirasome by single particle cryoelectron tomography. Proceedings of the National Academy of Sciences of the United States of America 2011;108:15196-200.
55. Wittig I, Schagger H. Supramolecular organization of ATP synthase and respiratory chain in mitochondrial membranes. Biochimica et biophysica acta 2009;1787:672-80.
56. Scarpulla RC. Nucleus-encoded regulators of mitochondrial function: integration of respiratory chain expression, nutrient sensing and metabolic stress. Biochimica et biophysica acta 2012;1819:1088-97.
57. Kukat C, Larsson NG. mtDNA makes a U-turn for the mitochondrial nucleoid. Trends in cell biology 2013;23:457-63.
58. Bastin J, Aubey F, Rotig A, Munnich A, Djouadi F. Activation of peroxisome proliferator-activated receptor pathway stimulates the mitochondrial respiratory chain and can correct deficiencies in patients' cells lacking its components. The Journal of clinical endocrinology and metabolism 2008;93:1433-41.
59. Fernandez-Marcos PJ, Auwerx J. Regulation of PGC-1alpha, a nodal regulator of mitochondrial biogenesis. The American journal of clinical nutrition 2011;93:884S-90.
60. St John JC, Facucho-Oliveira J, Jiang Y, Kelly R, Salah R. Mitochondrial DNA transmission, replication and inheritance: a journey from the gamete through the embryo and into offspring and embryonic stem cells. Human reproduction update 2010;16:488-509.
61. Gleyzer N, Vercauteren K, Scarpulla RC. Control of mitochondrial transcription specificity factors (TFB1M and TFB2M) by nuclear respiratory factors (NRF-1 and NRF-2) and

PGC-1 family coactivators. Molecular and cellular biology 2005;25:1354-66.
62. Ropp PA, Copeland WC. Cloning and characterization of the human mitochondrial DNA polymerase, DNA polymerase gamma. Genomics 1996;36:449-58.
63. Carrodeguas JA, Theis K, Bogenhagen DF, Kisker C. Crystal structure and deletion analysis show that the accessory subunit of mammalian DNA polymerase gamma, Pol gamma B, functions as a homodimer. Molecular cell 2001;7:43-54.
64. Takamatsu C, Umeda S, Ohsato T, et al. Regulation of mitochondrial D-loops by transcription factor A and single-stranded DNA-binding protein. EMBO reports 2002;3:451-6.
65. Clayton DA. Replication of animal mitochondrial DNA. Cell 1982;28:693-705.
66. Holt IJ, Lorimer HE, Jacobs HT. Coupled leading- and lagging-strand synthesis of mammalian mitochondrial DNA. Cell 2000;100:515-24.
67. Hackenbrock CR. Chemical and physical fixation of isolated mitochondria in low-energy and high-energy states. Proceedings of the National Academy of Sciences of the United States of America 1968;61:598-605.
68. Perkins GA, Renken CW, Frey TG, Ellisman MH. Membrane architecture of mitochondria in neurons of the central nervous system. Journal of neuroscience research 2001;66:857-65.
69. Mannella CA. Structure and dynamics of the mitochondrial inner membrane cristae. Biochimica et biophysica acta 2006;1763:542-8.
70. Hoch FL. Cardiolipins and biomembrane function. Biochimica et biophysica acta 1992;1113:71-133.
71. Schlame M, Rua D, Greenberg ML. The biosynthesis and functional role of cardiolipin. Progress in lipid research 2000;39:257-88.
72. Ott M, Robertson JD, Gogvadze V, Zhivotovsky B, Orrenius S. Cytochrome c release from mitochondria proceeds by a two-step process. Proceedings of the National Academy of Sciences of the United States of America 2002;99:1259-63.
73. Chicco AJ, Sparagna GC. Role of cardiolipin alterations in mitochondrial dysfunction and disease. American journal of physiology Cell physiology 2007;292:C33-44.

74. Fusaro G, Dasgupta P, Rastogi S, Joshi B, Chellappan S. Prohibitin induces the transcriptional activity of p53 and is exported from the nucleus upon apoptotic signaling. The Journal of biological chemistry 2003;278:47853-61.
75. Kasashima K, Ohta E, Kagawa Y, Endo H. Mitochondrial functions and estrogen receptor-dependent nuclear translocation of pleiotropic human prohibitin 2. The Journal of biological chemistry 2006;281:36401-10.
76. Tatsuta T, Model K, Langer T. Formation of membrane-bound ring complexes by prohibitins in mitochondria. Molecular biology of the cell 2005;16:248-59.
77. Merkwirth C, Dargazanli S, Tatsuta T, et al. Prohibitins control cell proliferation and apoptosis by regulating OPA1-dependent cristae morphogenesis in mitochondria. Genes & development 2008;22:476-88.
78. Pfanner N, van der Laan M, Amati P, et al. Uniform nomenclature for the mitochondrial contact site and cristae organizing system. The Journal of cell biology 2014;204:1083-6.
79. van der Laan M, Bohnert M, Wiedemann N, Pfanner N. Role of MINOS in mitochondrial membrane architecture and biogenesis. Trends in cell biology 2012;22:185-92.
80. Chacinska A, Koehler CM, Milenkovic D, Lithgow T, Pfanner N. Importing mitochondrial proteins: machineries and mechanisms. Cell 2009;138:628-44.
81. Bohnert M, Wenz LS, Zerbes RM, et al. Role of mitochondrial inner membrane organizing system in protein biogenesis of the mitochondrial outer membrane. Molecular biology of the cell 2012;23:3948-56.
82. Ott C, Ross K, Straub S, et al. Sam50 functions in mitochondrial intermembrane space bridging and biogenesis of respiratory complexes. Molecular and cellular biology 2012;32:1173-88.
83. Krause F, Reifschneider NH, Goto S, Dencher NA. Active oligomeric ATP synthases in mammalian mitochondria. Biochemical and biophysical research communications 2005;329:583-90.
84. Faccenda D, Campanella M. Molecular Regulation of the Mitochondrial F(1)F(o)-ATPsynthase: Physiological and Pathological Significance of the Inhibitory Factor 1 (IF(1)). International journal of cell biology 2012;2012:367934.

85. Allen RD, Schroeder CC, Fok AK. An investigation of mitochondrial inner membranes by rapid-freeze deep-etch techniques. The Journal of cell biology 1989;108:2233-40.
86. Paumard P, Vaillier J, Coulary B, et al. The ATP synthase is involved in generating mitochondrial cristae morphology. The EMBO journal 2002;21:221-30.
87. Misaka T, Miyashita T, Kubo Y. Primary structure of a dynamin-related mouse mitochondrial GTPase and its distribution in brain, subcellular localization, and effect on mitochondrial morphology. The Journal of biological chemistry 2002;277:15834-42.
88. Satoh M, Hamamoto T, Seo N, Kagawa Y, Endo H. Differential sublocalization of the dynamin-related protein OPA1 isoforms in mitochondria. Biochemical and biophysical research communications 2003;300:482-93.
89. Akepati VR, Muller EC, Otto A, Strauss HM, Portwich M, Alexander C. Characterization of OPA1 isoforms isolated from mouse tissues. Journal of neurochemistry 2008;106:372-83.
90. Griparic L, van der Wel NN, Orozco IJ, Peters PJ, van der Bliek AM. Loss of the intermembrane space protein Mgm1/OPA1 induces swelling and localized constrictions along the lengths of mitochondria. The Journal of biological chemistry 2004;279:18792-8.
91. Delettre C, Griffoin JM, Kaplan J, et al. Mutation spectrum and splicing variants in the OPA1 gene. Human genetics 2001;109:584-91.
92. Ishihara N, Fujita Y, Oka T, Mihara K. Regulation of mitochondrial morphology through proteolytic cleavage of OPA1. The EMBO journal 2006;25:2966-77.
93. Olichon A, Elachouri G, Baricault L, Delettre C, Belenguer P, Lenaers G. OPA1 alternate splicing uncouples an evolutionary conserved function in mitochondrial fusion from a vertebrate restricted function in apoptosis. Cell death and differentiation 2007;14:682-92.
94. Song Z, Chen H, Fiket M, Alexander C, Chan DC. OPA1 processing controls mitochondrial fusion and is regulated by mRNA splicing, membrane potential, and Yme1L. The Journal of cell biology 2007;178:749-55.
95. Anand R, Wai T, Baker MJ, et al. The i-AAA protease YME1L and OMA1 cleave OPA1 to balance mitochondrial fusion and fission. The Journal of cell biology 2014;204:919-29.

96. Baricault L, Segui B, Guegand L, et al. OPA1 cleavage depends on decreased mitochondrial ATP level and bivalent metals. Experimental cell research 2007;313:3800-8.
97. Duvezin-Caubet S, Jagasia R, Wagener J, et al. Proteolytic processing of OPA1 links mitochondrial dysfunction to alterations in mitochondrial morphology. The Journal of biological chemistry 2006;281:37972-9.
98. Griparic L, Kanazawa T, van der Bliek AM. Regulation of the mitochondrial dynamin-like protein Opa1 by proteolytic cleavage. The Journal of cell biology 2007;178:757-64.
99. Cipolat S, Rudka T, Hartmann D, et al. Mitochondrial rhomboid PARL regulates cytochrome c release during apoptosis via OPA1-dependent cristae remodeling. Cell 2006;126:163-75.
100. Duvezin-Caubet S, Koppen M, Wagener J, et al. OPA1 processing reconstituted in yeast depends on the subunit composition of the m-AAA protease in mitochondria. Molecular biology of the cell 2007;18:3582-90.
101. Ehses S, Raschke I, Mancuso G, et al. Regulation of OPA1 processing and mitochondrial fusion by m-AAA protease isoenzymes and OMA1. The Journal of cell biology 2009;187:1023-36.
102. Head B, Griparic L, Amiri M, Gandre-Babbe S, van der Bliek AM. Inducible proteolytic inactivation of OPA1 mediated by the OMA1 protease in mammalian cells. The Journal of cell biology 2009;187:959-66.
103. Chan DC. Fusion and fission: interlinked processes critical for mitochondrial health. Annual review of genetics 2012;46:265-87.
104. van der Bliek AM, Shen Q, Kawajiri S. Mechanisms of mitochondrial fission and fusion. Cold Spring Harbor perspectives in biology 2013;5.
105. Chen H, Chan DC. Physiological functions of mitochondrial fusion. Annals of the New York Academy of Sciences 2010;1201:21-5.
106. Gomes LC, Di Benedetto G, Scorrano L. During autophagy mitochondria elongate, are spared from degradation and sustain cell viability. Nature cell biology 2011;13:589-98.
107. Mitra K, Wunder C, Roysam B, Lin G, Lippincott-Schwartz J. A hyperfused mitochondrial state achieved at G1-S regulates cyclin E buildup and entry into S phase. Proceedings

of the National Academy of Sciences of the United States of America 2009;106:11960-5.
108. Twig G, Elorza A, Molina AJ, et al. Fission and selective fusion govern mitochondrial segregation and elimination by autophagy. The EMBO journal 2008;27:433-46.
109. Youle RJ, van der Bliek AM. Mitochondrial fission, fusion, and stress. Science 2012;337:1062-5.
110. Chen H, Detmer SA, Ewald AJ, Griffin EE, Fraser SE, Chan DC. Mitofusins Mfn1 and Mfn2 coordinately regulate mitochondrial fusion and are essential for embryonic development. The Journal of cell biology 2003;160:189-200.
111. Koshiba T, Detmer SA, Kaiser JT, Chen H, McCaffery JM, Chan DC. Structural basis of mitochondrial tethering by mitofusin complexes. Science 2004;305:858-62.
112. Ishihara N, Eura Y, Mihara K. Mitofusin 1 and 2 play distinct roles in mitochondrial fusion reactions via GTPase activity. Journal of cell science 2004;117:6535-46.
113. Malka F, Guillery O, Cifuentes-Diaz C, et al. Separate fusion of outer and inner mitochondrial membranes. EMBO reports 2005;6:853-9.
114. Frezza C, Cipolat S, Martins de Brito O, et al. OPA1 controls apoptotic cristae remodeling independently from mitochondrial fusion. Cell 2006;126:177-89.
115. Yamaguchi R, Lartigue L, Perkins G, et al. Opa1-mediated cristae opening is Bax/Bak and BH3 dependent, required for apoptosis, and independent of Bak oligomerization. Molecular cell 2008;31:557-69.
116. Smirnova E, Griparic L, Shurland DL, van der Bliek AM. Dynamin-related protein Drp1 is required for mitochondrial division in mammalian cells. Molecular biology of the cell 2001;12:2245-56.
117. Mears JA, Lackner LL, Fang S, Ingerman E, Nunnari J, Hinshaw JE. Conformational changes in Dnm1 support a contractile mechanism for mitochondrial fission. Nature structural & molecular biology 2011;18:20-6.
118. Elgass K, Pakay J, Ryan MT, Palmer CS. Recent advances into the understanding of mitochondrial fission. Biochimica et biophysica acta 2013;1833:150-61.
119. Kroemer G, Galluzzi L, Brenner C. Mitochondrial membrane permeabilization in cell death. Physiological reviews 2007;87:99-163.

120. Vaux DL. Apoptogenic factors released from mitochondria. Biochimica et biophysica acta 2011;1813:546-50.
121. Jiang X, Wang X. Cytochrome C-mediated apoptosis. Annual review of biochemistry 2004;73:87-106.
122. Suen DF, Norris KL, Youle RJ. Mitochondrial dynamics and apoptosis. Genes & development 2008;22:1577-90.
123. Jagasia R, Grote P, Westermann B, Conradt B. DRP-1-mediated mitochondrial fragmentation during EGL-1-induced cell death in C. elegans. Nature 2005;433:754-60.
124. Wasiak S, Zunino R, McBride HM. Bax/Bak promote sumoylation of DRP1 and its stable association with mitochondria during apoptotic cell death. The Journal of cell biology 2007;177:439-50.
125. Sugioka R, Shimizu S, Tsujimoto Y. Fzo1, a protein involved in mitochondrial fusion, inhibits apoptosis. The Journal of biological chemistry 2004;279:52726-34.
126. Scorrano L, Ashiya M, Buttle K, et al. A distinct pathway remodels mitochondrial cristae and mobilizes cytochrome c during apoptosis. Developmental cell 2002;2:55-67.
127. Olichon A, Baricault L, Gas N, et al. Loss of OPA1 perturbates the mitochondrial inner membrane structure and integrity, leading to cytochrome c release and apoptosis. The Journal of biological chemistry 2003;278:7743-6.
128. Cogliati S, Frezza C, Soriano ME, et al. Mitochondrial cristae shape determines respiratory chain supercomplexes assembly and respiratory efficiency. Cell 2013;155:160-71.
129. Narendra DP, Youle RJ. Targeting mitochondrial dysfunction: role for PINK1 and Parkin in mitochondrial quality control. Antioxidants & redox signaling 2011;14:1929-38.
130. Youle RJ, Narendra DP. Mechanisms of mitophagy. Nature reviews Molecular cell biology 2011;12:9-14.
131. Rambold AS, Kostelecky B, Elia N, Lippincott-Schwartz J. Tubular network formation protects mitochondria from autophagosomal degradation during nutrient starvation. Proceedings of the National Academy of Sciences of the United States of America 2011;108:10190-5.
132. Matsuda N, Sato S, Shiba K, et al. PINK1 stabilized by mitochondrial depolarization recruits Parkin to damaged mitochondria and activates latent Parkin for mitophagy. The Journal of cell biology 2010;189:211-21.

133. Narendra DP, Jin SM, Tanaka A, et al. PINK1 is selectively stabilized on impaired mitochondria to activate Parkin. PLoS biology 2010;8:e1000298.
134. Chan NC, Salazar AM, Pham AH, et al. Broad activation of the ubiquitin-proteasome system by Parkin is critical for mitophagy. Human molecular genetics 2011;20:1726-37.
135. Yoshii SR, Kishi C, Ishihara N, Mizushima N. Parkin mediates proteasome-dependent protein degradation and rupture of the outer mitochondrial membrane. The Journal of biological chemistry 2011;286:19630-40.
136. Ziviani E, Tao RN, Whitworth AJ. Drosophila parkin requires PINK1 for mitochondrial translocation and ubiquitinates mitofusin. Proceedings of the National Academy of Sciences of the United States of America 2010;107:5018-23.
137. Vincow ES, Merrihew G, Thomas RE, et al. The PINK1-Parkin pathway promotes both mitophagy and selective respiratory chain turnover in vivo. Proceedings of the National Academy of Sciences of the United States of America 2013;110:6400-5.
138. Hamalainen RH, Manninen T, Koivumaki H, Kislin M, Otonkoski T, Suomalainen A. Tissue- and cell-type-specific manifestations of heteroplasmic mtDNA 3243A>G mutation in human induced pluripotent stem cell-derived disease model. Proceedings of the National Academy of Sciences of the United States of America 2013;110:E3622-30.
139. Neupert W, Herrmann JM. Translocation of proteins into mitochondria. Annual review of biochemistry 2007;76:723-49.
140. Horvath SE, Daum G. Lipids of mitochondria. Progress in lipid research 2013;52:590-614.
141. Miller WL. Steroid hormone synthesis in mitochondria. Molecular and cellular endocrinology 2013;379:62-73.
142. Baughman JM, Perocchi F, Girgis HS, et al. Integrative genomics identifies MCU as an essential component of the mitochondrial calcium uniporter. Nature 2011;476:341-5.
143. De Stefani D, Raffaello A, Teardo E, Szabo I, Rizzuto R. A forty-kilodalton protein of the inner membrane is the mitochondrial calcium uniporter. Nature 2011;476:336-40.
144. Sibson NR, Dhankhar A, Mason GF, Rothman DL, Behar KL, Shulman RG. Stoichiometric coupling of brain glucose metabolism and glutamatergic neuronal activity. Proceedings of

the National Academy of Sciences of the United States of America 1998;95:316-21.
145. Waagepetersen HS, Sonnewald U, Gegelashvili G, Larsson OM, Schousboe A. Metabolic distinction between vesicular and cytosolic GABA in cultured GABAergic neurons using 13C magnetic resonance spectroscopy. Journal of neuroscience research 2001;63:347-55.
146. Ajioka RS, Phillips JD, Kushner JP. Biosynthesis of heme in mammals. Biochimica et biophysica acta 2006;1763:723-36.
147. Bernard DG, Gabilly ST, Dujardin G, Merchant S, Hamel PP. Overlapping specificities of the mitochondrial cytochrome c and c1 heme lyases. The Journal of biological chemistry 2003;278:49732-42.
148. Hederstedt L. Heme A biosynthesis. Biochimica et biophysica acta 2012;1817:920-7.
149. Antonicka H, Leary SC, Guercin GH, et al. Mutations in COX10 result in a defect in mitochondrial heme A biosynthesis and account for multiple, early-onset clinical phenotypes associated with isolated COX deficiency. Human molecular genetics 2003;12:2693-702.
150. Antonicka H, Mattman A, Carlson CG, et al. Mutations in COX15 produce a defect in the mitochondrial heme biosynthetic pathway, causing early-onset fatal hypertrophic cardiomyopathy. American journal of human genetics 2003;72:101-14.
151. Bugiani M, Tiranti V, Farina L, Uziel G, Zeviani M. Novel mutations in COX15 in a long surviving Leigh syndrome patient with cytochrome c oxidase deficiency. Journal of medical genetics 2005;42:e28.
152. Valnot I, von Kleist-Retzow JC, Barrientos A, et al. A mutation in the human heme A:farnesyltransferase gene (COX10) causes cytochrome c oxidase deficiency. Human molecular genetics 2000;9:1245-9.
153. Schaefer AM, Taylor RW, Turnbull DM, Chinnery PF. The epidemiology of mitochondrial disorders--past, present and future. Biochimica et biophysica acta 2004;1659:115-20.
154. Wallace DC, Fan W. Energetics, epigenetics, mitochondrial genetics. Mitochondrion 2010;10:12-31.
155. Wallace DC. A mitochondrial paradigm of metabolic and degenerative diseases, aging, and cancer: a dawn for

evolutionary medicine. Annual review of genetics 2005;39:359-407.
156. Mita S, Schmidt B, Schon EA, DiMauro S, Bonilla E. Detection of "deleted" mitochondrial genomes in cytochrome-c oxidase-deficient muscle fibers of a patient with Kearns-Sayre syndrome. Proceedings of the National Academy of Sciences of the United States of America 1989;86:9509-13.
157. Zeviani M, Di Donato S. Mitochondrial disorders. Brain : a journal of neurology 2004;127:2153-72.
158. Rahman S, Blok RB, Dahl HH, et al. Leigh syndrome: clinical features and biochemical and DNA abnormalities. Annals of neurology 1996;39:343-51.
159. Wallace DC, Singh G, Lott MT, et al. Mitochondrial DNA mutation associated with Leber's hereditary optic neuropathy. Science 1988;242:1427-30.
160. DiMauro S, Schon EA, Carelli V, Hirano M. The clinical maze of mitochondrial neurology. Nature reviews Neurology 2013;9:429-44.
161. Wallace DC, Chalkia D. Mitochondrial DNA genetics and the heteroplasmy conundrum in evolution and disease. Cold Spring Harbor perspectives in medicine 2013;3:a021220.
162. Van Goethem G, Martin JJ, Van Broeckhoven C. Progressive external ophthalmoplegia characterized by multiple deletions of mitochondrial DNA: unraveling the pathogenesis of human mitochondrial DNA instability and the initiation of a genetic classification. Neuromolecular medicine 2003;3:129-46.
163. Wallace DC. Mitochondrial defects in neurodegenerative disease. Mental retardation and developmental disabilities research reviews 2001;7:158-66.
164. Schon EA, Rizzuto R, Moraes CT, Nakase H, Zeviani M, DiMauro S. A direct repeat is a hotspot for large-scale deletion of human mitochondrial DNA. Science 1989;244:346-9.
165. Zeviani M, Carelli V. Mitochondrial disorders. Current opinion in neurology 2003;16:585-94.
166. Kaufmann P, Engelstad K, Wei Y, et al. Natural history of MELAS associated with mitochondrial DNA m.3243A>G genotype. Neurology 2011;77:1965-71.
167. Wallace DC, Zheng XX, Lott MT, et al. Familial mitochondrial encephalomyopathy (MERRF): genetic, pathophysiological, and biochemical characterization of a mitochondrial DNA disease. Cell 1988;55:601-10.

168. Man PY, Turnbull DM, Chinnery PF. Leber hereditary optic neuropathy. Journal of medical genetics 2002;39:162-9.
169. Schuelke M, Krude H, Finckh B, et al. Septo-optic dysplasia associated with a new mitochondrial cytochrome b mutation. Annals of neurology 2002;51:388-92.
170. Valnot I, Kassis J, Chretien D, et al. A mitochondrial cytochrome b mutation but no mutations of nuclearly encoded subunits in ubiquinol cytochrome c reductase (complex III) deficiency. Human genetics 1999;104:460-6.
171. Barrientos A, Barros MH, Valnot I, Rotig A, Rustin P, Tzagoloff A. Cytochrome oxidase in health and disease. Gene 2002;286:53-63.
172. Holt IJ, Harding AE, Petty RK, Morgan-Hughes JA. A new mitochondrial disease associated with mitochondrial DNA heteroplasmy. American journal of human genetics 1990;46:428-33.
173. Calvo SE, Mootha VK. The mitochondrial proteome and human disease. Annual review of genomics and human genetics 2010;11:25-44.
174. Fassone E, Rahman S. Complex I deficiency: clinical features, biochemistry and molecular genetics. Journal of medical genetics 2012;49:578-90.
175. Briere JJ, Favier J, El Ghouzzi V, et al. Succinate dehydrogenase deficiency in human. Cellular and molecular life sciences : CMLS 2005;62:2317-24.
176. Pagnamenta AT, Hargreaves IP, Duncan AJ, et al. Phenotypic variability of mitochondrial disease caused by a nuclear mutation in complex II. Molecular genetics and metabolism 2006;89:214-21.
177. Haut S, Brivet M, Touati G, et al. A deletion in the human QP-C gene causes a complex III deficiency resulting in hypoglycaemia and lactic acidosis. Human genetics 2003;113:118-22.
178. Barel O, Shorer Z, Flusser H, et al. Mitochondrial complex III deficiency associated with a homozygous mutation in UQCRQ. American journal of human genetics 2008;82:1211-6.
179. Miyake N, Yano S, Sakai C, et al. Mitochondrial complex III deficiency caused by a homozygous UQCRC2 mutation presenting with neonatal-onset recurrent metabolic decompensation. Human mutation 2013;34:446-52.

180. Gaignard P, Menezes M, Schiff M, et al. Mutations in CYC1, encoding cytochrome c1 subunit of respiratory chain complex III, cause insulin-responsive hyperglycemia. American journal of human genetics 2013;93:384-9.
181. Massa V, Fernandez-Vizarra E, Alshahwan S, et al. Severe infantile encephalomyopathy caused by a mutation in COX6B1, a nucleus-encoded subunit of cytochrome c oxidase. American journal of human genetics 2008;82:1281-9.
182. Shteyer E, Saada A, Shaag A, et al. Exocrine pancreatic insufficiency, dyserythropoeitic anemia, and calvarial hyperostosis are caused by a mutation in the COX4I2 gene. American journal of human genetics 2009;84:412-7.
183. Indrieri A, van Rahden VA, Tiranti V, et al. Mutations in COX7B cause microphthalmia with linear skin lesions, an unconventional mitochondrial disease. American journal of human genetics 2012;91:942-9.
184. Mayr JA, Havlickova V, Zimmermann F, et al. Mitochondrial ATP synthase deficiency due to a mutation in the ATP5E gene for the F1 epsilon subunit. Human molecular genetics 2010;19:3430-9.
185. Jonckheere AI, Renkema GH, Bras M, et al. A complex V ATP5A1 defect causes fatal neonatal mitochondrial encephalopathy. Brain : a journal of neurology 2013;136:1544-54.
186. Longley MJ, Clark S, Yu Wai Man C, et al. Mutant POLG2 disrupts DNA polymerase gamma subunits and causes progressive external ophthalmoplegia. American journal of human genetics 2006;78:1026-34.
187. Milone M, Massie R. Polymerase gamma 1 mutations: clinical correlations. The neurologist 2010;16:84-91.
188. Van Goethem G, Dermaut B, Lofgren A, Martin JJ, Van Broeckhoven C. Mutation of POLG is associated with progressive external ophthalmoplegia characterized by mtDNA deletions. Nature genetics 2001;28:211-2.
189. Nikali K, Suomalainen A, Saharinen J, et al. Infantile onset spinocerebellar ataxia is caused by recessive mutations in mitochondrial proteins Twinkle and Twinky. Human molecular genetics 2005;14:2981-90.
190. Mandel H, Hartman C, Berkowitz D, Elpeleg ON, Manov I, Iancu TC. The hepatic mitochondrial DNA depletion

syndrome: ultrastructural changes in liver biopsies. Hepatology 2001;34:776-84.
191. Saada A, Shaag A, Mandel H, Nevo Y, Eriksson S, Elpeleg O. Mutant mitochondrial thymidine kinase in mitochondrial DNA depletion myopathy. Nature genetics 2001;29:342-4.
192. Spinazzola A, Viscomi C, Fernandez-Vizarra E, et al. MPV17 encodes an inner mitochondrial membrane protein and is mutated in infantile hepatic mitochondrial DNA depletion. Nature genetics 2006;38:570-5.
193. Zanna C, Ghelli A, Porcelli AM, et al. OPA1 mutations associated with dominant optic atrophy impair oxidative phosphorylation and mitochondrial fusion. Brain : a journal of neurology 2008;131:352-67.
194. Debray FG, Morin C, Janvier A, et al. LRPPRC mutations cause a phenotypically distinct form of Leigh syndrome with cytochrome c oxidase deficiency. Journal of medical genetics 2011;48:183-9.
195. Mootha VK, Lepage P, Miller K, et al. Identification of a gene causing human cytochrome c oxidase deficiency by integrative genomics. Proceedings of the National Academy of Sciences of the United States of America 2003;100:605-10.
196. Baughman JM, Nilsson R, Gohil VM, Arlow DH, Gauhar Z, Mootha VK. A computational screen for regulators of oxidative phosphorylation implicates SLIRP in mitochondrial RNA homeostasis. PLoS genetics 2009;5:e1000590.
197. Gohil VM, Hayes P, Matsuyama S, Schagger H, Schlame M, Greenberg ML. Cardiolipin biosynthesis and mitochondrial respiratory chain function are interdependent. The Journal of biological chemistry 2004;279:42612-8.
198. Jiang F, Ryan MT, Schlame M, et al. Absence of cardiolipin in the crd1 null mutant results in decreased mitochondrial membrane potential and reduced mitochondrial function. The Journal of biological chemistry 2000;275:22387-94.
199. Barth PG, Wanders RJ, Vreken P. X-linked cardioskeletal myopathy and neutropenia (Barth syndrome)-MIM 302060. The Journal of pediatrics 1999;135:273-6.
200. Rotig A, Mollet J, Rio M, Munnich A. Infantile and pediatric quinone deficiency diseases. Mitochondrion 2007;7 Suppl:S112-21.

201. Quinzii CM, Hirano M, DiMauro S. CoQ10 deficiency diseases in adults. Mitochondrion 2007;7 Suppl:S122-6.
202. Okamoto K, Brinker A, Paschen SA, et al. The protein import motor of mitochondria: a targeted molecular ratchet driving unfolding and translocation. The EMBO journal 2002;21:3659-71.
203. Fenton WA. Mitochondrial protein transport--a system in search of mutations. American journal of human genetics 1995;57:235-8.
204. Roesch K, Curran SP, Tranebjaerg L, Koehler CM. Human deafness dystonia syndrome is caused by a defect in assembly of the DDP1/TIMM8a-TIMM13 complex. Human molecular genetics 2002;11:477-86.
205. Hansen JJ, Bross P, Westergaard M, et al. Genomic structure of the human mitochondrial chaperonin genes: HSP60 and HSP10 are localised head to head on chromosome 2 separated by a bidirectional promoter. Human genetics 2003;112:71-7.
206. Delettre C, Lenaers G, Pelloquin L, Belenguer P, Hamel CP. OPA1 (Kjer type) dominant optic atrophy: a novel mitochondrial disease. Molecular genetics and metabolism 2002;75:97-107.
207. Zuchner S, Vance JM. Emerging pathways for hereditary axonopathies. Journal of molecular medicine 2005;83:935-43.
208. Niemann A, Ruegg M, La Padula V, Schenone A, Suter U. Ganglioside-induced differentiation associated protein 1 is a regulator of the mitochondrial network: new implications for Charcot-Marie-Tooth disease. The Journal of cell biology 2005;170:1067-78.
209. Zuchner S, Mersiyanova IV, Muglia M, et al. Mutations in the mitochondrial GTPase mitofusin 2 cause Charcot-Marie-Tooth neuropathy type 2A. Nature genetics 2004;36:449-51.
210. Bai Y, Attardi G. The mtDNA-encoded ND6 subunit of mitochondrial NADH dehydrogenase is essential for the assembly of the membrane arm and the respiratory function of the enzyme. The EMBO journal 1998;17:4848-58.
211. Hofhaus G, Attardi G. Lack of assembly of mitochondrial DNA-encoded subunits of respiratory NADH dehydrogenase and loss of enzyme activity in a human cell mutant lacking the mitochondrial ND4 gene product. The EMBO journal 1993;12:3043-8.

212. Malfatti E, Bugiani M, Invernizzi F, et al. Novel mutations of ND genes in complex I deficiency associated with mitochondrial encephalopathy. Brain : a journal of neurology 2007;130:1894-904.
213. Ghezzi D, Goffrini P, Uziel G, et al. SDHAF1, encoding a LYR complex-II specific assembly factor, is mutated in SDH-defective infantile leukoencephalopathy. Nature genetics 2009;41:654-6.
214. De Meirleir L, Seneca S, Damis E, et al. Clinical and diagnostic characteristics of complex III deficiency due to mutations in the BCS1L gene. American journal of medical genetics Part A 2003;121A:126-31.
215. Ghezzi D, Arzuffi P, Zordan M, et al. Mutations in TTC19 cause mitochondrial complex III deficiency and neurological impairment in humans and flies. Nature genetics 2011;43:259-63.
216. Sanchez E, Lobo T, Fox JL, Zeviani M, Winge DR, Fernandez-Vizarra E. LYRM7/MZM1L is a UQCRFS1 chaperone involved in the last steps of mitochondrial Complex III assembly in human cells. Biochimica et biophysica acta 2013;1827:285-93.
217. Invernizzi F, Tigano M, Dallabona C, et al. A homozygous mutation in LYRM7/MZM1L associated with early onset encephalopathy, lactic acidosis, and severe reduction of mitochondrial complex III activity. Human mutation 2013;34:1619-22.
218. DiMauro S, Tanji K, Schon EA. The many clinical faces of cytochrome c oxidase deficiency. Advances in experimental medicine and biology 2012;748:341-57.
219. Diaz F. Cytochrome c oxidase deficiency: patients and animal models. Biochimica et biophysica acta 2010;1802:100-10.
220. Tiranti V, Hoertnagel K, Carrozzo R, et al. Mutations of SURF-1 in Leigh disease associated with cytochrome c oxidase deficiency. American journal of human genetics 1998;63:1609-21.
221. Leary SC, Cobine PA, Kaufman BA, et al. The human cytochrome c oxidase assembly factors SCO1 and SCO2 have regulatory roles in the maintenance of cellular copper homeostasis. Cell metabolism 2007;5:9-20.

222. Shoubridge EA. Cytochrome c oxidase deficiency. American journal of medical genetics 2001;106:46-52.
223. Papadopoulou LC, Sue CM, Davidson MM, et al. Fatal infantile cardioencephalomyopathy with COX deficiency and mutations in SCO2, a COX assembly gene. Nature genetics 1999;23:333-7.
224. Valnot I, Osmond S, Gigarel N, et al. Mutations of the SCO1 gene in mitochondrial cytochrome c oxidase deficiency with neonatal-onset hepatic failure and encephalopathy. American journal of human genetics 2000;67:1104-9.
225. Coenen MJ, van den Heuvel LP, Ugalde C, et al. Cytochrome c oxidase biogenesis in a patient with a mutation in COX10 gene. Annals of neurology 2004;56:560-4.
226. Oquendo CE, Antonicka H, Shoubridge EA, Reardon W, Brown GK. Functional and genetic studies demonstrate that mutation in the COX15 gene can cause Leigh syndrome. Journal of medical genetics 2004;41:540-4.
227. De Meirleir L, Seneca S, Lissens W, et al. Respiratory chain complex V deficiency due to a mutation in the assembly gene ATP12. Journal of medical genetics 2004;41:120-4.
228. Cizkova A, Stranecky V, Mayr JA, et al. TMEM70 mutations cause isolated ATP synthase deficiency and neonatal mitochondrial encephalocardiomyopathy. Nature genetics 2008;40:1288-90.
229. Wenz T, Diaz F, Spiegelman BM, Moraes CT. Activation of the PPAR/PGC-1alpha pathway prevents a bioenergetic deficit and effectively improves a mitochondrial myopathy phenotype. Cell metabolism 2008;8:249-56.
230. Cerutti R, Pirinen E, Lamperti C, et al. NAD-Dependent Activation of Sirt1 Corrects the Phenotype in a Mouse Model of Mitochondrial Disease. Cell metabolism 2014.
231. Johnson SC, Yanos ME, Kayser EB, et al. mTOR inhibition alleviates mitochondrial disease in a mouse model of Leigh syndrome. Science 2013;342:1524-8.
232. Santra S, Gilkerson RW, Davidson M, Schon EA. Ketogenic treatment reduces deleted mitochondrial DNAs in cultured human cells. Annals of neurology 2004;56:662-9.
233. Ahola-Erkkila S, Carroll CJ, Peltola-Mjosund K, et al. Ketogenic diet slows down mitochondrial myopathy progression in mice. Human molecular genetics 2010;19:1974-84.

234. Gilkerson RW, Schon EA, Hernandez E, Davidson MM. Mitochondrial nucleoids maintain genetic autonomy but allow for functional complementation. The Journal of cell biology 2008;181:1117-28.
235. Bough KJ, Wetherington J, Hassel B, et al. Mitochondrial biogenesis in the anticonvulsant mechanism of the ketogenic diet. Annals of neurology 2006;60:223-35.
236. Wenz T, Luca C, Torraco A, Moraes CT. mTERF2 regulates oxidative phosphorylation by modulating mtDNA transcription. Cell metabolism 2009;9:499-511.
237. Tanaka M, Borgeld HJ, Zhang J, et al. Gene therapy for mitochondrial disease by delivering restriction endonuclease SmaI into mitochondria. Journal of biomedical science 2002;9:534-41.
238. Gammage PA, Rorbach J, Vincent AI, Rebar EJ, Minczuk M. Mitochondrially targeted ZFNs for selective degradation of pathogenic mitochondrial genomes bearing large-scale deletions or point mutations. EMBO molecular medicine 2014;6:458-66.
239. Minczuk M, Papworth MA, Kolasinska P, Murphy MP, Klug A. Sequence-specific modification of mitochondrial DNA using a chimeric zinc finger methylase. Proceedings of the National Academy of Sciences of the United States of America 2006;103:19689-94.
240. Bacman SR, Williams SL, Pinto M, Peralta S, Moraes CT. Specific elimination of mutant mitochondrial genomes in patient-derived cells by mitoTALENs. Nature medicine 2013;19:1111-3.
241. Tiranti V, Viscomi C, Hildebrandt T, et al. Loss of ETHE1, a mitochondrial dioxygenase, causes fatal sulfide toxicity in ethylmalonic encephalopathy. Nature medicine 2009;15:200-5.
242. Viscomi C, Burlina AB, Dweikat I, et al. Combined treatment with oral metronidazole and N-acetylcysteine is effective in ethylmalonic encephalopathy. Nature medicine 2010;16:869-71.
243. Bratic A, Larsson NG. The role of mitochondria in aging. The Journal of clinical investigation 2013;123:951-7.
244. Kanabus M, Heales SJ, Rahman S. Development of pharmacological strategies for mitochondrial disorders. British journal of pharmacology 2014;171:1798-817.

245. Hakkaart GA, Dassa EP, Jacobs HT, Rustin P. Allotopic expression of a mitochondrial alternative oxidase confers cyanide resistance to human cell respiration. EMBO reports 2006;7:341-5.
246. El-Khoury R, Dufour E, Rak M, et al. Alternative oxidase expression in the mouse enables bypassing cytochrome c oxidase blockade and limits mitochondrial ROS overproduction. PLoS genetics 2013;9:e1003182.
247. Dassa EP, Dufour E, Goncalves S, et al. Expression of the alternative oxidase complements cytochrome c oxidase deficiency in human cells. EMBO molecular medicine 2009;1:30-6.
248. Perales-Clemente E, Bayona-Bafaluy MP, Perez-Martos A, Barrientos A, Fernandez-Silva P, Enriquez JA. Restoration of electron transport without proton pumping in mammalian mitochondria. Proceedings of the National Academy of Sciences of the United States of America 2008;105:18735-9.
249. Fernandez-Ayala DJ, Sanz A, Vartiainen S, et al. Expression of the Ciona intestinalis alternative oxidase (AOX) in Drosophila complements defects in mitochondrial oxidative phosphorylation. Cell metabolism 2009;9:449-60.
250. Kemppainen KK, Rinne J, Sriram A, et al. Expression of alternative oxidase in Drosophila ameliorates diverse phenotypes due to cytochrome oxidase deficiency. Human molecular genetics 2014;23:2078-93.
251. Sanz A, Soikkeli M, Portero-Otin M, et al. Expression of the yeast NADH dehydrogenase Ndi1 in Drosophila confers increased lifespan independently of dietary restriction. Proceedings of the National Academy of Sciences of the United States of America 2010;107:9105-10.
252. Rustin P, Jacobs HT. Respiratory chain alternative enzymes as tools to better understand and counteract respiratory chain deficiencies in human cells and animals. Physiol Plant 2009;137:362-70.
253. Mingozzi F, High KA. Therapeutic in vivo gene transfer for genetic disease using AAV: progress and challenges. Nature reviews Genetics 2011;12:341-55.
254. Gao GP, Alvira MR, Wang L, Calcedo R, Johnston J, Wilson JM. Novel adeno-associated viruses from rhesus monkeys as vectors for human gene therapy. Proceedings of

the National Academy of Sciences of the United States of America 2002;99:11854-9.
255. Chen H, Vermulst M, Wang YE, et al. Mitochondrial fusion is required for mtDNA stability in skeletal muscle and tolerance of mtDNA mutations. Cell 2010;141:280-9.
256. Reddy PH. Inhibitors of mitochondrial fission as a therapeutic strategy for diseases with oxidative stress and mitochondrial dysfunction. Journal of Alzheimer's disease : JAD 2014;40:245-56.
257. Wang D, Wang J, Bonamy GM, et al. A small molecule promotes mitochondrial fusion in mammalian cells. Angewandte Chemie 2012;51:9302-5.
258. Antonicka H, Ogilvie I, Taivassalo T, et al. Identification and characterization of a common set of complex I assembly intermediates in mitochondria from patients with complex I deficiency. The Journal of biological chemistry 2003;278:43081-8.
259. Benit P, Beugnot R, Chretien D, et al. Mutant NDUFV2 subunit of mitochondrial complex I causes early onset hypertrophic cardiomyopathy and encephalopathy. Human mutation 2003;21:582-6.
260. Kruse SE, Watt WC, Marcinek DJ, Kapur RP, Schenkman KA, Palmiter RD. Mice with mitochondrial complex I deficiency develop a fatal encephalomyopathy. Cell metabolism 2008;7:312-20.
261. Quintana A, Kruse SE, Kapur RP, Sanz E, Palmiter RD. Complex I deficiency due to loss of Ndufs4 in the brain results in progressive encephalopathy resembling Leigh syndrome. Proceedings of the National Academy of Sciences of the United States of America 2010;107:10996-1001.
262. Vesela K, Hulkova H, Hansikova H, Zeman J, Elleder M. Structural analysis of tissues affected by cytochrome C oxidase deficiency due to mutations in the SCO2 gene. APMIS : acta pathologica, microbiologica, et immunologica Scandinavica 2008;116:41-9.
263. Yang H, Brosel S, Acin-Perez R, et al. Analysis of mouse models of cytochrome c oxidase deficiency owing to mutations in Sco2. Human molecular genetics 2010;19:170-80.
264. Zordan MA, Cisotto P, Benna C, et al. Post-transcriptional silencing and functional characterization of the

Drosophila melanogaster homolog of human Surf1. Genetics 2006;172:229-41.
265. Clozel M, Hess P, Fischli W, et al. Age-dependent hypertension in Mpv17-deficient mice, a transgenic model of glomerulosclerosis and inner ear disease. Experimental gerontology 1999;34:1007-15.

Chapter 2

Opa1 overexpression ameliorates the clinical phenotype of two mitochondrial disease mouse models.

Gabriele Civiletto[1,2,5], Tatiana Varanita[3,5], Tatiana Gorletta[1], Serena Barbaro[1], Silvia Marchet[1], Costanza Lamperti[1], Carlo Viscomi[1,2], Luca Scorrano[3,4,5*], Massimo Zeviani[1,2,5*]

[1] Fondazione IRCCS Istituto Neurologico "C. Besta", Milan, Italy
[2] MRC-Mitochondrial Biology Unit, Cambridge, UK
[3] Dulbecco Telethon Institute, Venetian Institute of Molecular Medicine, Padova, Italy
[4] Dept. of Biology, University of Padova, Padova, Italy
[5] These authors equally contributed to the work

Submitted Cell Metabolism

Abstract

Increased levels of the mitochondria-shaping protein Opa1 increase respiratory chain efficiency and protect from tissue damage, suggesting that it could be an attractive target to counteract mitochondrial dysfunction. Here we show that *Opa1* overexpression ameliorates two mouse models of defective mitochondrial bioenergetics. The offspring from crosses of a constitutive knockout for the structural complex I component *Ndufs4* (*Ndufs4*$^{-/-}$), as well as of a muscle-specific conditional knockout for the complex IV assembly factor *Cox15* (*Cox15*$^{sm/sm}$) with *Opa1* transgenic (*Opa1*^{tg}) mice were clinically and biochemically improved. Whilst the amelioration was significant but limited in *Ndufs4*$^{-/-}$*::Opa1*^{tg} mice, mitochondrial ultrastructure and respiration correction, motor performance improvement and survival prolongation were remarkable in *Cox15*$^{sm/sm}$*::Opa1*^{tg} mice. Mechanistically, respiratory chain supercomplexes containing active complex IV were increased in *Cox15*$^{sm/sm}$*::Opa1*^{tg} mice, resulting in residual monomeric complex IV stabilization. In conclusion, amelioration of cristae shape by controlled *Opa1* overexpression improves two mouse models of mitochondrial disease.

Introduction

Mutations in mitochondrial DNA (mtDNA), and in the vast repertoire of nuclear genes that converge on the formation and function of the mitochondrial respiratory chain (MRC), are responsible for primary “mitochondrial disorders”, a group of

highly heterogeneous conditions, hallmarked by faulty oxidative phosphorylation (OXPHOS), that can affect any organ, at any age and by any mode of transmission [266]. When taken as a whole, mitochondrial disorders are among the most frequent genetic diseases, affecting >1 in 5,000 individuals in the European population [267]. Despite substantial progress in mitochondrial medicine, the complexity of mitochondrial biology and genetics still constitutes a major challenge for understanding the mechanistic basis of mitochondrial disorders, and explains, at least in part, their huge clinical and biochemical variability, which is also a major hurdle toward effective treatment. However, the development of “general” therapeutic strategies, extendable to diverse disease-associated OXPHOS defects, is now a realistic goal, based on rapidly expanding knowledge of the molecular mechanisms underpinning mitochondrial biogenesis, quality control and signalling pathways. Several of these mechanisms are related to the control of mitochondrial shape and organization of the mitochondrial network.

Mitochondria are highly dynamic organelles that fuse and divide to adapt their structure and morphology to the energetic needs of the cell [268]. Dynamin-related GTPases located on the inner and outer mitochondrial membranes (IMM and OMM) control the fission and fusion processes [269]. Mitochondrial fission and fusion regulate a number of cellular processes, including organelle distribution during cell proliferation, bioenergetics proficiency, mitochondrial calcium flux, mitochondrial apoptosis,

autophagy, and even complex morphogenetic processes such as the formation of dendritic spines [268]. Fission is regulated by the OMM protein Dynamin-related protein 1 (Drp1) and by its partners Fission 1 (Fis1), Mitochondrial Fission Factor (MFF) and Mitochondrial Division (Mid) 49 and 51; fusion is controlled by the OMM proteins Mitofusins 1 and 2 (Mfn1 and 2) and by the IMM protein Optic atrophy 1 (Opa1). In humans, eight Opa1 isoforms are produced by alternative splicing of a single gene [91] that are further processed by at least three proteases to form several long (L) and short (S) Opa1 protein species [92,94,95,98,101,102] which oligomerize to form functionally active oligomers [114]. In addition to its role in mitochondrial fusion, Opa1 controls the cristae remodelling arm of mitochondrial apoptosis [114] and the physical and functional organization of the MRC complexes in MRC supercomplexes [128]. These functional quaternary structures increase electron flow channelling through MRCs during respiration, thus minimizing electron leaks [270,271], and stabilize individual MRCs such as complex III [272]. Consequently, Opa1 levels directly affect mitochondrial respiratory efficiency [128] and proteolytic inactivation of Opa1 has been shown to occur in cells from mitochondrial disease patients [100]. However, the role of Opa1 in vivo and the potential of its stabilization as a strategy to combat mitochondrial dysfunction and disease is unclear. Genetic ablation of Opa1 is lethal during embryonic development [273] and causes massive dysfunction also in postmitotic tissues (Tezze et al., submitted). On the other hand, high levels of Opa1 overexpression are toxic

in cells, leading to mitochondrial hyperfragmentation [274]. In order to avoid these paradoxical effects, we have used X-chromosome targeted Opa1 transgenesis (Opa1tg) to obtain moderate, ubiquitous overexpression in a mouse line [128]. Remarkably, Opa1tg mice are fertile, viable, live normally and are protected from a panoply of tissue insults, including denervation-induced skeletal muscle atrophy, brain and heart ischemia-reperfusion, and liver failure caused by Fas-ligand induced apoptosis (Varanita et al, 2014 manuscript in preparation). We therefore reasoned that Opa1 overexpression could be exploited to correct the biochemical impairment and mitigate the clinical derangement associated with genetically determined OXPHOS failure in available mouse models of mitochondrial disease. To this aim, we crossed the Opa1tg mouse with (1) a constitutive knockout mouse for Ndufs4, (Ndufs4-/-) [260,261,275,276], encoding the 18 kDa subunit of complex I (cI) and (2) a skeletal muscle-specific knockout mouse for Cox15, in which the Cre recombinase-driven ablation of Cox15 is dependent upon the muscle-specific actin gene promoter (Cox15sm/sm) [277]. Cox15 encodes a key enzyme in the biosynthesis of heme a, an essential catalytic redox component of complex IV (cIV, cytochrome c oxidase, COX) [278-283]. In humans, mutations in NDUFS4 are associated with early-onset, fatal Leigh syndrome due to severe cI deficiency [284-286]. Mutations in COX15 have been reported in children with severe, isolated cardiomyopathy, encephalopathy or cardioencephalomyopathy [150,151,287]. Here we report that the

mild Opa1 overexpression achieved in the Opa1tg mice corrects these two models of cI and cIV deficiency, the latter to a greater extent.

Materials and Methods

Reagents and materials

Antibodies (Cox1, Cox4, Uqcrc2, Ndufa9, Atp5a, SdhA) were from Mitoscience, Gapdh were from Millipore, P62 was from Sigma, LC3-I/II was from Cell Signaling, Lamp1 was from Sigma, Opa1 was from BD Biosciences.

Animal work

All procedures were conducted under the UK Animals (Scientific Procedures) Act, 1986, approved by Home Office license (PPL: 7538) and local ethical review. The mice were kept on a C57Bl6/129Sv mixed background, and wild-type littermates were used as controls. The animals were maintained in a temperature- and humidity-controlled animal-care facility, with a 12 hr light/dark cycle and free access to water and food, and were sacrificed by cervical dislocation.

Behavioural analysis

A treadmill apparatus (Columbus Instruments, Columbus, OH) was used to measure motor exercise endurance according to the number of falls in the motivational grid during a gradually accelerating program with speed initially at 6.5 m/min and increasing by 0.5 m/min every 3 min. The test was terminated

by exhaustion, defined as >10 falls/min into the motivational grid.

A rotarod apparatus (Ugo Basile, Italy) was used to assess coordination skills. After two acclimation sessions the mice underwent three trial sessions at least 20 minutes apart, using a standard acceleration protocol pre-set by the constructor.

Oxygen consumption studies

Mouse brains were homogenized in 0.075 M sucrose, 0.225 M mannitol, 1 mM EGTA, 0.01% fatty acids free BSA pH 7.4; skeletal muscle were homogenized in 150 mM sucrose, 50 mM Tris-HCl, 50 mM KCl, 10 mM EDTA, 0.2% BSA, pH 7.4, subtilisin 1mg/gram of muscle (frezza 2007). Mitochondria isolated by differential centrifugation and resuspended 25mM sucrose, 75 mM sorbitol, 100mM KCl, 0.05 mM EDTA, 5 mM $MgCl_2$, 10 mM Tris-HCl pH7.4, 10 mM H_3PO_4, pH 7.4 [288]

For oxygraphic measurements, 250-500 µg of mitochondrial proteins were incubated in a buffer containing 225 mM sucrose, 75 mM mannitol, 10 mM Tris-HCl pH 7.4, 10 mM KCl, 10 mM KH_2PO_4, 5 mM $MgCl_2$, 1 mg/ml fatty acids free BSA, pH 7.4. Oxygen consumption was evaluated by a Clark oxygen electrode (Hansatech, Instruments, Norfolk, UK), using the following substrates and inhibitors concentrations: 5 mM glutamate and 2.5 mM malate for cI-dependent respiration, 5 mM succinate and 2 µM rotenone for cII-dependent respiration, 6 mM ascorbate and 300 µM TMPD and antimycin A 0.25 µg/ml for cIV-dependent respiration. 100 µM ADP was added to

stimulate ATP-coupled oxygen consumption. 100μM NaCN was added to completely inhibit respiration [289].

Blue Native Gel Electrophoresis (BNGE)

For BNGE analysis, 250 μg of mitochondria isolated as described above were resuspended in native page buffer (Invitrogen), protease inhibitors and 4% digitonin and incubated for 1h on ice before centrifuging at 20000g at 4°. 5% Coomassie G250 was added to the supernatant. 30μg were separated by 3%–12% gradient BNGE and either stained with for in gel activities, or electroblotted on PVDF membranes for immunodetection [290].

Morphological Analysis

For histochemical analysis, tissues were frozen in liquid-nitrogen pre-cooled isopentane. 8 μm thick sections were stained for COX and SDH, as described [291]. For ultrastructural studies, samples were fixed with 2.5% glutaraldehyde in 10 mM phosphate buffer (pH 7.4).

Biochemical Analysis of MRC Complexes

Brain and skeletal muscle samples were snap-frozen in liquid nitrogen and homogenized in 10 mM phosphate buffer (pH 7.4). The spectrophotometric activity of cI, cII, cIII, and cIV, as well as citrate synthase (CS), was measured as described [292].

Real-Time PCR

MtDNA content and transcripts analysis was carried out by SYBR Green real-time PCR, as described (Viscomi et al., 2011).

Western-Blot Analysis

Mouse tissues were homogenized in ten volumes of 10 mM potassium phosphate buffer (pH 7.4). Mitochondrial-enriched fractions were collected after centrifugation at 800 g for 10 min in the presence of protease inhibitors, and frozen and thawed three times in liquid nitrogen. Protein concentration was determined by the Lowry method. Aliquots, 70 µg each, were run through a 4-12% SDS-PAGE and electroblotted onto a nitrocellulose membrane, which was then immunodecorated with different antibodies.

Results

Generation of Ndufs4$^{-/-}$::Opa1^{tg} and Cox15$^{sm/sm}$::Opa1^{tg} mouse lines

To obtain transgenic overexpression of *Opa1* in OXPHOS defective mouse lines, we crossed the *Opa1^{tg}* mouse with *Ndufs4$^{-/-}$* and with *Cox15$^{sm/sm}$* mice, two mouse models of primary mitochondrial disorders. The constitutive *Ndufs4$^{-/-}$* mouse shows severe cI deficiency with the accumulation of a catalytically inactive 830 kDa cI assembly intermediate, associated with the onset of a rapidly progressive, invariably fatal syndrome, dominated by neurological impairment starting

at approximately 40 days after birth [260,293]. The *Cox15*$^{sm/sm}$ mouse shows profound skeletal muscle COX deficiency, leading to muscle wasting, severe motor performance impairment, and markedly reduced survival [277].

Ndufs4$^{-/-}$::Opa1^{tg} mice live longer and show better motor coordination than Ndufs4$^{-/-}$ mice.

The *Ndufs4*$^{-/-}$*::Opa1*^{tg} double mutant individuals showed a significant, albeit modest, increase in both motor coordination and lifespan, compared to *Ndufs4*$^{-/-}$. Motor coordination, measured by weekly-performed rotarod test, showed steady downhill in both *Ndufs4*$^{-/-}$*::Opa1*^{tg} and *Ndufs4*$^{-/-}$ groups, each composed of six individuals. However, the scores that were identical in the two groups at the beginning of the observation (week 4th after birth) showed significant differences in the subsequent measurements, with the *Ndufs4*$^{-/-}$*::Opa1*^{tg} group performing consistently better than the *Ndufs4*$^{-/-}$ group in weeks 5th and 6th. At week 7th both groups were virtually unable to perform the test at any rate, due to collapse of neurological conditions or death (Figure 1A). Kaplan-Meier analysis showed that survival probability was moderately, but significantly, prolonged in *Ndufs4*$^{-/-}$*::Opa1*^{tg} vs. *Ndufs4*$^{-/-}$ littermates (log rank test p=0.015) (Figure 1B). The survival median was 53.5 days and 62.0 days for *Ndufs4*$^{-/-}$ and *Ndufs4*$^{-/-}$*::Opa1*^{tg}, respectively. This clinical phenotype was associated with moderately but significantly increased glutamate-malate dependent state-3 oxygen consumption rate of isolated brain mitochondria

(reflecting cI-driven respiration), which nevertheless remained well below the values obtained in brain mitochondria of WT and *Opa1*^{tg} littermates (Figure 1C). No change was detected in cI activity of isolated brain mitochondria between *Ndufs4*$^{-/-}$*::Opa1*^{tg} vs. *Ndufs4*$^{-/-}$ littermates, measured by spectrophotometric assay, whereas the activity of complex II was slightly but significantly ($P<0.05$) increased (Figure 1D). BNGE-based in-gel activity of cI and cI-containing supercomplexes showed hardly any reactive band in both *Ndufs4*$^{-/-}$*::Opa1*^{tg} double mutants and *Ndufs4*$^{-/-}$ littermates (Figure 1E), Accordingly, Western-blot analysis showed in both samples the catalytically inactive 830 kDa cI assembly intermediate and a 830 kDa+cIII$_2$ supercomplex, but neither cI holocomplex nor cI supercomplexes (Figure S1).

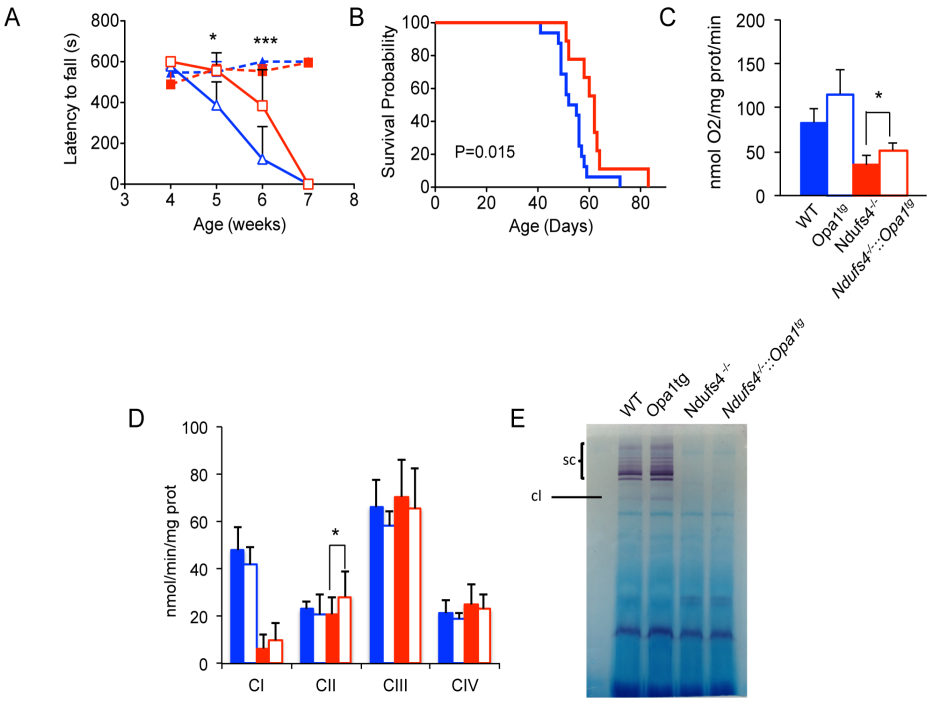

Figure 1. ***Slight motor function and lifespan amelioration in Ndufs4$^{-/-}$::Opa1^{tg} double mutants***

A) Rotarod analysis (n=6/group). Dashed blue: *WT*; dashed red: *Opa1^{tg}*; solid blue: *Ndufs4$^{-/-}$*; solid red: *Ndufs4$^{-/-}$::Opa1^{tg}*. Error bars represent SD. The asterisks represent the significance levels calculate by unpaired, 2-tail Student's t test *p<0.05, ***p<0.005, and refer to the comparison between *Ndufs4$^{-/-}$::Opa1^{tg}* and *Ndufs4$^{-/-}$*.

B) Kaplan–Meier survival probability. Significance was assessed by log-rank test. Solid blue: *Ndufs4$^{-/-}$* (n=16); solid red: *Ndufs4$^{-/-}$/Opa1^{tg}* (n=9).

C) Oxygen consumption measurements (nmoles O_2/min/mg of protein). Solid blue: *WT* (n=5); blue outline: *Opa1^{tg}* (n=5); solid red: *Ndufs4$^{-/-}$* (n=5); red outline: *Ndufs4$^{-/-}$::Opa1^{tg}* (n=6). The asterisks represent the significance levels calculate by unpaired, 2-tail Student's t test *p<0.05.

D) MRC activities (nmoles/min/mg of protein) in brain mitochondria. Solid blue: *WT* (n=6); blue outline: *Opa1^{tg}* (n=4); solid red: *Ndufs4$^{-/-}$* (n=4); red outline: *Ndufs4$^{-/-}$::Opa1^{tg}* (n=6). Error bars represent SD. The asterisks represent the significance levels calculate by unpaired, 2-tail Student's t test *p<0.05.

E) BNGE- in-gel activity of cI. Note the absence of BNGE-based in-gel activity of cI and cI-containing supercomplexes (sc) band in *Ndufs4$^{-/-}$* and *Ndufs4$^{-/-}$::Opa1^{tg}* samples.

Survival and functional improvement in the double mutant Cox15$^{sm/sm}$::Opa1^{tg} mice

Similar to *Cox15$^{sm/sm}$::Opa1^{tg},* male and female *Cox15$^{sm/sm}$::Opa1^{tg}* mice were smaller than WT or *Opat^{tg}* littermates ($p<0.005$; n=4 for each genotype; data not shown). To test muscle performance, we monthly monitored motor endurance by a standard treadmill test starting at 2 months of age. Albeit still significantly lower than WT (n=8) and *Opa1^{tg}* (n=9) littermates, the scores of the *Cox15$^{sm/sm}$::Opa1^{tg}* double mutant group (n=8) were significantly and consistently higher than those of the *Cox15$^{sm/sm}$* group (n=10) ($p<0.005$ at each time point; Figure 2A). On average, the distance covered by *Cox15$^{sm/sm}$::Opa1^{tg}* individuals was 3 times that of the *Cox15$^{sm/sm}$* littermates (169±20 vs. 58±6 meters, $p=2.59x10^{-6}$). This improvement was recorded in both homozygous females and hemizygous males (Figure S2). Interestingly, *Opa1^{Tg}* performed better than WT littermates (890±50 vs. 803±27 meters, $p<0.001$). We followed the animals up to 6 months of age. Notably, *Cox15$^{sm/sm}$::Opa1^{tg}* double mutants showed a remarkable increase in survival probability compared to their *Cox15$^{sm/sm}$* littermates (log rank test $p=0.0003$). Only 1/17 (7%) *Cox15$^{sm/sm}$::Opa1^{tg}* animal died during our observation period, vs. 12/23 (50%) *Cox15$^{sm/sm}$* littermates (Figure 2B). In conclusion, controlled *Opa1* overexpression ameliorates life expectancy and motor function of a mouse model of complex IV deficiency.

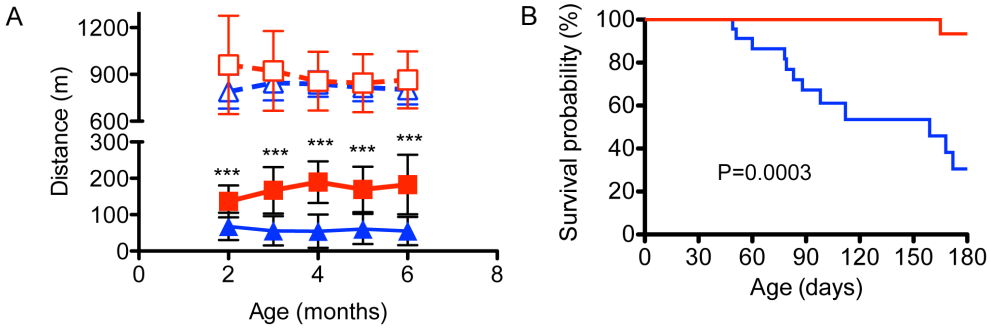

Figure 2. ***Marked motor function and lifespan amelioration in Cox15$^{sm/sm}$::Opa1^{Tg} individuals***

A) Treadmill analysis of motor performance. Dashed blue: *WT* (n=8); dashed red: *Opa1^{tg}* (n=9); solid blue: *Cox15$^{sm/sm}$* (n=10); solid red *Cox15$^{sm/sm}$::Opa1^{tg}* (n=8). Error bars represent SD. The asterisks represent the significance levels calculate by unpaired, 2-tail Student's t test ***p<0.005, and refer to the comparison between *Cox15$^{sm/sm}$::Opa1^{tg}* and *Cox15$^{sm/sm}$*.

B) Kaplan–Meier survival probability. Significance was assessed by log-rank test. Solid blue: *Cox15$^{sm/sm}$* (n=23); solid red: *Cox15$^{sm/sm}$::Opa1^{tg}* (n=17).

Amelioration of skeletal muscle mitochondrial ultrastructure and respiration in Cox15$^{sm/sm}$::Opa1^{tg} mice.

Post-mortem examination performed at 6 months of age showed that the skeletal muscles of both *Cox15$^{sm/sm}$::Opa1^{tg}* and *Cox15$^{sm/sm}$* were smaller than those of their WT and *Opa1^{Tg}* littermates, suggesting no effect of *Opa1* overexpression in preventing muscle hypotrophy associated with *Cox15$^{sm/sm}$* myopathy [277]. This was confirmed by quantitative measurement of the cross-sectional area at the midportion of the gastrocnemius muscles (Figure S3A). In both groups, histological examination of the same muscle revealed the presence of numerous centralized nuclei and atrophic fibres (Figure S3B). We therefore tested whether the muscle

hypotrophy and dystrophic features of the *Cox15*$^{sm/sm}$ mice was associated with increased apoptosis or altered autophagy that are blocked by increased *Opa1* expression in vivo (Varanita et al. 2014 manuscript in preparation). However, TUNEL staining in muscle sections did reveal hardly any positive fibre in both *Cox15*$^{sm/sm}$ and *Cox15*$^{sm/sm}$*::Opa1*^{tg}, similar to WT and *Opa1*^{Tg} (not shown), suggesting that apoptosis is not a major player in the pathogenesis of *Cox15*$^{sm/sm}$ myopathy. Conversely, immunostaining of muscle sections with Lamp1 and P62 antibodies revealed hugely increased reactions in *Cox15*$^{sm/sm}$ samples compared to WT and *Opa1*^{Tg}, which did not obviously change in *Cox15*$^{sm/sm}$*::Opa1*^{tg} (Figure S4A). Western-blot immunovisualization of P62 and LC3B-I/LC3B-II confirmed the variable increase of autophagic markers in both *Cox15*$^{sm/sm}$ and *Cox15*$^{sm/sm}$*::Opa1*^{tg} (Figure S4B). These data indicate that inhibition of apoptosis and autophagy are unlikely to contribute to the amelioration of *Cox15*$^{sm/sm}$ phenotype when crossed with the *Opa1*^{tg} mice.

We therefore turned back to the analysis of mitochondrial structure. Ultrastructural examination of tibialis anterior muscle revealed marked improvement of mitochondrial morphology and myofibrillary organization in *Cox15*$^{sm/sm}$*::Opa1*^{tg} compared to *Cox15*$^{sm/sm}$. Whilst *Cox15*$^{sm/sm}$ muscle mitochondria showed profound cristae disorganization and prominent vacuolar degeneration of the inner mitochondrial compartment (Figure 3A), the *Cox15*$^{sm/sm}$*::Opa1*^{tg} cristae were organized in an ordered and parallel array and were tightly folded (Figure 3B),

similar to what observed in WT and *Opa1*^{tg} littermate specimens (Figure 3C, D). No hyperfused organelles were observed in *Opa1*^{Tg} muscle. Likewise, myofibrils, which in *Cox15*$^{sm/sm}$ appeared disorganized and separated from each other by the accumulation of membranous and granular material, showed a compact orderly array in *Cox15*$^{sm/sm}$*::Opa1*^{tg}, again resembling those of WT and *Opa1*^{tg} specimens.

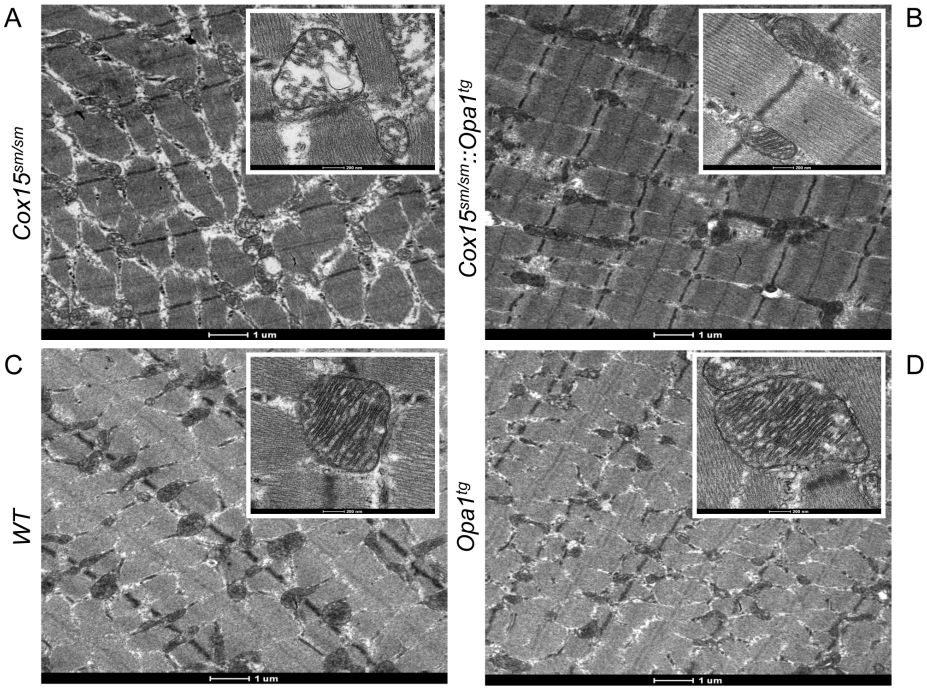

Figure 3. Mitochondrial ultrastructure is ameliorated in Cox15$^{sm/sm}$::Opa1^{Tg}

A) *Cox15*$^{sm/sm}$. Note the accumulation of inter-myofibrillar amorphous material, and the disorganization of the mitochondrial cristae (inset). Scale bar 1 µm.

B) *Cox15*$^{sm/sm}$*::Opa1*^{tg}. Note that the myofibrillar and cristae (inset) structure is well preserved.

C) *WT*.

D) *Opa1*^{Tg}. Note that mitochondria appear larger and with denser cristae than in *WT*.

To test whether the clinical and morphological improvements observed in *Cox15*$^{sm/sm}$*::Opa1*^{tg} individuals were associated with biochemical correction, we first measured respiration in isolated muscle mitochondria. Glutamate-malate dependent state-3 oxygen consumption rate (reflecting cI-driven respiration) was decreased in *Cox15*$^{sm/sm}$ individuals (128±37 nmol/min/mg protein), but increased significantly in *Cox15*$^{sm/sm}$*::Opa1*^{tg} (190±48 nmol/min/mg; $p<0.05$), up to lower normal values, not significantly different from those obtained in WT (250±84 nmol/min/mg) and *Opa1*^{Tg} (276±101 nmol/min/mg) samples (Figure 4A). Similar results were obtained by measuring succinate- and TMPD/ascorbate-dependent state-3 oxygen consumption rate (reflecting cII- and cIV-driven respiration, respectively) (Figure 4A). We then analysed the activity of the single respiratory complexes by spectrophotometric assay. The specific activity of cIV normalized to that of citrate synthase (CS) was significantly increased ($p<0.05$) in *Cox15*$^{sm/sm}$*::Opa1*^{tg} (16±3) vs. *Cox15*$^{sm/sm}$ (10±4) muscle homogenates, albeit still much lower than that of WT (47±18) or *Opa1*^{Tg} (44±7) muscles (Figure 4B). These results were qualitatively confirmed by histochemical COX staining, which showed reduced COX-negative fibres in COX/SDH double reaction in *Cox15*$^{sm/sm}$*::Opa1*^{tg} vs. *Cox15*$^{sm/sm}$ muscle fibres (Figure 4C).

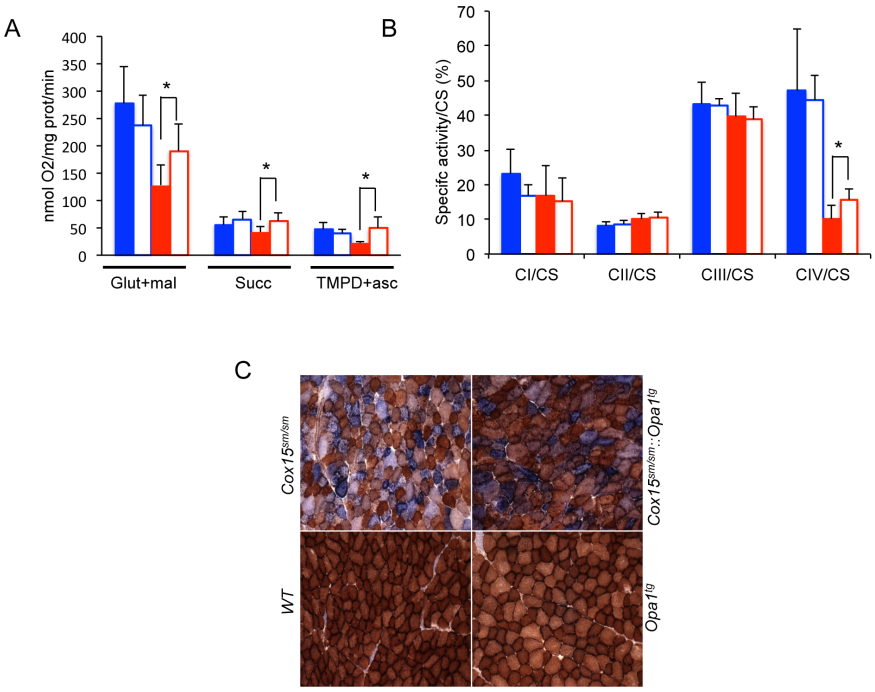

Figure 4. Skeletal muscle *Cox15$^{sm/sm}$::Opa1^{Tg}* mitochondrial respiration is recovered

A) Oxygen consumption measurements (nmoles O_2/min/mg of protein). Solid blue: *WT* (n=5); blue outline: *Opa1^{tg}* (n=5); solid red: *Cox15$^{sm/sm}$* (n=5); red outline: *Cox15$^{sm/sm}$::Opa1^{tg}* (n=6). Error bars represent SD. The asterisks represent the significance levels calculate by unpaired, 2-tail Student's t test *p<0.05.

B) MRC activities (nmoles/min/mg of protein) in skeletal muscle mitochondria. MRC activities (nmoles/min/mg of protein) in brain mitochondria. Solid blue: *WT* (n=5); blue outline: *Opa1^{tg}* (n=5); solid red: *Cox15$^{sm/sm}$* (n=5); red outline: *Cox15$^{sm/sm}$::Opa1^{tg}* (n=6). Error bars represent SD. The asterisks represent the significance levels calculate by unpaired, 2-tail Student's t test *p<0.05.

C) COX/SDH histochemical double staining.

Mitochondrial respiratory chain supercomplexes are increased in Cox15$^{sm/sm}$::Opa1^{tg} mice

In order to understand the molecular bases for the observed correction of mitochondrial respiration in Cox15$^{sm/sm}$::Opa1^{tg} animals, we analysed the amount of subunits specific to each MRC complex by Western-blotting of isolated muscle mitochondrial proteins separated by SDS-PAGE. The amounts of both Cox1, the mtDNA-encoded, largest cIV subunit, which contains the two heme-a moieties, and Cox4, a nucleus encoded, early assembled cIV subunit, were reduced in Cox15$^{sm/sm}$ compared to WT and Opa1^{Tg} samples, but did increase in those from Cox15$^{sm/sm}$::Opa1^{tg} animals (Figure 5A and Figure S5A). In both Cox15$^{sm/sm}$ and Cox15$^{sm/sm}$::Opa1^{tg} samples, subunits of other MRC complexes were generally increased, particularly the Uqcrc2 subunit of cIII, suggesting compensatory activation of MRC biogenesis induced by cIV deficiency. Interestingly, analysis of mitochondrial and nuclear transcripts of cIV subunits revealed a specific, marked reduction of Cox1 mRNA in Cox15$^{sm/sm}$ samples, which was fully rescued in Cox15$^{sm/sm}$::Opa1^{tg} samples (Figure 5B). Conversely, other mtDNA- (Cox2) and nucleus-encoded (Cox4 and Cox5a) transcripts were unchanged in Cox15$^{sm/sm}$ vs. WT mice and were not affected by Opa1 overexpression (Figure 5B). Importantly, the Cox15 transcript level measured in skeletal muscle of Cox15$^{sm/sm}$: was approximately 9% of that present in WT and Opa1^{tg} littermates, and did not change significantly in Cox15$^{sm/sm}$::Opa1^{tg} (Figure S5B), ruling out a direct effect of

Opa1 overexpression on Cox15 transcription. We did not detect any quantitative changes in any group of animals for transcripts encoding Tfam and Pgc1α. The mtDNA copy number, which was increased in Cox15$^{sm/sm}$ returned to WT levels in Cox15$^{sm/sm}$::Opa1^{tg}, suggesting normalization of the homeostatic control on mtDNA maintenance (Figure S5C). Together, these data suggest that Opa1 overexpression leads to stabilization in cIV protein and transcript levels.

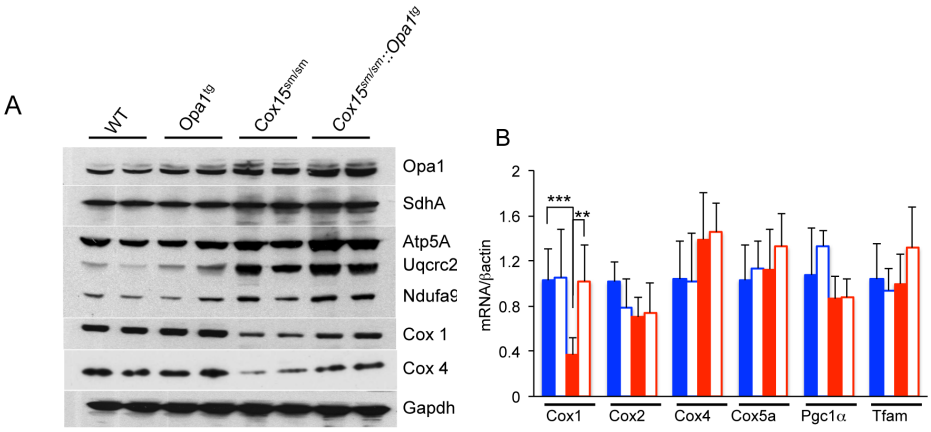

Figure 5. ***Molecular analysis of Cox15$^{sm/sm}$::Opa1^{tg} skeletal muscle***

A) Western blot immunovisualization of Opa1, SdhA (cII), Atp5A (cV), Uqcrc2 (cIII), Ndufa9 (cI), Cox1, and Cox4 (cIV); Gapdh was taken as a loading reference.

B) mRNA expression analysis of cIV- and mitochondrial biogenesis-related genes. Gene transcripts, retrotranscribed into cDNA, were normalized to the β-Actin gene transcript, taken as a standard, and expressed as time fold variation relative to the WT. Error bars represent SD. Comparison among groups was carried out by one way ANOVA, and Bonferroni correction: **p < 0.01; ***p < 0.005.

Individual MRC stability depends on their assembly in respiratory chain supercomplexes (RCS) [272]. We therefore analysed cI and cIV Blue-Native Gel Electrophoresis (BNGE) in-gel activities in digitonin-treated isolated muscle mitochondria. In Cox15sm/sm mitochondria, the intensity of the band corresponding to individual cIV holocomplex was markedly reduced, and there was hardly any reaction in the high molecular weight area harbouring RCS. However, individual cIV in-gel activity was increased and cIV reactive high-molecular weight bands were clearly detected in Cox15sm/sm::Opa1tg mitochondria (Figure 6A) indicating remarkable stabilization of cIV holocomplex and cIV-containing RCS. Likewise, several high-molecular weight cI-reactive bands, corresponding to cI- and cIV-containing RCS, were virtually absent in the same Cox15sm/sm samples, but were clearly, albeit weakly, visible in the Cox15sm/sm::Opa1tg samples (Figure 6B). Western-blot analysis on BNGE samples using an anti-Cox1 specific antibody confirmed the results of in-gel activity: a band corresponding to cIV holocomplex was increased in Cox15sm/sm::Opa1tg compared to Cox15sm/sm and high molecular-weight Cox1-reactive bands that were detected in WT and Opa1Tg samples were absent, even upon long exposure, in Cox15sm/sm, but clearly, albeit weakly, visible in Cox15sm/sm::Opa1tg samples (Figure 6C). Similarly, immunodetection of cI-containing RCS with an anti-Ndufa9 antibody were slightly increased in Cox15sm/sm::Opa1tg vs. Cox15sm/sm (Figure 6D). In total, our results indicate that

increased Opa1 levels stabilize RCS and residual complex IV in Cox15sm/sm mice.

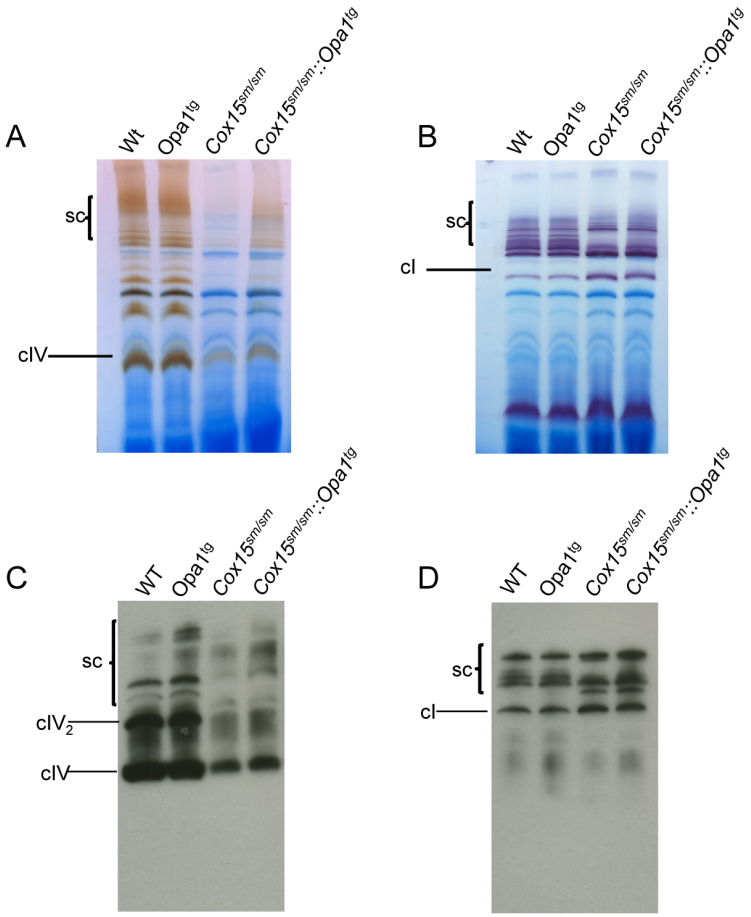

Figure 6. CI and cIV activities *in skeletal muscle.*
A) cIV-specific BNGE in-gel activity. Note the increased staining in the bands corresponding to cIV-holoenzyme and cIV-containing supercomplexes (sc) in *Cox15*$^{sm/sm}$*::Opa1*^{tg} vs. *Cox15*$^{sm/sm}$.
B) cI-specific BNGE in-gel activity. Note the increased staining in the bands corresponding to the supercomplexes (sc) in *Cox15*$^{sm/sm}$*::Opa1*^{tg} vs. *Cox15*$^{sm/sm}$.
C) Western-blot immunovisualization of MRC cIV from BNGE of digitonin-treated isolated mitochondria
D) Western-blot immunovisualization of MRC cI from BNGE of digitonin-treated isolated mitochondria

Discussion

The moderate overexpression of *Opa1* achieved in the *Opa1*^{tg} mouse model is well tolerated and compatible with normal development, fertility and lifespan. Increased *Opa1* amount in key tissues, including skeletal and cardiac muscle, brain and liver, confer remarkable protection against a wide spectrum of experimental tissue damage models (Varanita et al, 2014 manuscript in preparation). Here, we demonstrate that this effect can be exploited to improve the clinical, biochemical and molecular phenotype of two mouse models of genetically determined OXPHOS failure.

The *Ndufs4*$^{-/-}$ mouse is characterised by the complete absence of a structural component of cI. In the current map of mammalian cI, the Ndufs4 18 kDa subunit has been modelled into a density in a cleft between the 75 kDa subunit and the 49 kDa, 30 kDa and Ndufs8 (TYKY) subunits [294]. This location may explain why disease mutations in the 18 kDa subunit lead to accumulation of late-stage interrupted-assembly intermediates lacking the NADH-dehydrogenase module [293]. The indispensable role of Ndufs4 in preserving the cI structure and redox activity can also explain the limited improvement of the clinical and biochemical phenotypes observed in *Ndufs4*$^{-/-}$ *::Opa1*^{tg} double mutants. Inhibition of mTOR recently shown to alleviate the clinical phenotype also failed to correct the cI defect of rapamycin-treated *Ndufs4*$^{-/-}$ mice [231]. However, the cristae-centric approach used here to treat cI deficiency improved survival to levels comparable to those achieved by

every other day rapamycin administration [231]. It would be interesting to verify if the combination of Opa1 overexpression and mTOR inhibition is additive and can achieve even better clinical amelioration.

The *Cox15*$^{sm/sm}$ mouse model is based on muscle-specific ablation of *Cox15*, dependent on the activity of the *Cre* recombinase under the control of the skeletal muscle-specific actin promoter. Although *Cox15*$^{sm/sm}$ individuals display early-onset, progressive mitochondrial myopathy, characterized by profound muscle weakness and wasting leading to early death, the genetic lesion underpinning this phenotype can be considered as a hypomorphic mutant allele, the effects of which on COX activity and MRC proficiency are severe but partial. Accordingly, *Cox15* transcript was drastically decreased, but not absent, in *Cox15*$^{sm/sm}$ and *Cox15*$^{sm/sm}$*::Opa1*^{tg} muscles, explaining the presence of some residual COX activity in muscle of adult individuals, and the ”mosaic” like distribution of the histochemical reaction to COX, which is preserved in scattered muscle fibres (Figure 4C). The molecular *Cox15*$^{sm/sm}$ defect resembles that of the majority of mitochondrial disorders, i.e. partial rather than complete biochemical impairment, due to decreased but not abolished function of the mutant gene product. Incidentally, this category of mitochondrial disease includes also the few *COX15* mutant patients reported in the literature [150,151,287]. These considerations may explain the marked and persistent improvement of the clinical phenotype observed in *Cox15*$^{sm/sm}$*::Opa1*^{tg} double mutants, and suggest

that OXPHOS impairment due to decreased but not abolished function of the mutant gene product, is amenable to correction by potentiating the effects of Opa1 on mitochondrial cristae shape and MRC function.

The *Cox15*$^{sm/sm}$*::Opa1*^{tg} animals displayed dramatic increase in motor endurance but also showed remarkable extension of survival, up to, and in most cases well beyond, the six-month period of observation of our experimental protocol. These clinical effects were associated with robust increase of muscle mitochondrial respiration, which was accompanied by milder but significant increase of muscle COX activity. The discrepancy between the nearly complete reversion to normal in the respiratory rate and the modest increment of COX activity may be explained by increased stabilization of cIV holocomplex and cIV-associated supercomplexes, as indicated by results of BNGE in-gel activity and immunoblotting. The clinical and biochemical recovery of the *Cox15*$^{sm/sm}$*::Opa1*^{tg} double mutants was associated with marked correction of the profound ultrastructural alteration in cristae morphology associated with *Cox15* ablation. This effect is likely to be directly connected with the role of Opa1 in cristae shape and may be correlated to partial stabilization of the cIV holocomplex and supercomplex organization in the cristae membrane. Accordingly, both nucleus- and mitochondria-encoded MRC subunits were increased in *Cox15*$^{sm/sm}$*::Opa1*^{tg} vs. *Cox15*$^{sm/sm}$ muscles, while the corresponding transcripts were unchanged, with the notable exception of *Cox1* mRNA. Cox1 is the mtDNA-encoded

catalytic cIV subunit, which contains the heme-*a* moieties essential for Cox1 stabilization [278]. The concordant decrease of both Cox1 protein and mRNA in *Cox15*$^{sm/sm}$ was completely reverted in *Cox15*$^{sm/sm}$*::Opa1*^{tg}. Taken together, these results substantiate the possibility that in mammals, as in *Saccharomyces cerevisiae*, Cox1 biosynthesis is regulated by a feedback mechanism linking translation and post-translation processing to transcription [295]. In yeast, a key role in this homeostatic loop is carried out by the *Cox1* specific translation activators Mss51 and Pet309 [295]. The mammalian orthologue of Pet309 has been identified as the leucine-rich pentatricopeptide repeat containing (LRPPRC) protein, an RNA binding factor that is mutated in French-Canadian, COX defective Leigh-like syndrome in humans [195]. However, as there are no obvious mammalian orthologs of Mss51, and the 5' UTR sequence of the yeast *Cox1* mRNA, to which Mss51 binds, is virtually absent in the mammalian transcript, these feedback mechanisms are probably different in their molecular details between yeast and mammalian systems.

Finally, whilst apoptosis seems not to play a significant role in *Cox15*$^{sm/sm}$ myopathy, and is not increased in *Cox15*$^{sm/sm}$*::Opa1*^{tg} samples, immunoanalysis revealed hugely increased levels of several autophagy markers in both *Cox15*$^{sm/sm}$ and *Cox15*$^{sm/sm}$*::Opa1*^{tg} muscle fibres. These findings suggest that autophagy is activated in response to *Cox15* ablation, but whether it is relevant to the pathogenesis of the disease is unclear.

Our study demonstrates that Opa1-dependent mitochondrial cristae and RCS stabilization is effective in correcting mitochondrial disease conditions characterized by partial, however severe, MRC defects. Opa1 can even partially improve defects caused by complete lack of mitochondrial cI, via an unknown mechanism. Our results indicate Opa1 as a new target for effective therapy of primary mitochondrial disorders. From a translational point of view, future work is warranted to elucidate the molecular details underpinning these remarkable effects, extend the experimental observation to additional OXPHOS-defective models, and eventually transfer this set of proof-of-principle observations into effective therapeutic approaches, by e.g. selecting compounds or bioreactors able to control the expression or stability of Opa1 in suitable mammalian cell systems and animal models.

Acknowledgments

This work was supported by: the Pierfranco and Luisa Mariani Foundation Italy (to MZ), Telethon-Italy GPP10005 (to MZ, LS), GGP11011 (to MZ), GGP12162, GGP14187A (to LS), AIRC Italy (to LS), Cariplo 2011-0526 (to MZ), ERC FP7-322424 (to MZ) and FP7-282280 (to LS), FP7 CIG PCIG13-GA-2013-618697 (to LS), Italian Ministry of Research FIRB RBAP11Z3YA_005 (to LS) and Italian Ministry of health GR-2010-2306-756 (to CV). We are grateful to the personnel at Phenomics and ARES animal care facilities for skilful technical assistance. We thank Dr. Raffaele Cerutti for excellent assistance in histological analysis.

References

Acin-Perez, R., Bayona-Bafaluy, M.P., Fernandez-Silva, P., Moreno-Loshuertos, R., Perez-Martos, A., Bruno, C., Moraes, C.T., and Enriquez, J.A. (2004). Respiratory complex III is required to maintain complex I in mammalian mitochondria. Molecular cell *13*, 805-815.

Acin-Perez, R., and Enriquez, J.A. (2014). The function of the respiratory supercomplexes: the plasticity model. Biochimica et biophysica acta *1837*, 444-450.

Alfadhel, M., Lillquist, Y.P., Waters, P.J., Sinclair, G., Struys, E., McFadden, D., Hendson, G., Hyams, L., Shoffner, J., and Vallance, H.D. (2011). Infantile cardioencephalopathy due to a COX15 gene defect: report and review. American journal of medical genetics. Part A *155A*, 840-844.

Anand, R., Wai, T., Baker, M.J., Kladt, N., Schauss, A.C., Rugarli, E., and Langer, T. (2014). The i-AAA protease YME1L and OMA1 cleave OPA1 to balance mitochondrial fusion and fission. The Journal of cell biology *204*, 919-929.

Antonicka, H., Mattman, A., Carlson, C.G., Glerum, D.M., Hoffbuhr, K.C., Leary, S.C., Kennaway, N.G., and Shoubridge, E.A. (2003). Mutations in COX15 produce a defect in the mitochondrial heme biosynthetic pathway, causing early-onset fatal hypertrophic cardiomyopathy. American journal of human genetics *72*, 101-114.

Bareth, B., Dennerlein, S., Mick, D.U., Nikolov, M., Urlaub, H., and Rehling, P. (2013). The heme a synthase Cox15 associates with cytochrome c oxidase assembly intermediates during Cox1 maturation. Molecular and cellular biology *33*, 4128-4137.

Barros, M.H., Carlson, C.G., Glerum, D.M., and Tzagoloff, A. (2001). Involvement of mitochondrial ferredoxin and Cox15p in hydroxylation of heme O. FEBS letters *492*, 133-138.

Barros, M.H., and Tzagoloff, A. (2002). Regulation of the heme A biosynthetic pathway in Saccharomyces cerevisiae. FEBS letters *516*, 119-123.

Bugiani, M., Invernizzi, F., Alberio, S., Briem, E., Lamantea, E., Carrara, F., Moroni, I., Farina, L., Spada, M., Donati, M.A., et al. (2004). Clinical and molecular findings in children with complex I deficiency. Biochim Biophys Acta *1659*, 136-147.

Bugiani, M., Tiranti, V., Farina, L., Uziel, G., and Zeviani, M. (2005). Novel mutations in COX15 in a long surviving Leigh syndrome patient with cytochrome c oxidase deficiency. Journal of medical genetics *42*, e28.
Calvaruso, M.A., Willems, P., van den Brand, M., Valsecchi, F., Kruse, S., Palmiter, R., Smeitink, J., and Nijtmans, L. (2012). Mitochondrial complex III stabilizes complex I in the absence of NDUFS4 to provide partial activity. Human molecular genetics *21*, 115-120.
Cipolat, S., Martins de Brito, O., Dal Zilio, B., and Scorrano, L. (2004). OPA1 requires mitofusin 1 to promote mitochondrial fusion. Proceedings of the National Academy of Sciences of the United States of America *101*, 15927-15932.
Cogliati, S., Frezza, C., Soriano, M.E., Varanita, T., Quintana-Cabrera, R., Corrado, M., Cipolat, S., Costa, V., Casarin, A., Gomes, L.C., et al. (2013). Mitochondrial cristae shape determines respiratory chain supercomplexes assembly and respiratory efficiency. Cell *155*, 160-171.
Delettre, C., Griffoin, J.M., Kaplan, J., Dollfus, H., Lorenz, B., Faivre, L., Lenaers, G., Belenguer, P., and Hamel, C.P. (2001). Mutation spectrum and splicing variants in the OPA1 gene. Human genetics *109*, 584-591.
Duvezin-Caubet, S., Koppen, M., Wagener, J., Zick, M., Israel, L., Bernacchia, A., Jagasia, R., Rugarli, E.I., Imhof, A., Neupert, W., et al. (2007). OPA1 processing reconstituted in yeast depends on the subunit composition of the m-AAA protease in mitochondria. Molecular biology of the cell *18*, 3582-3590.
Ehses, S., Raschke, I., Mancuso, G., Bernacchia, A., Geimer, S., Tondera, D., Martinou, J.C., Westermann, B., Rugarli, E.I., and Langer, T. (2009). Regulation of OPA1 processing and mitochondrial fusion by m-AAA protease isoenzymes and OMA1. The Journal of cell biology *187*, 1023-1036.
Elliott, H.R., Samuels, D.C., Eden, J.A., Relton, C.L., and Chinnery, P.F. (2008). Pathogenic mitochondrial DNA mutations are common in the general population. Am J Hum Genet *83*, 254-260.
Enriquez, J.A., and Lenaz, G. (2014). Coenzyme q and the respiratory chain: coenzyme q pool and mitochondrial supercomplexes. Molecular syndromology *5*, 119-140.

Fernandez-Vizarra, E., Lopez-Perez, M.J., and Enriquez, J.A. (2002). Isolation of biogenetically competent mitochondria from mammalian tissues and cultured cells. Methods *26*, 292-297.
Frezza, C., Cipolat, S., Martins de Brito, O., Micaroni, M., Beznoussenko, G.V., Rudka, T., Bartoli, D., Polishuck, R.S., Danial, N.N., De Strooper, B., et al. (2006). OPA1 controls apoptotic cristae remodeling independently from mitochondrial fusion. Cell *126*, 177-189.
Frezza, C., Cipolat, S., and Scorrano, L. (2007). Organelle isolation: functional mitochondria from mouse liver, muscle and cultured fibroblasts. Nature protocols *2*, 287-295.
Glerum, D.M., Muroff, I., Jin, C., and Tzagoloff, A. (1997). COX15 codes for a mitochondrial protein essential for the assembly of yeast cytochrome oxidase. The Journal of biological chemistry *272*, 19088-19094.
Griparic, L., Kanazawa, T., and van der Bliek, A.M. (2007). Regulation of the mitochondrial dynamin-like protein Opa1 by proteolytic cleavage. The Journal of cell biology *178*, 757-764.
Griparic, L., and van der Bliek, A.M. (2001). The many shapes of mitochondrial membranes. Traffic *2*, 235-244.
Head, B., Griparic, L., Amiri, M., Gandre-Babbe, S., and van der Bliek, A.M. (2009). Inducible proteolytic inactivation of OPA1 mediated by the OMA1 protease in mammalian cells. The Journal of cell biology *187*, 959-966.
Herrmann, J.M., Woellhaf, M.W., and Bonnefoy, N. (2013). Control of protein synthesis in yeast mitochondria: the concept of translational activators. Biochimica et biophysica acta *1833*, 286-294.
Ishihara, N., Fujita, Y., Oka, T., and Mihara, K. (2006). Regulation of mitochondrial morphology through proteolytic cleavage of OPA1. The EMBO journal *25*, 2966-2977.
Johnson, S.C., Yanos, M.E., Kayser, E.B., Quintana, A., Sangesland, M., Castanza, A., Uhde, L., Hui, J., Wall, V.Z., Gagnidze, A., et al. (2013). mTOR inhibition alleviates mitochondrial disease in a mouse model of Leigh syndrome. Science *342*, 1524-1528.
Karamanlidis, G., Lee, C.F., Garcia-Menendez, L., Kolwicz, S.C., Jr., Suthammarak, W., Gong, G., Sedensky, M.M., Morgan, P.G., Wang, W., and Tian, R. (2013). Mitochondrial complex I deficiency increases protein acetylation and accelerates heart failure. Cell metabolism *18*, 239-250.

Kasahara, A., and Scorrano, L. (2014). Mitochondria: from cell death executioners to regulators of cell differentiation. Trends in cell biology.
Koopman, W.J., Willems, P.H., and Smeitink, J.A. (2012). Monogenic mitochondrial disorders. N Engl J Med *366*, 1132-1141.
Kruse, S.E., Watt, W.C., Marcinek, D.J., Kapur, R.P., Schenkman, K.A., and Palmiter, R.D. (2008). Mice with mitochondrial complex I deficiency develop a fatal encephalomyopathy. Cell metabolism *7*, 312-320.
Mootha, V.K., Lepage, P., Miller, K., Bunkenborg, J., Reich, M., Hjerrild, M., Delmonte, T., Villeneuve, A., Sladek, R., Xu, F., et al. (2003). Identification of a gene causing human cytochrome c oxidase deficiency by integrative genomics. Proceedings of the National Academy of Sciences of the United States of America *100*, 605-610.
Nijtmans, L.G., Henderson, N.S., and Holt, I.J. (2002). Blue Native electrophoresis to study mitochondrial and other protein complexes. Methods *26*, 327-334.
Petruzzella, V., Tiranti, V., Fernandez, P., Ianna, P., Carrozzo, R., and Zeviani, M. (1998). Identification and characterization of human cDNAs specific to BCS1, PET112, SCO1, COX15, and COX11, five genes involved in the formation and function of the mitochondrial respiratory chain. Genomics *54*, 494-504.
Petruzzella, V., Vergari, R., Puzziferri, I., Boffoli, D., Lamantea, E., Zeviani, M., and Papa, S. (2001). A nonsense mutation in the NDUFS4 gene encoding the 18 kDa (AQDQ) subunit of complex I abolishes assembly and activity of the complex in a patient with Leigh-like syndrome. Human molecular genetics *10*, 529-535.
Quintana, A., Kruse, S.E., Kapur, R.P., Sanz, E., and Palmiter, R.D. (2010). Complex I deficiency due to loss of Ndufs4 in the brain results in progressive encephalopathy resembling Leigh syndrome. Proceedings of the National Academy of Sciences of the United States of America *107*, 10996-11001.
Quintana, A., Morgan, P.G., Kruse, S.E., Palmiter, R.D., and Sedensky, M.M. (2012). Altered anesthetic sensitivity of mice lacking Ndufs4, a subunit of mitochondrial complex I. PloS one *7*, e42904.

Rahn, J.J., Stackley, K.D., and Chan, S.S. (2013). Opa1 is required for proper mitochondrial metabolism in early development. PloS one *8*, e59218.
Scacco, S., Petruzzella, V., Budde, S., Vergari, R., Tamborra, R., Panelli, D., van den Heuvel, L.P., Smeitink, J.A., and Papa, S. (2003). Pathological mutations of the human NDUFS4 gene of the 18-kDa (AQDQ) subunit of complex I affect the expression of the protein and the assembly and function of the complex. The Journal of biological chemistry *278*, 44161-44167.
Sciacco, M., and Bonilla, E. (1996). Cytochemistry and immunocytochemistry of mitochondria in tissue sections. Methods Enzymol *264*, 509-521.
Song, Z., Chen, H., Fiket, M., Alexander, C., and Chan, D.C. (2007). OPA1 processing controls mitochondrial fusion and is regulated by mRNA splicing, membrane potential, and Yme1L. The Journal of cell biology *178*, 749-755.
van den Heuvel, L., Ruitenbeek, W., Smeets, R., Gelman-Kohan, Z., Elpeleg, O., Loeffen, J., Trijbels, F., Mariman, E., de Bruijn, D., and Smeitink, J. (1998). Demonstration of a new pathogenic mutation in human complex I deficiency: a 5-bp duplication in the nuclear gene encoding the 18-kD (AQDQ) subunit. American journal of human genetics *62*, 262-268.
Vinothkumar, K.R., Zhu, J., and Hirst, J. (2014). Architecture of mammalian respiratory complex I. Nature.
Viscomi, C., Bottani, E., Civiletto, G., Cerutti, R., Moggio, M., Fagiolari, G., Schon, E.A., Lamperti, C., and Zeviani, M. (2011). In vivo correction of COX deficiency by activation of the AMPK/PGC-1alpha axis. Cell metabolism *14*, 80-90.
Wang, Z., Wang, Y., and Hegg, E.L. (2009). Regulation of the heme A biosynthetic pathway: differential regulation of heme A synthase and heme O synthase in Saccharomyces cerevisiae. The Journal of biological chemistry *284*, 839-847.

Supplemental Information

Supplemental data

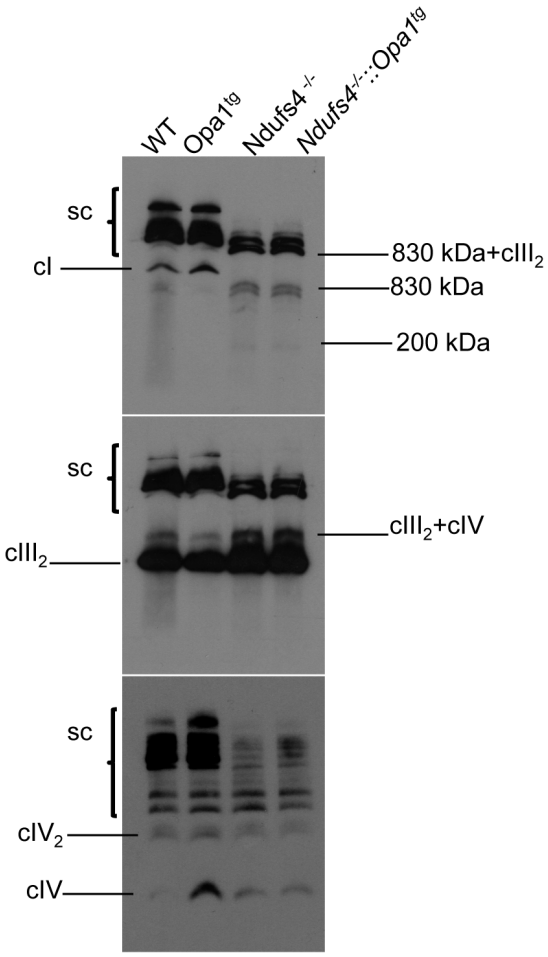

Figure S1, related to figure 1. Western-blot immunovisualization of MRC cI (upper panel), cIII (middle panel), and cIV (lower panel) from BNGE of digitonin-treated isolated mitochondria of *WT, Opa1^{tg}, Ndufs4$^{-/-}$, Ndufs4$^{-/-}$::Opa1^{tg}* samples.

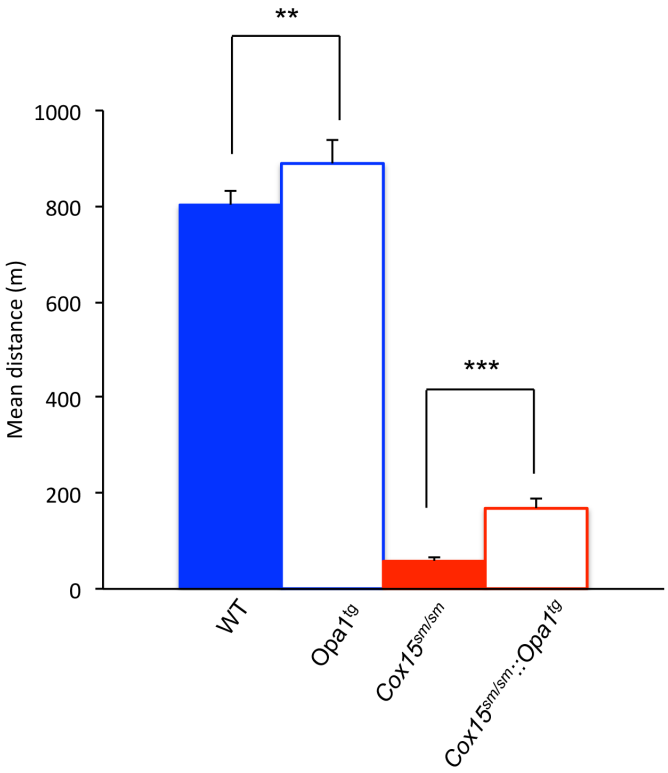

Figure S2, **related to figure 2.**
Means of weekly performed treadmill tests over 5 weeks. Solid blue: *WT* (n=8); blue outline: *Opa1*^{tg} (n=9); solid red: *Cox15*$^{sm/sm}$ (n=9); red outline: *Cox15*$^{sm/sm}$*::Opa1*^{tg} (n=10). Error bars represent SD. Statistical significance was calculated by unpaired, 2-tail Student's t test: **p<0.01: ***p<0.005.

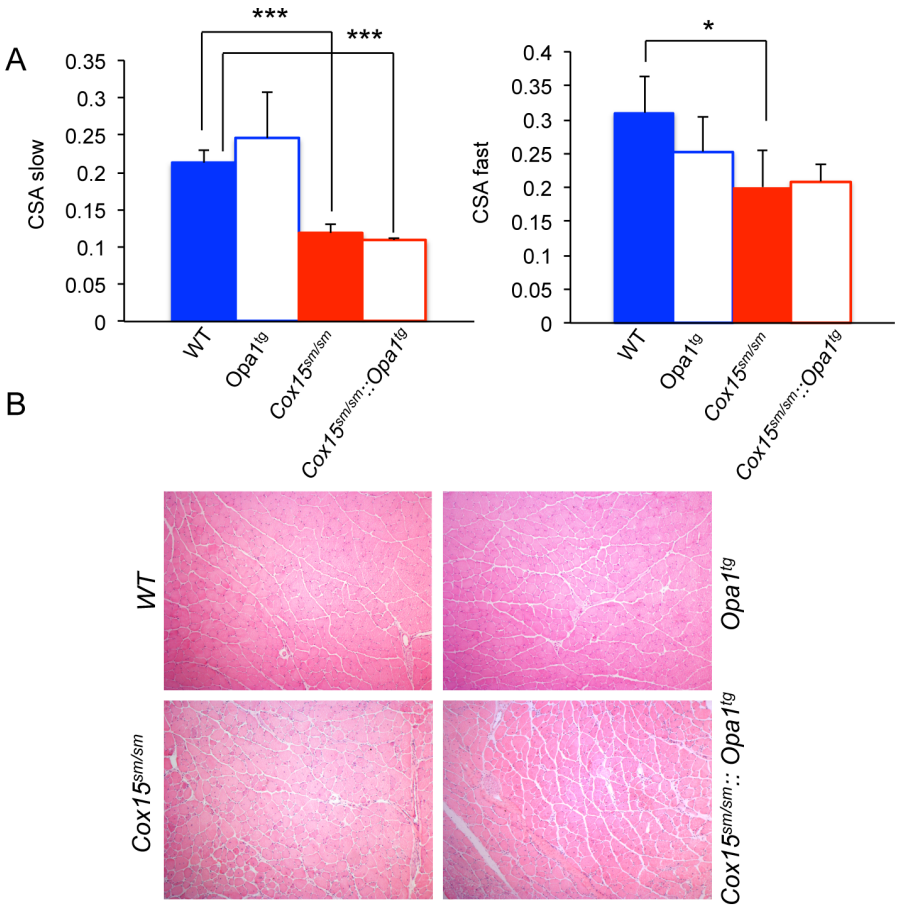

Figure S3, related to figure 3.

A: cross sectional area of the slow (left) and fast (right) fibres of gastrocnemius muscle. Solid blue: *WT* (n=3); blue outline: *Opa1*^{tg} (n=3); solid red: *Cox15*$^{sm/sm}$ (n=3); red outline: *Cox15*$^{sm/sm}$*::Opa1*^{tg} (n=3). Statistical significance was calculated by unpaired, 2-tail Student's t test: **p<0.01: ***p<0.005: *p<0.05; **p<0.01; ***p<0.005.

B: Haematoxylin and Eosing (H&E) staining of skeletal muscle.

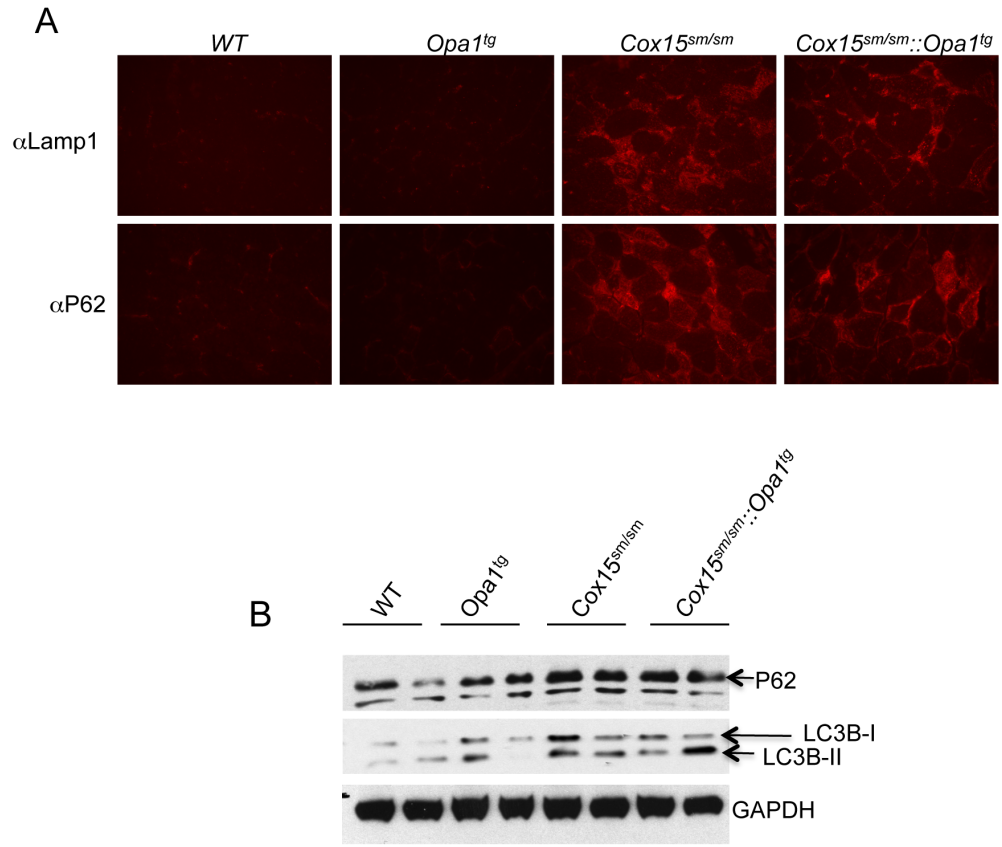

Figure S4: Autophagic markers in skeletal muscle
A: Immunofluorescence using **α**-Lamp1 (upper panels) and an **α**-P62 antibodies on specimens from the four genotypes.
B: Western blot immunovisualization of P62 and LC3B-I and LC3B-II on skeletal muscle homogenates from the four genotypes.

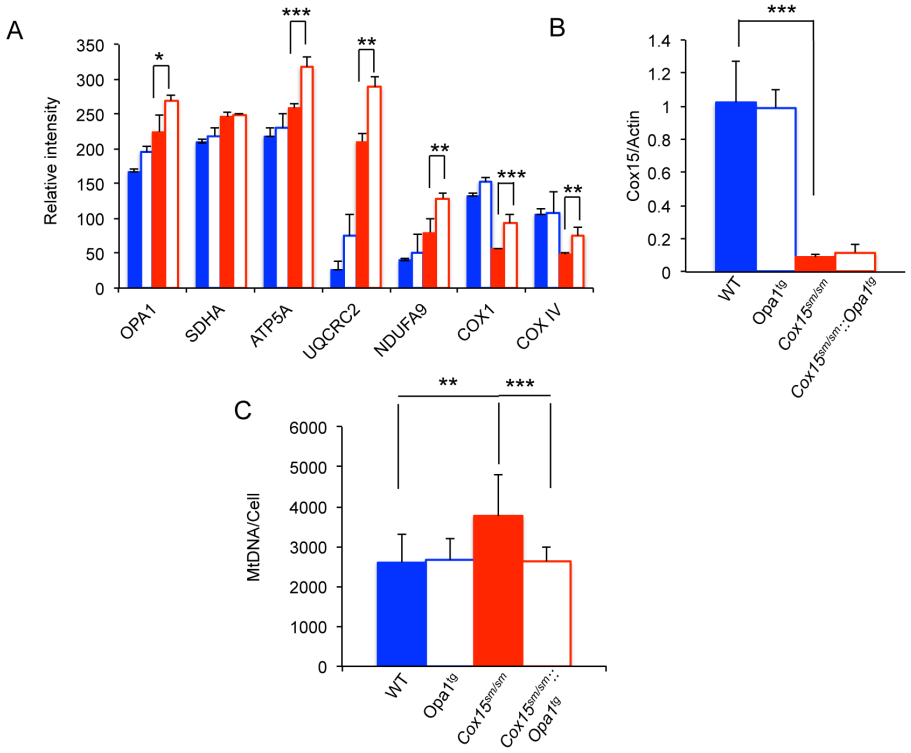

Figure S5, related to figure 5.

A: Densitometric analysis on n=4 samples for each genotype. Error bars represent SD. Statistical significance was calculated by unpaired, 2-tail Student's t test: *p<0.05; **p<0.01; ***p<0.005.

B: Quantification of Cox15 transcript. Solid blue: *WT* (n=4); blue outline: *Opa1*^{tg} (n=4); solid red: *Cox15*$^{sm/sm}$ (n=4); red outline: *Cox15*$^{sm/sm}$*::Opa1*^{tg} (n=4). Error bars represent SD. Statistical significance was calculated by unpaired, 2-tail Student's t test: ***p<0.005.

C: Quantification of mtDNA copy number. Solid blue: *WT* (n=4); blue outline: *Opa1*^{tg} (n=4); solid red: *Cox15*$^{sm/sm}$(n=4); red outline: *Cox15*$^{sm/sm}$*::Opa1*^{tg} (n=4). Error bars represent SD. Statistical significance was calculated by unpaired, 2-tail Student's t test: *p<0.05; **p<0.01; ***p<0.005.

Chapter 3

In Vivo Correction of COX Deficiency by Activation of the AMPK/PGC-1α Axis

Carlo Viscomi,[1,4] Emanuela Bottani,[1,4] **Gabriele Civiletto**,[1] Raffaele Cerutti,[1] Maurizio Moggio,[2] Gigliola Fagiolari,[2] Eric A. Schon,[3] Costanza Lamperti,[1] and Massimo Zeviani[1,*]

[1] Unit of Molecular Neurogenetics, The Foundation ''Carlo Besta'' Institute of Neurology–IRCCS, 20126 Milan, Italy
[2] Neuromuscular Unit, Department of Neurology, The Foundation Ca` Granda-Ospedale Maggiore-Policlinico and University of Milan–IRCCS, 20122 Milan, Italy
[3] Department of Neurology, College of Physicians and Surgeons, Columbia University, New York, NY 10032, USA
[4] These authors equally contributed to the work

Cell Metabolism 2011;14:80-90

Abstract

Increased mitochondrial biogenesis by activation of PPAR- or AMPK/PGC-1α-dependent homeostatic pathways has been proposed as a treatment for mitochondrial disease. We tested this hypothesis on three recombinant mouse models characterized by defective cytochrome c-oxidase (COX) activity: a knockout (KO) mouse for Surf1, a knockout/knockin mouse for Sco2, and a muscle-restricted KO mouse for Cox15. First, we demonstrated that double- recombinant animals overexpressing PGC-1α in skeletal muscle on a Surf1 KO background showed robust induction of mitochondrial biogenesis and increase of mitochondrial respiratory chain activities, including COX. No such effect was obtained by treating both $Surf1^{-/-}$ and $Cox15^{-/-}$ mice with the pan- PPAR agonist bezafibrate, which instead showed adverse effects in either model. Contrariwise, treat-ment with the AMPK agonist AICAR led to partial correction of COX deficiency in all three models, and, importantly, significant motor improvement up to normal in the $Sco2^{KO/KI}$ mouse. These results open new perspectives for therapy of mitochondrial disease.

Introduction

Present in virtually all eukaryotes, mitochondria are the major source of the high-energy phosphate molecule adenosine tri-phosphate (ATP), which is synthesized by the mitochondrial respiratory chain (MRC) through the process of oxidative phosphorylation (OXPHOS) (Wallace, 2005). ATP is the

principal energy substrate required for all active processes within the cell, and ATP deficiency leads to cellular dysfunction and ultimately cell death. A host of pathways and enzymatic functions residing within mitochondria can modify and influence OXPHOS, and OXPHOS abnormalities can in turn generate signals that trigger either homeostatic pathways, e.g., mitochondrial biogenesis, or execution programs, e.g., mitophagy, which eliminates single dysfunctional organelles, or apoptosis, which eliminates the whole dysfunctional cell (Goldman et al., 2010).

A complex, finely tuned homeostatic system senses the dynamic balance between energy demand and expenditure and regulates the biogenesis, activity, and coupling of mitochondria, according to type, function, and metabolic status of cells and tissues (Wallace and Fan, 2010). In mammals, a master regulator of mitochondrial biogenesis is PPAR-gamma Coactivator 1 alpha (PGC-1α), a transcriptional coactivator that is physiologically induced or activated by conditions of shortage of, or increased demand for, energy, such as cold, physical activity and fasting (Handschin and Spiegelman, 2006). PGC-1α acts by interacting with, and increasing the activity of, a number of transcription factors that in turn induce genes directly or indirectly related to mitochondrial proliferation, oxidative catabolism, and respiration. For instance, PGC-1α interacts with, and potentiates the function of, nuclear respiratory factors (NRF1 and NRF2) and a, b/d, and g isoforms of the peroxisomal proliferator activated receptors (PPARs). Both

NRF1 and NRF2 induce the expression of several nucleus-encoded subunits of MRC complexes, and of genes involved in replication and transcription of mtDNA, including Tfam (Kelly and Scarpulla, 2004). PPARs are tissue-specific, or ubiquitously expressed, nuclear receptors of fatty acids, which act as their activating ligands. The principal action of PPARs is to induce transcription of genes encoding enzymes involved in cellular and organelle uptake of fatty acids and fatty acid oxidation (FAO), in both mitochondria and peroxisomes (Lefebvre et al., 2006; Barish et al., 2006). PGC-1α is activated by posttranslational modifications, including phosphorylation and deacetylation. Phosphorylation at PGC-1α T177 and S538 residues is operated by the AMP- dependent kinase (AMPK) (Jagger et al., 2007). Again, this activation responds to a physiological homeostatic mechanism, since ATP and AMP are part of the same nucleotide pool, their levels being inversely related, so that when shortage of the former occurs, the latter increases, and vice versa. As a consequence of increased AMP levels, reflecting low ATP availability and low energy reserve, AMPK is activated, resulting in a cascade of phosphorylation-dependent adaptive modifications of several factors, including PGC-1α, that ultimately determine the shut- down of anabolic, energy-consuming processes, whereas catabolic, energy-producing pathways, such as FAO and MRC, are switched on. AMPK activates PGC-1α not only by direct phosphorylation but also by indirect means, for instance by activating the NAD+-dependent deacetylase sirtuin 1, Sirt1, which in turn increases

the amount of deacetylated, active form of PGC-1α (Canto´ et al., 2009). Sirt1 activation by AMPK is mainly due to increased NAD+/NADH ratio, a condition that stimulates Sirt1, as a consequence of AMPK-mediated in- creased expression of FAO (and OXPHOS) genes, and also of the Nampt gene, encoding the enzyme that converts nicotinamide into NAD+ (Canto´ et al., 2009). AMPK is a heterotrimer consisting of a catalytic a subunit and two regulatory subunits, b and g. The latter subunits exist as multiple isoforms, giving 12 different possible combinations of holoenzyme with different tissue distribution and subcellular localization. AMPK is allosterically stimulated by AMP and is itself regulated by phosphorylation via two main upstream AMPK kinases (Cantò and Auwerx, 2010; Steinberg and Kemp, 2009). The major regulatory phosphorylation site of AMPK has been identified as T172 within the catalytic loop between the DFG and APE motifs of the “a” subunit (Fogarty et al., 2010). Besides physiological conditions, PGC-1α and PPARs can also be stimulated or induced pharmacologically. For instance, bezafibrate is a pan-PPAR agonist that is widely used to treat the metabolic syndrome and hyperlipidemias (Tenenbaum et al., 2005). Resveratrol, a natural poly- phenol compound, activates PGC-1α via Sirt1 (Lagouge et al., 2006), and 5-aminoimidazole-4-carboxamide ribonucleoside (AICAR) does so by generating inosine monophosphate, which acts as an AMPK agonist by mimicking AMP (Corton et al., 1995; Merrill et al., 1997).

Mitochondrial disorders are clinical entities associated with

defects of OXPHOS, which are ultimately genetically determined (Wallace, 2010). Mitochondrial disorders can be determined by mutations in mtDNA, or in OXPHOS-related nuclear genes (Zeviani and Di Donato, 2004). Many pathogenic mtDNA mutations are heteroplasmic, i.e., they coexist with a variable percentage of wild-type mtDNA. Clinical symptoms typically ensue when the amount of mutant mtDNA offsets a critical threshold, usually >50%–60% of total mtDNA, below which the mutation has virtually no clinical impact. Likewise, most of the mitochondrial syndromes due to mutations in nuclear genes behave as recessive traits and in many cases are determined either by mutations in ‘‘ancillary’’ proteins that play an arguably relevant, but nevertheless not essential, often partially redundant, role in OXPHOS, or by hypomorphic mutant alleles encoding a crippled but still partially functional protein. These observations have suggested the hypothesis that the deleterious effects of either mtDNA- or nuclear-gene mutations could be overcome, at least partially, by increasing the total amount of mitochondria and/or of functionally active ‘‘MRC units,’’ via activation of the mitochondrial biogenesis program in critical tissues (Bastin et al., 2008; Wenz et al., 2008). This idea has first been tested in cells from mitochondrial disease patients, by overexpressing recombinant *PGC-1*α or by adding bezafibrate in the medium (Bastin et al., 2008; Srivastava et al., 2009). Both treatments showed mutant cells to partially recover MRC activities and increase ATP production. Oral bezafibrate has later been reported to ameliorate the clinical conditions and

the biochemical impairment of a *cre*-lox murine model of COX-defective myopathy, determined by muscle-specific ablation of Cox10, the *heme b* farnesyl transferase, by expressing the cre recombinase under the myosin light-chain 1F (MLC1F) promoter. Here, we report the results of experimental treatments carried out on three other mouse models of COX deficiency: (1) a Surf1 constitutive knockout (KO) mouse, (2) a muscle-specific Cox15 KO mouse, and (3) a constitutive knockout/knockin Sco2 mouse ($Sco2^{KO/KI}$) (Yang et al., 2010) carrying a null Sco2 allele and a second Sco2 allele with a missense mutation E129K, corresponding to the E140K recurrent, pathogenic change in SCO2 mutant patients. Absence of Surf1, an assembly factor of COX, causes severe COX deficiency and fatal Leigh syndrome in children, but milder COX deficiency, and hardly any clinical sign, in mice (Dell'Agnello et al., 2007). Mutations in Cox15, the key enzyme for the conversion of heme o into heme a (Khalimonchuk and Ro¨del, 2005), lead to fatal encephalocardiomyopathy in children (Antonicka et al., 2003; Bugiani et al., 2005) and severe myopathy with marked COX deficiency in muscle-restricted KO mice (this paper). Sco2 is a metallochaperone involved in copper metallation of COX (Leary et al., 2009), mutations in which lead to infantile fatal encephalocardiomyopathy (Papadopoulou et al., 1999).

Materials and Methods

Reagents and Materials

AICAR was from Toronto Research Chemicals. Anti-PGC-1a antibody was from Abcam; anti-AMPK and anti-AMPK-P antibodies were from Cell Signaling; anti-COI and -COX5a were from Invitrogen; anti-GAPDH was from Millipore. Anti-rabbit and anti-mouse secondary antibodies were from Amersham. Chemicals were from Sigma. MCK-PGC-1a and ACTA-Cre transgenic mice were obtained from Jackson Laboratory, Bar Harbor, USA. Oligonucleotides were from PRIMM, Italy. The sequences of all the primers used in this study are available on request.

Western Blot Analysis

Total homogenates were prepared in RIPA buffer (50 mM Tris HCl [pH 8], 150 mM NaCl, 1% NP-40, 0.5% sodium deoxycholate, 0.1% SDS) with the addition of a protease inhibitor cocktail (Roche). Protein concentration was determined by the Lowry method. Aliquots, 80 mg each, were run through a 12% SDS-PAGE and electroblotted onto a nitrocellulose membrane, which was then matched with different antibodies.

In Vivo Experiments

Animal studies were in accordance with the Italian Law D.L. 116/1992 and the EU directive 86/609/CEE. Standard food and water were given ad libitum. Mice were maintained in a temperature- and humidity-controlled animal-care facility, with a

12 hr light/dark cycle and free access to water and food (Standard Diet, Mucedola, Italy). Bezafibrate (Sigma) 0.5% was added to a standard diet (Mucedola, Italy) and administered for 1 month. AICAR or vehicle was administered for 4 weeks with a single daily subcutaneous injection. No difference in daily monitored water and food intake was detected between the treated versus untreated groups of animals during the experiment. Animals were sacrificed by cervical dislocation.

Treadmill Test

A treadmill apparatus (Columbus Instruments, Columbus, OH) was used to measure motor exercise endurance according to the number of falls in the motivational grid during a gradually accelerating program with speed initially at 6.5 m/min and increasing by 0.5 m/min every 3 min. The test was terminated by exhaustion, defined as >10 falls/min into the motivational grid.

Morphological Analysis

Histochemical and ultrastructural analyses were performed as described (Sciacco and Bonilla, 1996; Dubowitz, 1985). TUNEL reaction was performed following the manufacturer's instructions (In Situ Cell Death Detection Kit, Roche, Germany).

Biochemical Analysis of MRC Complexes

Muscle quadriceps samples stored in liquid nitrogen were homogenized in 10 mM phosphate buffer (pH 7.4), and the

spectrophotometric activity of cI, cII, cIII and cIV, as well as CS, was measured as described (Bugiani et al., 2004).

Real-Time PCR

For mtDNA content analysis, SYBR Green real-time PCR was performed using primers specific to a mouse mtDNA region in the *COI* gene and primers specific to RNaseP, a single copy gene taken as a nuclear gene reference, as described (Viscomi et al., 2009). For the analysis of transcripts, total RNA was extracted from liquid nitrogen snap frozen muscle by Trizol, according to the manufacturer's instructions (Invitrogen, Carlsbad, CA, USA). Of total RNA, 2 mg was treated with RNase free-DNase and retrotranscribed using the ''cDNA cycle'' kit (Invitrogen, Carlsbad, CA, USA). Approximately 2–5 ng of cDNA was used for real-time PCR assay using primers specific for amplification of several genes.

Creation of a Recombinant Cox15 KO Mouse

A mouse genomic region spanning *Cox15* exons 1–2 was PCR amplified with suitable oligos to introduce a *loxP* site, and cloned into a vector containing a Neomycin resistance cassette, flanked by two *Flp* sites, and a second *loxP* site. The short and long arms of homology were amplified by PCR using suitable oligos and cloned into the vector containing the floxed region. The final targeting vector was linearized by digestion with XhoI and electroporated in 129Sv cells. A total of 600 clones were PCR screened by PCR (see legend of Figure S2). In one

recombinant clone, homologous recombination was ascertained on the long arm by long-range PCR (see Figure S2). Injection into C57Bl/6 blastocysts was followed by selection of chimaeric individuals, which were then backcrossed to a C57Bl/6 female. The recombinant mice were crossed to a general deleter *cre* transgenic mouse to obtain *Cox15+/-* heterozygous mice, which were then crossed to a *Flpe* transgenic mouse in order to eliminate the neomycin-resistance cassette, resulting in *Cox15lox/lox* individuals. *ACTA-Cox15*$^{-/-}$ mice were eventually obtained by crossing *Cox15*$^{lox/lox}$ with *ACTA-Cre* mice.

Results

Overexpression of PGC-1α increases MRC activities

We first investigated a transgenic mouse that overexpresses *PGC-1*α under the promoter of the skeletal-muscle-specific creatine-kinase (MCK) gene (*MCK-PGC-1*α). Muscle-restricted overexpression of the *PGC-1*α gene in the transgenic individuals was 10.7 ± 2.9-fold that of controls, resulting in a 4-fold steady- state increase in the amount of the PGC-1α protein (Figure 1A). The *MCK-PGC-1*α mice are vital, with hardly any clinically relevant features; however, they did show a 3- to 4-fold increase in both muscle mtDNA content (from 1900 ± 674 to 6706 ± 394 copies/cell) and citrate synthase (CS) activity in muscle homogenate (from 337.9 ± 48.6 to 948.4 ± 139.3 nmol/min/mg of protein), two indexes of mitochondrial mass, compared to WT littermates (Figures 1B and 1C). We also

determined the expression levels of the immediate targets of PGC-1α, i.e., *Nrf1* and *Nrf2*, and of several downstream targets of the latter factors, including *Tfam*, *COI*, *COII*, *COXIV*, and *COX5a* (Figure 1D). The mRNA levels of both *Nrf* genes remained unchanged, whereas the downstream genes were all overexpressed 2- to 3-fold in *MCK-PGC-1*α muscle samples, compared to those of WT littermates. These findings are fully compatible with the role of PGC-1α as a coactivator that increases the transcriptional activity of several factors, including the Nrf's, but is not a transcription factor by itself. Increased expression of COX subunit transcripts was correlated to increased amount of the corresponding proteins, demonstrated by quantitative western blot (WB) immunovisualization (Figure 1A), which resulted in a 1.5- to 2-fold increase in the specific activities of MRC complexes, cI cII, cIII, and cIV (Figure 1C).

PGC-1α is also known to activate factors, e.g., PPARs, that increase the cellular and organelle uptake, and the catabolic oxidation, of fatty acids (FAO). This effect was reflected by a 3.5-fold increased expression in *MCK-PGC-1*α mouse muscle of *CD36/FAT*, a gene encoding the plasma membrane transporter of fatty acids (Figure 1D).

In order to test whether PGC-1α overexpression may correct specific MRC defects in vivo, we then carried out suitable crosses that transferred the MCK-PGC-1α allele into a COX-defective model due to the constitutive ablation of Surf1. Surf1 is a putative assembly factor specific to COX, its absence being associated with profound COX deficiency in humans (%10%–

15% of the lower normal limit in different cell types) and, albeit milder, in mice as well (typically 30%–40% of the lower normal limit). While the loss of Surf1 causes early onset, invariably fatal Leigh encephalopathy in patients, recombinant null mice showed hardly any clinically deleterious consequence, and standard treadmill test showed no locomotor impairment.

The skeletal muscle of Surf1$^{-/-}$/MCK-PGC-1α double mutant mice did show the same effects detected in MCK-PGC-1α trans- genic muscles: increased mtDNA content (from 2078 ± 693 to 4079 ± 824 copies/cell) and CS activity (from 343 ± 33 to 934 ± 226 nmol/min/mg) (Figures 1B and 1C), increased levels of CD36/FAT transcript, and increased levels of COX-specific mRNA and protein subunits (Figures 1A and 1D). These changes resulted in (1) partial but significant recovery of COX specific activity (1.6-fold, from 104 ± 24 to 162 ± 42 nmol/min/mg; $p = 0.02$) (Figure 1C), which nevertheless remained well below the normal range (370 ± 49 nmol/min/mg); and (2) increased histochemical reaction to COX (Figure 1E). Taken together, these data suggest that overexpression of PGC-1α induces mitochondrial biogenesis and can partially correct a specific defect of COX in vivo.

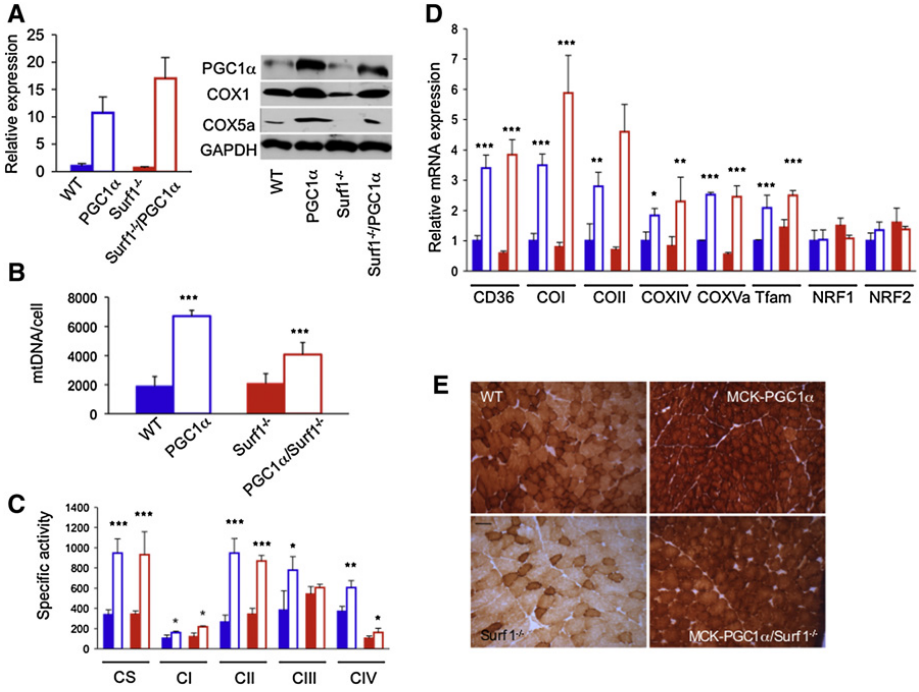

Figure 1: Effects of PGC-1α Overexpression in Surf1$^{-/-}$ Mice

(A) Expression analysis of PGC-1α. (Left panel). Solid blue, WT; blue outline, PGC-1α: MCK-PGC-1α transgenic mouse; solid red, Surf1$^{-/-}$, constitutive Surf1 knockout mouse; red outline, Surf1$^{-/-}$/PGC-1α: Surf1$^{-/-}$/MCK-PGC-1α double mutant mouse. Error bars represent the standard deviation (SD). (Right panel) Western blot immunovisualization of skeletal muscle proteins of the different genotypes, listed as above.

(B) MtDNA analysis in different genotypes MtDNA is expressed as number of DNA molecules per cell.

(C) MRC activities in the different genotypes, expressed as nmoles/min/mg of protein. Note that the activity of cII has been multiplied by 10 for visualization clarity.). CS, citrate synthase; CI-IV, MRC complexes I–IV. The asterisks represent the significance levels calculated by unpaired, Student's two-tailed t test: *p < 0.05; **p < 0.01; ***p < 0.001.

(D) Expression analysis of FAO- and OXPHOS-related genes

(E) COX staining in muscles from different mouse lines. Scale bar, 25 mm, magnification 20x.

Bezafibrate induces Expression of FAO- but not OXPHOS-related genes

In a second set of experiments, we then tested the effects of PPAR activation in the *Surf1*$^{-/-}$ mouse model. To this end, the same genes, proteins, and activities measured in the *MCK-PGC-1*α and *Surf1*$^{-/-}$*/MCK-PGC-1*α mouse models were also measured in *Surf1*$^{-/-}$ and WT littermates exposed to 0.5% bezafibrate, mixed in standard food for 1 month (Wenz et al., 2008). We observed significant body weight loss during the treatment and marked hepatomegaly at the end of treatment, in both *Surf1*$^{-/-}$ and WT animals (Figure S1), indicating toxicity of this drug in mice. As expected, the expression of PPAR β/δ and PPAR α, the two PPAR isoforms present in skeletal muscle, was significantly increased in treated animals, along with FAO-related genes, including *CD36/FAT*, *ACOX*, encoding acylCoA oxidase, and *SCAD*, encoding short-chain acylCoA dehydrogenase (Figure 2A). Taken together, these data clearly demonstrated that bezafibrate treatment was indeed effective on the main targets specific for this drug in vivo. Contrariwise, no significant change in mtDNA content, CS, and MRC activities was measured in treated versus untreated *Surf1*$^{-/-}$ or WT muscles (Figures 2B and 2C), and the histochemical reaction to COX was equally defective in both treated and untreated *Surf1*$^{-/-}$ specimens (Figure 2D). Accordingly, the expression of *PGC-1*α, both *NRFs*, and *Tfam* remained unchanged among the different groups of animals, as did several COX subunit transcripts from either nuclear (e.g.,

COXIV) or mtDNA (*COI* and *COII*) genes (Figure 2A).

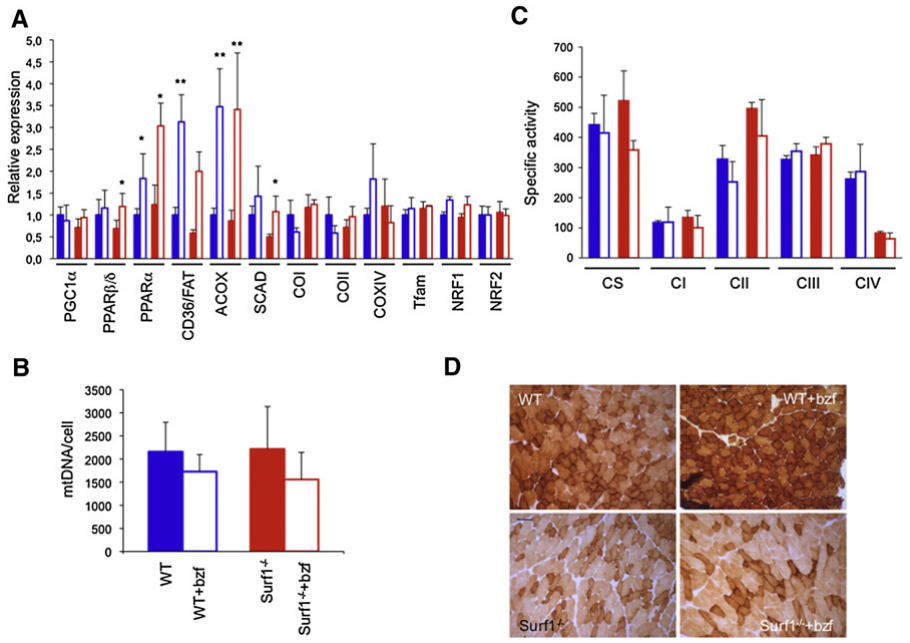

Figure 2. Bezafibrate treatment on the Surf1$^{-/-}$ mouse model
(A) Expression analysis of FAO- and OXPHOS- related genes in Surf1$^{-/-}$ and WT muscles of bezafibrate (bzf)-treated and untreated mice. Solid blue, WT, untreated; blue outline, bzf-treated WT; solid red, Surf1$^{-/-}$, untreated; red outline, bzf- treated Surf1$^{-/-}$.
(B) MtDNA content analysis in the different genotypes.
(C) MRC activities in the different genotypes, expressed as nmoles/min/mg of protein. Note that the activity of cII has been multiplied by 10 for visualization clarity.
(D) COX staining in muscles from *Surf1*$^{-/-}$ and WT muscles of bzf-treated and untreated mice. Scale bar, 25 mm, magnification 20x.

A muscle-specific Cox15 KO mouse displays COX-defective mitochondrial myopathy

Since our results failed to confirm those on bezafibrate treatment reported in the *MLC1F-Cox10*$^{-/-}$ mouse model (Wenz et al., 2008), we created a KO mouse for the *Cox15* gene, using the *cre*-lox technology (Figures S2A and S2B). The *Cox15* gene product is the enzyme that comes next to Cox10 in the biosynthetic pathway of *heme a*, the COX-specific *heme* moiety. Cox10 adds a farnesyl chain to *heme b*, converting it into *heme o*, which can then be inserted into the protein backbone of nascent COX. Cox15 eventually converts *heme o* into functionally active *heme a* by oxidation of the C8-methyl group (Khalimonchuk and Ro¨ del, 2005). The constitutive *Cox15*$^{-/-}$ animals, obtained by crossing *Cox15loxP/loxP* mice with a general *cre*-deleter transgenic mouse, showed consistent embryonic lethality at 7.5 dpc (not shown). We then produced a muscle-specific *Cox15*$^{-/-}$ model by crossing *Cox15loxP/loxP* with a transgenic mouse expressing the *cre* recombinase under the control of the human skeletal muscle-specific a-actin (ACTA1) promoter (*ACTA-Cox15 or Cox15*$^{sm/sm}$ mouse).

Recombination of the *Cox15* locus by the *cre* recombinase was detected only in skeletal muscle and, in trace amount, in the heart, whereas no recombination occurs in other tissues (Figure S2C). Accordingly, the amount of *Cox15* mRNA in *ACTA-Cox15*$^{-/-}$ mouse skeletal muscle was ≈16% than that of WT muscle (Figure 3A), and so was the COX/CS ratio (0.05 ± 0.02 in *ACTA-Cox15*$^{-/-}$ versus 0.66 ± 0.06 in WT), whereas there was

no significant difference in other tissues (Figure 3B). Albeit born at the expected mendelian ratio, the *ACTA-Cox15*$^{-/-}$ mice were smaller than WT littermates at 30 days after birth (data not shown) and had significantly reduced motor performance measured by a standard treadmill test, initially administered to 4-week-old individuals, and then repeated at 6, 8, 12, and 16 weeks (Figure 3C). Histochemical analysis in skeletal muscle confirmed severe reduction of COX and compensatory proliferation of aberrant mitochondria (Figure 3D), which was confirmed by increased mtDNA content (Figure 3E), increased cII and CS activities (Table S1), and increased SDH histochemical reaction (data not shown), in *ACTA-Cox15*$^{-/-}$ muscles. COX histochemistry was normal in other tissues (data not shown). Except for cII activity, which increased from 24.2 ± 4.2 in WT to 34.9 ± 7.8 in *ACTA-Cox15*$^{-/-}$ muscle homogenate, other MRC activities, including cI and cIII, in muscle (Table S1), and all the MRC activities in non muscle tissues (data not shown), of *ACTA-Cox15*$^{-/-}$ were comparable to those of WT littermates.

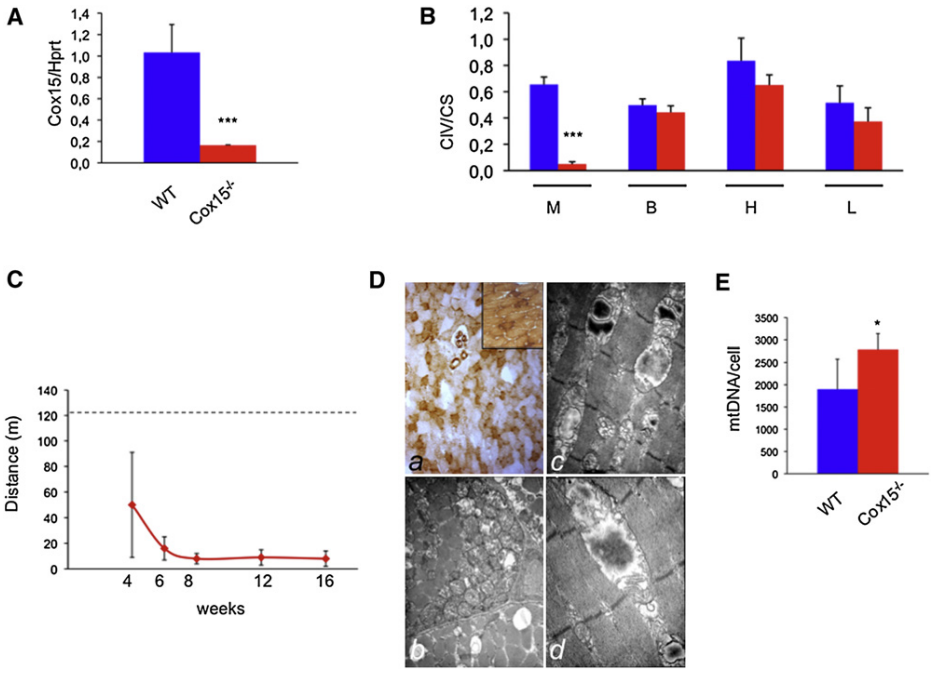

Figure 3. Characterization of the ACTA-Cox15$^{-/-}$ mouse model
(A) *Cox15* transcript levels in skeletal muscle. The *Cox15*-specific mRNA content is ≈ 15% in *ACTA-Cox15*$^{-/-}$ relative to the parental *Cox15*$^{lox/lox}$ mouse line, considered as wild-type (WT).
(B) COX (CIV)-specific activity normalized to that of citrate synthase (CS) in tissues from *ACTA-Cox15*$^{-/-}$ mice. M, muscle; B, brain; H, heart; L, liver.
(C) Treadmill analysis of *ACTA-Cox15*$^{-/-}$ mice at different time points. The dotted line indicates the lower limit of the motor performance of the parental *Cox15*$^{lox/lox}$ mouse line, considered as WT.
(D) (Top) COX staining from *ACTA-Cox15*$^{-/-}$ skeletal muscle. Magnification 20x. (Bottom) Electron microscopy analysis of *ACTA-Cox15*$^{-/-}$ skeletal muscle (magnification 7000x)
(E) MtDNA content in *Cox15*$^{lox/lox}$ (WT) and *ACTA-Cox15*$^{-/-}$ skeletal muscles.

Bezafibrate is highly toxic to ACTA-Cox15$^{-/-}$ mice

We then tested the response of eight *ACTA-Cox15*$^{-/-}$ female mice to bezafibrate, according to the same protocol used on the *Surf1*$^{-/-}$ and *MLC1F-Cox10*$^{-/-}$ models. However, after 24–48 hr

from the treatment start, the *ACTA-Cox15*$^{-/-}$ animals became critically ill, prompting us to euthanize them. We found worsening of the mitochondrial myopathy (Figures S3A and S3B), and massive apoptosis, demonstrated by numerous TUNEL-positive nuclei (Figures S3C and S3D), corresponding ultrastructurally to chromatin condensation and apoptotic bodies (Figures S3E and S3F). No increased levels of plasma creatine kinase, urea, creatinine, or lactate were detected in plasma of euthanized animals, as observed in massive rhabdo- myolysis and acute kidney failure, an adverse effect occasionally reported in patients under bezafibrate treatment (Charach et al., 2005; Wu et al., 2009).

AICAR Induces FAO and OXPHOS Genes in Surf1$^{-/-}$, Sco2$^{KO/KI}$, and ACTA-Cox15$^{-/-}$ Muscle

In a third set of experiments, we tested the capacity of AICAR, an AMPK agonist, to activate PGC-1α in our animal models. AICAR was given for 1 month in daily subcutaneous injections of 0.25 mg/day/gm of body weight to 2-month-old *Surf1*$^{-/-}$, *Sco2*$^{KO/KI}$, and WT littermates, and of 0.5 mg/day/gm to 2-month-old *ACTA-Cox15*$^{-/-}$ animals and WT littermates, each group being composed of three/four individuals (see legends of Figures 4–6 for details). At the end of treatment, the mtDNA content (data not shown) and CS activity in skeletal muscle (Table S2) were similar in each treated group versus the corresponding untreated group. Analysis of selected transcripts (Figures 4A, 5A, and 6A) showed that, similar to the *MCK-PGC-1α* overexpressing mice, *Nrf1* and *Nrf2* gene expression was

unchanged in all groups; however, both *Tfam* and the COX subunit encoding genes were significantly increased in treated versus untreated *Surf1*$^{-/-}$ ($p < 0.05$), *Sco2*$^{KO/KI}$ ($p < 0.01$), and *ACTA-Cox15*$^{-/-}$ muscles ($p < 0.01$). Increased expression of these genes was observed in treated WT mice exposed to the higher (0.5 mg/gm) but not to the lower (0.25 mg/gm) dosage ($p < 0.01$). The expression of the FAO- related *CD36/FAT* gene was significantly increased in all treated groups. *PDK4* and *UCP3*, two genes that are activated by AMPK independently from PGC-1α, were also increased under AICAR treatment. Immunovisualization of selected proteins (Figures 4B, 5B, and 6B) showed that increased expression of COX subunit genes was paralleled by increased amount of COX1 and COX5a proteins in treated *Surf1*$^{-/-}$, *Sco2*$^{KO/KI}$, and *ACTA-Cox15*$^{-/-}$ mice, resulting in significantly increased COX-specific activity (Figures 4C, 5C, and 6C and Tables S2–S4; $p < 0.01$). We also immunovisualized T172-phosphorylated (AMPK-PT172) versus total muscle AMPK (Figures 4B, 5B, and 6B). Interestingly, the levels of AMPK-PT172 were already 8-fold higher in untreated *Surf1*$^{-/-}$ than in untreated WT mice, whereas total AMPK was unchanged. A similar result was obtained in the untreated *ACTA-Cox15*$^{-/-}$ and, albeit less pronounced, in *Sco2*$^{KO/KI}$ muscles. AICAR further increased AMPK phosphorylation in all three COX-defective models, and in WT littermates as well. The quantitative biochemical results obtained by spectrophotometric assays (Figures 4C, 5C, and 6C and Tables S2, S3, and S4) were paralleled by a similar, albeit merely qualitative, trend

shown by histochemical reactions to COX (Figures 4D, 5D, and 6D), SDH (Figures 5D and 6D), and, in treated *ACTA-Cox15*$^{-/-}$ mice, by marked decrease of ultrastructural abnormalities in mitochondria (Figure 6D). Taken together, these results indicate a compensatory activation of the AMPK-Pgc1α axis in conditions of defective COX activity.

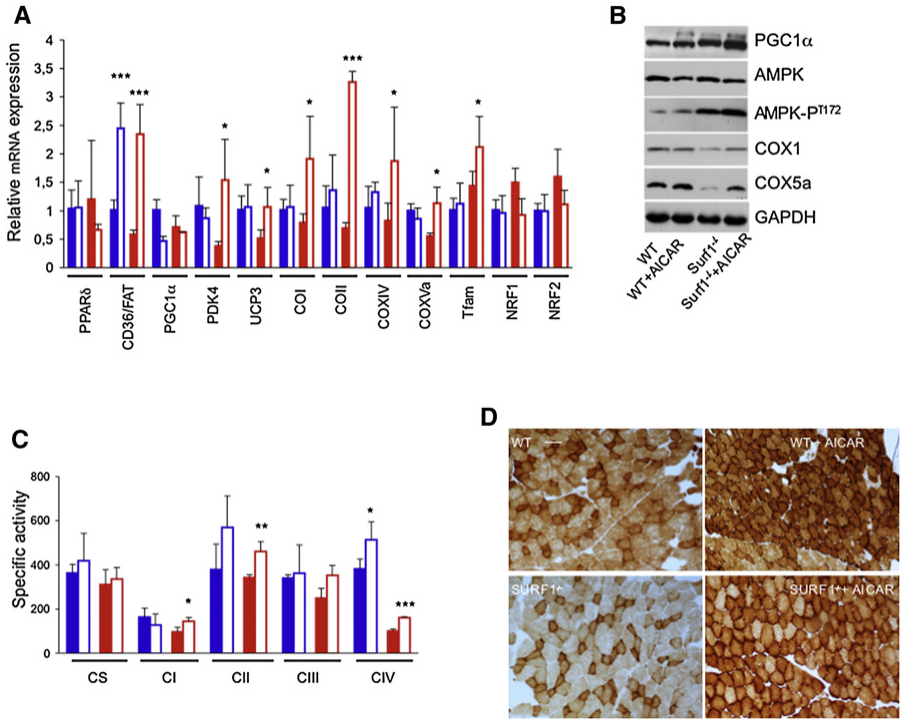

Figure 4. AICAR Treatment in Surf1$^{-/-}$ Mice

(A) Expression analysis of FAO- and OXPHOS- related genes in *Surf1*$^{-/-}$ and WT muscles of AICAR-treated (0.25 mg/day/gm) and untreated mice. Solid blue, WT, untreated; blue outline, AICAR-treated WT; solid red, *Surf1*$^{-/-}$, untreated; red outline, AICAR-treated *Surf1*$^{-/-}$.

(B) Western blot immunovisualization of skeletal muscle proteins of the different genotypes, listed as above.

(C) MRC activities in the different genotypes, AICAR-treated or untreated. Note that the activity of cII has been multiplied by 10 for visualization clarity

D) COX staining in skeletal muscles from AICAR-treated and untreated

Surf1$^{-/-}$ and WT littermates. Magnification 20x

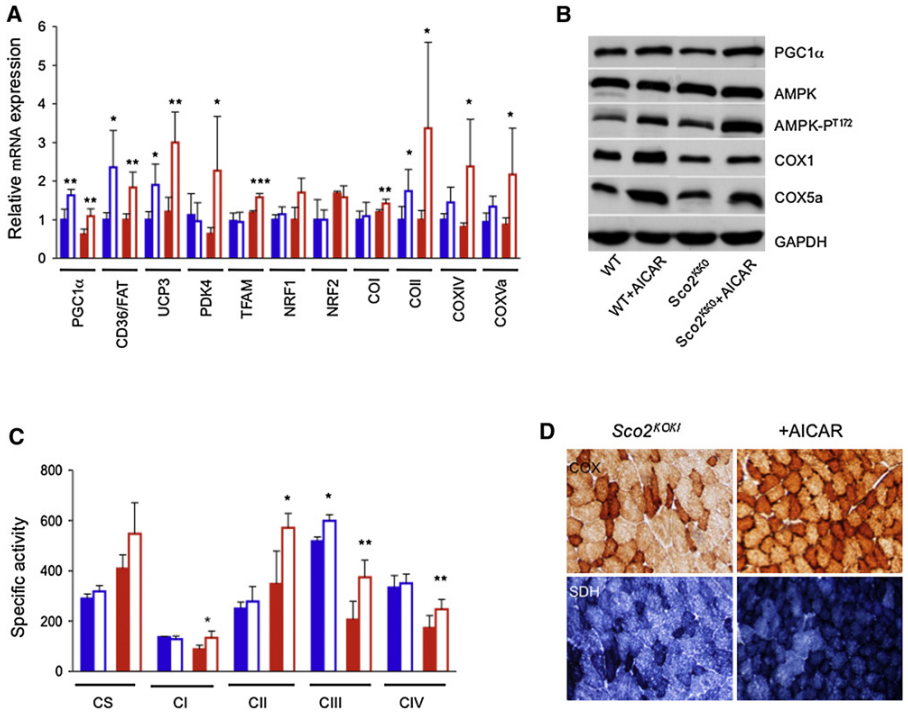

Figure 5. AICAR Treatment in Sco2$^{KO/KI}$ Mice

(A) Expression analysis of FAO- and OXPHOS-related genes in *Sco2*$^{KO/KI}$ and WT muscles of AICAR-treated (0.25 mg/day/gm) and untreated mice. Solid blue, WT, untreated; blue outline, AICAR-treated WT; solid red, *Sco2*$^{KO/KI}$, untreated; red outline, AICAR-treated *Sco2*$^{KO/KI}$.

(B) Western blot immunovisualization of skeletal muscle proteins of the different genotypes, listed as above.

(C) MRC-specific activities in the different genotypes, AICAR-treated or untreated, expressed as nmoles/min/mg of protein. Note that the activity of cII has been multiplied by 10 for visualization clarity.

(D) COX and SDH staining in skeletal muscles from AICAR-treated and untreated *Sco2*$^{KO/KI}$ and WT littermates.

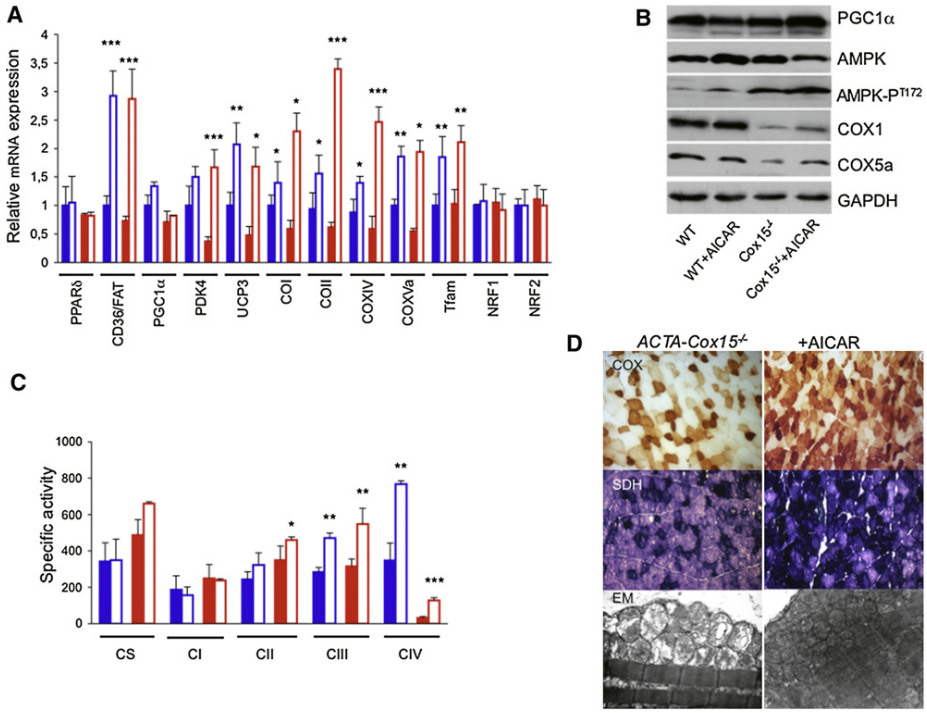

Figure 6. AICAR Treatment in ACTA-Cox15$^{-/-}$ Mice

(A) Expression analysis of FAO- and OXPHOS-related genes in *ACTA-Cox15*$^{-/-}$ and WT muscles of AICAR-treated (0.5 mg/day/gm) and untreated mice. Solid blue, WT, untreated; blue outline, AICAR-treated WT; solid red, *ACTA-Cox15*$^{-/-}$.

(B) Western blot immunovisualization of skeletal muscle proteins of the different genotypes, listed as above.

C) MRC-specific activities in the different genotypes, AICAR-treated or untreated, expressed as nmoles/min/mg of protein. Note that the activity of cII has been multiplied by 10 for visualization clarity.

(D) COX (upper panel) and SDH (middle panel) staining in AICAR-treated and untreated *ACTA-Cox15*$^{-/-}$ and WT muscle. Magnification, 20x. (Bottom) EM of muscles from untreated and AICAR-treated muscles.

Effect of AICAR Treatment on Motor Performance

In order to evaluate the clinical effect of treatment, we administered a standard, quantitative incremental motor endurance test using a treadmill device. The motor performance was similar to WT littermates in untreated *Surf1*$^{-/-}$ mice, significantly impaired in *Sco2*$^{KO/KI}$ mice, and extremely impaired in *ACTA-Cox15*$^{-/-}$ mice, which were able to walk on the treadmill for just a couple of minutes (Figure 7A). Since no motor phenotype was detected in *Surf1*$^{-/-}$ mice, we focused our analysis on the other two COX-defective models that did show motor impairment. In treated *Sco2*$^{KO/KI}$ mice, the biochemical improvement was mirrored by marked amelioration of motor performance, which reached the same score as the untrained WT littermates by the first to second week of treatment (Figure 7B). Contrariwise, and in spite of partial biochemical recovery, we found no change by treadmill test in *ACTA-Cox15*$^{-/-}$ mice, suggesting that the mitochondrial myopathy was too severe for AICAR treatment to achieve a clinically detectable effect (Figure 7C).

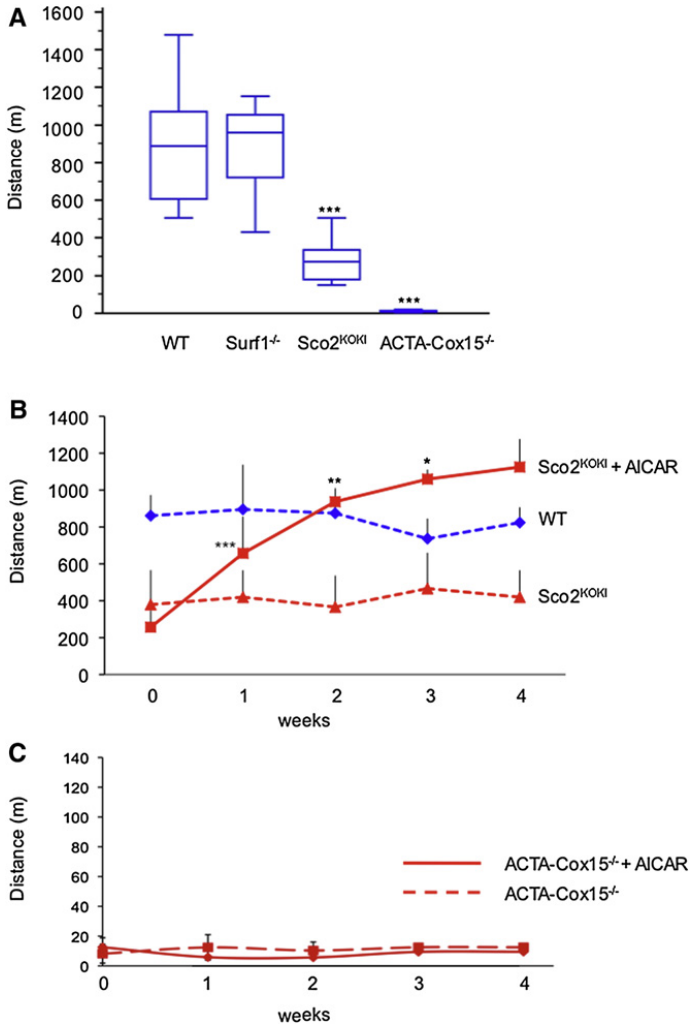

Figure 7. Treadmill test

(A) Box-and-whisker plot of treadmill tests administered to WT (n. 16), *Surf1*$^{-/-}$ (n. 11), *Sco2*$^{KO/KI}$ (n. 9), and *ACTA-Cox15*$^{-/-}$ (n. 11) mice at 3 months of age.

(B) Treadmill test in AICAR-treated *Sco2*$^{KO/KI}$ and in untreated *Sco2KO/KI* and WT littermates. Each group was composed of four individuals.

(C) Treadmill test in untreated and AICAR-treated *ACTA-Cox15*$^{-/-}$ mice.

Acknowledgments

This work was supported by the Pierfranco and Luisa Mariani Foundation Italy; Fondazione Telethon-Italy grants numbers GGP07019 and GPP10005; Fondazione Tomasello and Associazione Mitocon to M.Z.; the National Institutes of Health (grant HD32062), the Muscular Dystrophy Association, and the Marriott Mitochondrial Disorder Clinical Research Fund to E.A.S.; and the ‘‘Associazione Amici del Centro Dino Ferrari’’ to M.M.

References

Antonicka, H., Mattman, A., Carlson, C.G., Glerum, D.M., Hoffbuhr, K.C., Leary, S.C., Kennaway, N.G., and Shoubridge, E.A. (2003). Mutations in COX15 produce a defect in the mitochondrial heme biosynthetic pathway, causing early-onset fatal hypertrophic cardiomyopathy. Am. J. Hum. Genet. *72*, 101–114.

Barish, G.D., Narkar, V.A., and Evans, R.M. (2006). PPAR delta: a dagger in the heart of the metabolic syndrome. J. Clin. Invest. *116*, 590–597.

Bastin, J., Aubey, F., Rotig, A., Munnich, A., and Djouadi, F. (2008). Activation of peroxisome proliferator activated receptor pathway stimulates the mitochondrial respiratory chain and can correct deficiencies in patients’ cells lacking its components. J. Clin. Endocrinol. Metab. *4*, 1433–1441.

Bugiani, M., Invernizzi, F., Alberio, S., Briem, E., Lamantea, E., Carrara, F., Moroni, I., Farina, L., Spada, M., Donati, M.A., et al. (2004). Clinical and molecular findings in children with complex I deficiency. Biochim. Biophys. Acta *1659*, 136–147.

Bugiani, M., Tiranti, V., Farina, L., Uziel, G., and Zeviani, M. (2005). Novel mutations in COX15 in a long surviving Leigh syndrome patient with cytochrome c oxidase deficiency. J. Med. Genet. *42*, e28. 10.1136/jmg.2004. 029926.

Canto´ C., and Auwerx, J. (2010). AMP-activated protein kinase and its down- stream transcriptional pathways. Cell. Mol. Life Sci. *67*, 3407–3423.

Cantò, C., Gerhart-Hines, Z., Feige, J.N., Lagouge, M., Noriega, L., Milne, J.C., Elliott, P.J., Puigserver, P., and Auwerx, J. (2009). AMPK regulates energy expenditure by modulating NAD+ metabolism and SIRT1 activity. Nature *458*, 1056–1060.
Charach, G., Grosskopf, I., Rotmensch, H.H., Kitzis, I., and Weintraub, M. (2005). Bezafibrates cause moderate, reversible impairment in renal function in patients without prior renal disease. Nephron Clin. Pract. *100*, c120–c125. Corton, J.M., Gillespie, J.G., Hawley, S.A., and Hardie, D.G. (1995). 5-amino-imidazole-4-carboxamide ribonucleoside. A specific method for activating AMP-activated protein kinase in intact cells? Eur. J. Biochem. *229*, 558–565. Cree, L.M., Patel, S.K., Pyle, A., Lynn, S., Turnbull, D.M., Chinnery, P.F., and Walker, M. (2008). Age-related decline in mitochondrial DNA copy number in isolated human pancreatic islets. Diabetologia *51*, 1440–1443.
Dell'Agnello, C., Leo, S., Agostino, A., Szabadkai, G., Tiveron, C., Zulian, A., Prelle, A., Roubertoux, P., Rizzuto, R., and Zeviani, M. (2007). Increased longevity and refractoriness to Ca(2+)-dependent neurodegeneration in Surf1 knockout mice. Hum. Mol. Genet. *16*, 431–444.
Dubowitz, V. (1985). Muscle Biopsy, A Practical Approach, 2nd ed. (London: Baillie` re Tindall). Fogarty, S., Hawley, S.A., Green, K.A., Saner, N., Mustard, K.J., and Hardie, D.G. (2010). Calmodulin-dependent protein kinase kinase-b activates AMPK without forming a stable complex: synergistic effects of Ca2+ and AMP. Biochem. J. *426*, 109–118.
Gerhart-Hines, Z., Rodgers, J.T., Bare, O., Lerin, C., Kim, S.H., Mostoslavsky, R., Alt, F.W., Wu, Z., and Puigserver, P. (2007). Metabolic control of muscle mitochondrial function and fatty acid oxidation through SIRT1/PGC-1alpha. EMBO J. *26*, 1913–1923.
Goldman, S.J., Taylor, R., Zhang, Y., and Jin, S. (2010). Autophagy and the degradation of mitochondria. Mitochondrion *10*, 309–315. Handschin, C., and Spiegelman, B.M. (2006). Peroxisome proliferator- activated receptor gamma coactivator 1 coactivators, energy homeostasis, and metabolism. Endocr. Rev. *27*, 728–735.
Ja¨ger, S., Handschin, C., St-Pierre, J., and Spiegelman, B.M. (2007). AMP- activated protein kinase (AMPK) action in skeletal muscle via direct phosphorylation of PGC-1alpha. Proc. Natl.

Acad. Sci. USA *104*, 12017–12022. Kelly, D.P., and Scarpulla, R.C. (2004). Transcriptional regulatory circuits controlling mitochondrial biogenesis and function. Genes Dev. *18*, 357–368. Khalimonchuk, O., and Ro¨ del, G. (2005). Biogenesis of cytochrome c oxidase. Mitochondrion *5*, 363–388.
Kleiner, S., Nguyen-Tran, V., Bare´ , O., Huang, X., Spiegelman, B., and Wu, Z. (2009). PPAR{delta} agonism activates fatty acid oxidation via PGC-1{alpha} but does not increase mitochondrial gene expression and function. J. Biol. Chem. *284*, 18624–18633.
Lagouge, M., Argmann, C., Gerhart-Hines, Z., Meziane, H., Lerin, C., Daussin, F., Messadeq, N., Milne, J., Lambert, P., Elliott, P., et al. (2006). Resveratrol improves mitochondrial function and protects against metabolic disease by activating SIRT1 and PGC-1alpha. Cell *127*, 1109–1122.
Leary, S.C., Sasarman, F., Nishimura, T., and Shoubridge, E.A. (2009). Human SCO2 is required for the synthesis of CO II and as a thiol-disulphide oxidore- ductase for SCO1. Hum. Mol. Genet. *18*, 2230–2240. Lefebvre, P., Chinetti, G., Fruchart, J.C., and Staels, B. (2006). Sorting out the roles of PPAR alpha in energy metabolism and vascular homeostasis. J. Clin. Invest. *116*, 571–580.
Lin, J., Wu, H., Tarr, P.T., Zhang, C.-Y., Wu, Z., Boss, O., Michael, L.F., Puigserver, P., Isotani, E., Olson, E.N., et al. (2002). Transcriptional co-acti- vator PGC-1a drives the formation of slow-twitch muscle fibers. Nature *418*, 797–801.
Luquet, S., Lopez-Soriano, J., Holst, D., Fredenrich, A., Melki, J., Rassoulzadegan, M., and Grimaldi, P.A. (2003). Peroxisome proliferator-acti- vated receptor delta controls muscle development and oxidative capability. FASEB J. *17*, 2299–2301.
Merrill, G.F., Kurth, E.J., Hardie, D.G., and Winder, W.W. (1997). AICA riboside increases AMP-activated protein kinase, fatty acid oxidation, and glucose uptake in rat muscle. Am. J. Physiol. *273*, 1107–1112.
Papadopoulou, L.C., Sue, C.M., Davidson, M.M., Tanji, K., Nishino, I., Sadlock, J.E., Krishna, S., Walker, W., Selby, J., Glerum, D.M., et al. (1999). Fatal infantile cardioencephalomyopathy with COX deficiency and mutations in SCO2, a COX assembly gene. Nat. Genet. *23*, 333–337.

Sciacco, M., and Bonilla, E. (1996). Cytochemistry and immunocytochemistry of mitochondria in tissue sections. Methods Enzymol. *264*, 509–521.
Srivastava, S., Diaz, F., Iommarini, L., Aure, K., Lombes, A., and Moraes, C.T. (2009). PGC-1alpha/beta induced expression partially compensates for respiratory chain defects in cells from patients with mitochondrial disorders. Hum. Mol. Genet. *18*, 1805–1812.
Steinberg, G.R., and Kemp, B.E. (2009). AMPK in health and disease. Physiol. Rev. *89*, 1025–1078.
Tenenbaum, A., Motro, M., and Fisman, E.Z. (2005). Dual and pan-peroxisome proliferator-activated receptors (PPAR) co-agonism: the bezafibrate lessons. Cardiovasc. Diabetol. *16*, 4–14.
Tiranti, V., Galimberti, C., Nijtmans, L., Bovolenta, S., Perini, M.P., and Zeviani, M. (1999). Characterization of SURF-1 expression and Surf-1p function in normal and disease conditions. Hum. Mol. Genet. *8*, 2533–2540.
Viscomi, C., Spinazzola, A., Maggioni, M., Fernandez-Vizarra, E., Massa, V., Pagano, C., Vettor, R., Mora, M., and Zeviani, M. (2009). Early-onset liver mtDNA depletion and late-onset proteinuric nephropathy in Mpv17 knockout mice. Hum. Mol. Genet. *18*, 12–26.
Wallace, D.C. (2005). A mitochondrial paradigm of metabolic and degenerative diseases, aging, and cancer: a dawn for evolutionary medicine. Annu. Rev. Genet. *39*, 359–407.
Wallace, D.C. (2010). Mitochondrial energetics and therapeutics. Annu. Rev. Pathol. *5*, 297–348.
Wallace, D.C., and Fan, W. (2010). Energetics, epigenetics, mitochondrial genetics. Mitochondrion *10*, 12–31.
Wang, Y.X., Zhang, C.L., Yu, R.T., Cho, H.K., Nelson, M.C., Bayuga-Ocampo, C.R., Ham, J., Kang, H., and Evans, R.M. (2004). Regulation of muscle fiber type and running endurance by PPARdelta. PLoS Biol. *2*, e294. 10.1371/journal.pbio.0020294.
Wenz, T., Diaz, F., Spiegelman, B.M., and Moraes, C.T. (2008). Activation of the PPAR/PGC-1alpha pathway prevents a bioenergetic deficit and effectively improves a mitochondrial myopathy phenotype. Cell Metab. *8*, 249–256.

Wu, J., Song, Y., Li, H., and Chen, J. (2009). Rhabdomyolysis associated with fibrate therapy: review of 76 published cases and a new case report. Eur. J. Clin. Pharmacol. *65*, 1169–1174.
Yang, H., Brosel, S., Acin-Perez, R., Slavkovich, V., Nishino, I., Khan, R., Goldberg, I.J., Graziano, J., Manfredi, G., and Schon, E.A. (2010). Analysis of mouse models of cytochrome c oxidase deficiency owing to mutations in Sco2. Hum. Mol. Genet. *19*, 170–180.
Zeviani, M., and Di Donato, S. (2004). Mitochondrial disorders. Brain *127*, 2153–2172.

Supplemental information

Table S1: Specific activities of citrate synthase (CS) and MRC complexes (CI-IV) in ACTA-Cox15$^{-/-}$ mice (n.3) and COX15$^{lox/lox}$ (n.3), considered as WT. Values are expressed as nanomoles/min/mg protein

	CS	**CI**	**CII***	**CIII**	**CIV*****
CTR	354.7±103.5	186.0±77.4	24.2±4.2	283.3±26.4	347.0±97.1
Cox15$^{-/-}$	487.3±84.9	248.0±77.8	35.0±7.8	314.7±41	30.7±9.2

* Student's *t* test p<0.05
*** Student's *t* test p<0.005

Table S2. Specific activities of MRC complexes CI-IV and citrate synthase (CS) of Surf1$^{-/-}$ and WT littermates. Values are expressed as nanomoles/min/mg protein

	CS	**CI**	**CII**	**CIII**	**CIV**
WT	363.3±39.2	163.3±39.7	37.9±11.5	339.9±15.5	382.5±45.2
WT AICAR	418.8±124.0	127.5±50.2	56.9±14.3	362.6±127.2	514.3±80.5*
Surf1$^{-/-}$	310.8±66.8	96.2±21.2	34.2±13.7	249.7±44.3	100.6±7.8
Surf1$^{-/-}$+AICAR	336.4±52.3	144.6±18.1*	46.1±4.4**	352.6±45.8*	161.0±3.5***

Student's *t* test *p<0.05; **p<0.01; ***p<0.001

Table S3. Specific activities of MRC complexes CI-IV and citrate synthase (CS) of Sco2^{KOKI} and WT littermates. Values are expressed as nanomoles/min/mg protein

	CS	**CI**	**CII**	**CIII**	**CIV**
WT	289.0±104.0	136.3±77.3	24.9±2.6	517.3±17.5	332.8±48.2
WT+AICAR	349.0±115.1	156.5±47.2	32.3±6.7	598.6±24.2*	350.3±36.0
Sco2^{KOKI}	408.0±55.4	88.2±16.2	34.7±13.7	206.0±41.3	172.6±49.8
Sco2^{KOKI} AICAR	546.2±123.2	134.6±26.1*	57.1±5.6*	374.6±85.8*	247.0±39.5**

Student's *t* test *p<0.05; **p<0.01

Table S4. Specific activities of MRC complexes CI-IV and citrate synthase (CS) of ACTA-Cox15$^{-/-}$ and WT littermates. Values are expressed as nanomoles/min/mg protein

	CS	**CI**	**CII**	**CIII**	**CIV**
WT	341.2±104.6	186.1±77.3	24.2±4.2	283.1±26.7	347.2±97.2
WT AICAR	349.2±115.3	156.6±47.5	32.3±6.7	471.4±27.3**	768.2±17.2**
Cox15$^{-/-}$	487.3±85.1	248.0±78.1	34.9±7.8	315.3±41.2	30.7±9.0
Cox15$^{-/-}$+AICAR	661.1±9.1	237.6±10.2	46.0±17.6*	549.3±86.1**	127.5±15.4***

Student's *t* test *p<0.05; **p<0.01; ***p<0.001

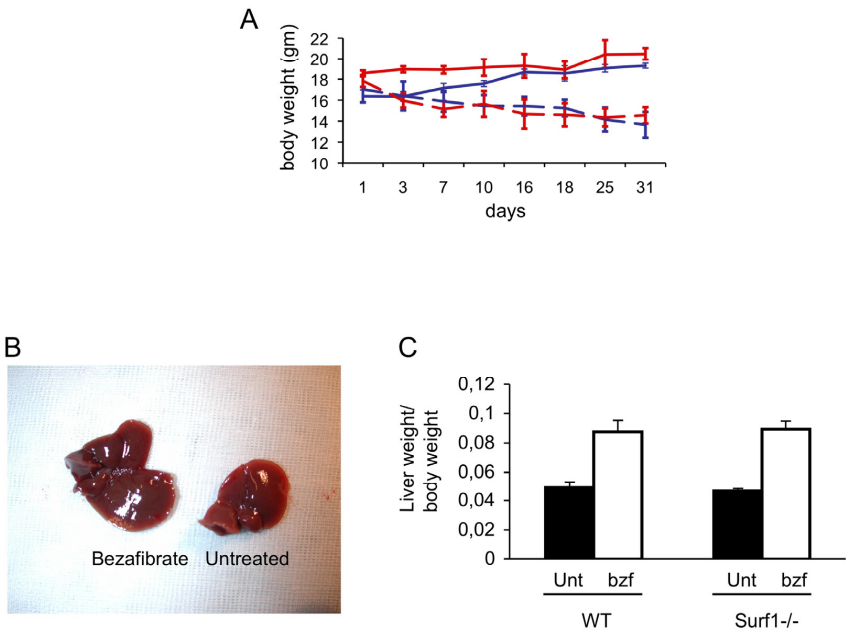

Figure S1. Bezafibrate treatment in Surf1$^{-/-}$ mice.

A: body weight during treatment. Red lines: Surf1$^{-/-}$ mice (n. 3). Blue lines: WT littermates (n. 3). Continuous lines: untreated animals. Dotted lines: treated animals (see main text for details).

B: liver enlargement at autopsy of a treated vs. an untreated Surf1$^{-/-}$ mice.

C: liver weight/body weight in untreated (Unt) vs. treated (bzf) animals (n. 3 for each group).

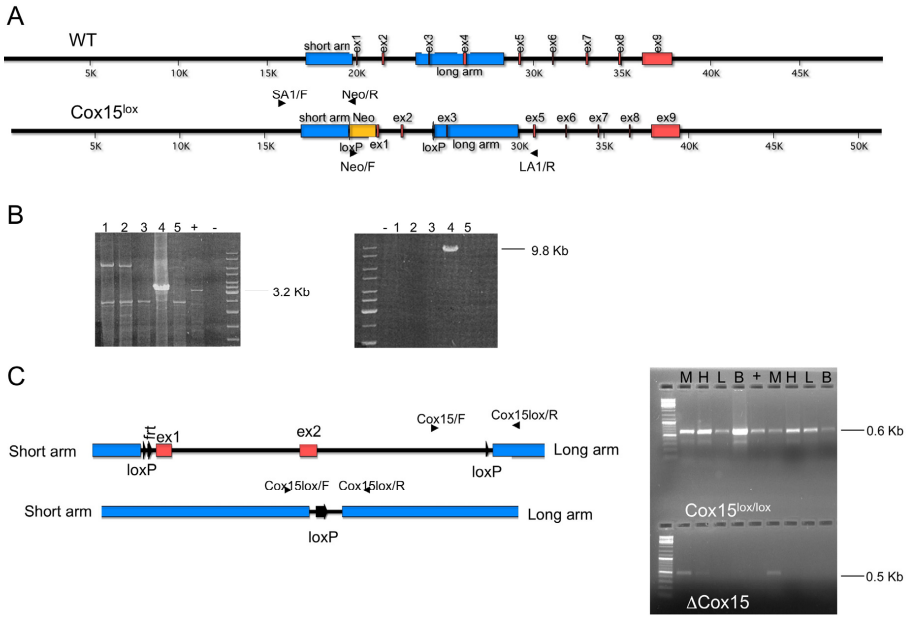

Figure S2. Cox15^{lox} and ACTA-Cox15$^{-/-}$ recombinant alleles

A: Schematic structure of wild type (WT) and recombinant Cox15^{lox} allele. Short and long arm of homology are shown in blue. A neomycin-resistance cassette is shown in yellow. Two lox-P sites are located in introns flanking exons 1 and 2. Arrowheads indicate the position of primers used specific to the short arm (SA1/F and Neo/R) and the long arm (Neo/F and LA1/R) for the screening of recombinant ES cells. Note that both SA1/F and LA1/R are located in regions outside the recombinant construct.

B: PCR-based screening of positive ES clones using the primer pairs SA1/F and Neo/R (left panel) specific for the short arm, and Neo/F and LA1/R (right panel) specific for the long arm. Clone 4 shows the expected fragments at 3.2kb (short arm) and 9.8 kb (long arm).

C: Left: schematic structure of the recombinant Cox15^{lox} allele before (top) and after (bottom) cre-mediated recombination of the region encompassed by the two lox-P sites. Arrowheads indicate the position of the primer pairs Cox15lox/F and Cox15lox/R used for the genotype analysis. Right: PCR-based genotyping in muscle (M), heart (H), liver (L) and brain (B) of Cox15$^{lox/lox}$ vs ACTA-Cox15$^{-/-}$ alleles of two recombinant animals. Note that the diagnostic band specific to the ACTA-Cox15$^{-/-}$ allele is present only in skeletal muscle and, in trace amount, in the heart.

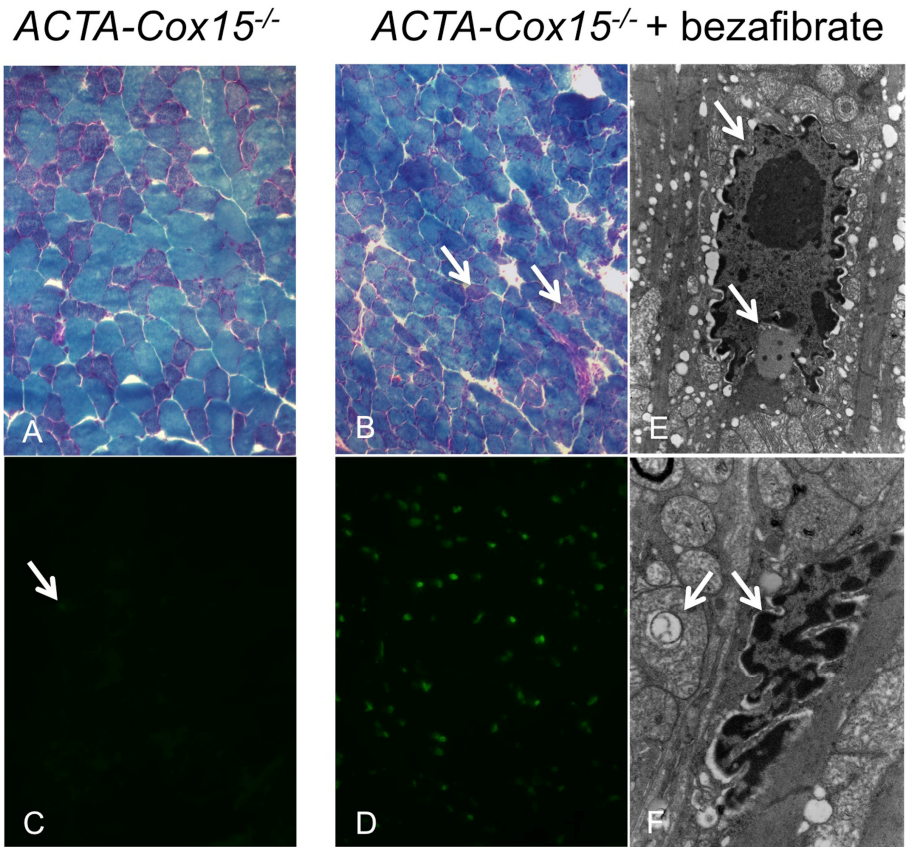

Figure S3: Effects of bezafibrate of ACTA-Cox15$^{-/-}$ mice.
Gomori trichrome staining of muscle from A) an ACTA-Cox15$^{-/-}$ untreated mouse (panel A) and bezafibrate-treated ACTA-Cox15$^{-/-}$ mouse (panel B). Note the increase of ragged-red fibers, fiber-size variation and central nuclei in the bezafibrate-treated muscle. Arrows indicate two degenerated fibers. Magnification 20x. TUNEL staining in sections serial to those shown in panels A and B. The bezafibrate-treated muscle (panel D) contains numerous TUNEL-positive fluorescent green nuclei, compared to a single weakly TUNEL-positive nucleus present in untreated muscle, indicated by an arrow (panel C).Panel E: Electron microscopy (EM) of a nucleus in a muscle fiber from a bezafibrate-treated ACTA-Cox15$^{-/-}$ mouse. Note the gaps in the nuclear membrane and an apoptotic body (arrows). Magnification 20000x. Panel F: EM of a piknotic nucleus and a vacuolated mitochondrion (arrows) in a muscle fiber from a bezafibrate-treated ACTA-Cox15$^{-/-}$ mouse. Magnification 20000x.

Chapter 4

AAV-mediated Liver-specific MPV17 Expression Restores mtDNA Levels and Prevents Diet-induced Liver Failure

Emanuela Bottani[1], Carla Giordano[2], **Gabriele Civiletto[1]**, Ivano Di Meo[1], Alberto Auricchio[3], Emilio Ciusani[4], Silvia Marchet[1], Costanza Lamperti[1], Giulia d'Amati[2], Carlo Viscomi[1] and Massimo Zeviani[1,5]

[1]Unit of Molecular Neurogenetics, The Foundation "Carlo Besta" Institute of Neurology IRCCS, Milan, Italy;
[2]Department of Radiological, Oncological, and Pathological Sciences, Sapienza University, Roma, Italy;
[3]Department of Pediatrics, Division of Medical Genetics, Telethon Institute of Genetics and Medicine, "Federico II" University, Naples, Italy;
[4]Laboratory of Clinical Pathology and Medical Genetics, The Foundation "Carlo Besta" Institute of Neurology IRCCS, Milan, Italy;
[5]MRC-Mitochondrial Biology Unit, Cambridge, UK

Molecular Therapy 2014;22:10-17

Abstract

Mutations in human *MPV17* cause a hepatocerebral form of mitochondrial DNA depletion syndrome (MDS) hallmarked by early-onset liver failure, leading to premature death. Liver transplantation and frequent feeding using slow-release carbohydrates are the only available therapies, although surviving patients eventually develop slowly progressive peripheral and central neuropathy. The physiological role of Mpv17, including its functional link to mitochondrial DNA (mtDNA) maintenance, is still unclear. We show here that Mpv17 is part of a high molecular weight complex of unknown composition, which is essential for mtDNA maintenance in critical tissues, *i.e.* liver, of a Mpv17 knockout mouse model. On a standard diet, Mpv17$^{-/-}$ mouse shows hardly any symptom of liver dysfunction, but a ketogenic diet (KD) leads these animals to liver cirrhosis and failure. However, when expression of human *MPV17* is carried out by adeno-associated virus (AAV)-mediated gene replacement, the Mpv17 knockout mice are able to reconstitute the Mpv17-containing supramolecular complex, restore liver mtDNA copy number and oxidative phosphorylation (OXPHOS) proficiency, and prevent liver failure induced by the KD. These results open new therapeutic perspectives for the treatment of MPV17-related liver-specific MDS.

Introduction

The term mitochondrial DNA depletion syndrome (MDS) indicates a heterogeneous group of diseases characterized by profound reduction in mitochondrial DNA (mtDNA) copy number in one or several tissues.[1] Myopathic, encephalomyopathic, and hepatocerebral forms of MDS are known, due to mutations in gene products involved in mtDNA maintenance, either by controlling the supply of deoxynucleotides for, or by carrying out, the synthesis of mtDNA. MDS is considered rare, with an estimated prevalence of 1:100,000,[2] although the number of genes associated with this condition is rapidly expanding, and a systematic diagnostic screening is hampered by tissue specificity. For instance, thymidine kinase 2[3] and guanosine kinase[4] are the two enzymes involved in deoxynucleotide recycling in mitochondria; p53-ribo- nucleotide reductase subunit 25 and thymidine phosphorylase[6] are the two cytosolic enzymes controlling the *de novo* biosynthesis of deoxynucleotides (p53-ribonucleotide reductase subunit 2) and the catabolism of nucleotides (thymidine phosphorylase), respectively; polymerase γ[7] is the mitochondrion-specific DNA polymerase and Twinkle,[8] the mtDNA helicase. MPV17[9–16], a small protein of the inner mitochondrial membrane, is a prominent cause of hepatocerebral MDS, accounting for about 50% of the cases. More than 20 different *MPV17* mutations in >70 patients have been reported so far. However, the functional and mechanistic links between Mpv17 and mtDNA maintenance are still missing. Nevertheless, studies on SYM1, the MPV17

yeast ortholog, suggest a role for this protein in controlling the flux of Krebs cycle intermediates across the inner mitochondrial membrane. How this functional data relate to mtDNA maintenance and integrity are unknown. In addition, studies based on blue native gel electrophoresis have demonstrated that SYM1 is present within a high molecular weight complex of ~600 kDa, the composition of which is, however, unknown.[17]

Liver involvement associated with severe hypoglycemic crises and rapidly progressive deterioration of hepatic function, leading to liver cirrhosis and failure, are early and predominant features of *MPV17*-dependent MDS. Unlike other MDS, neurological involvement in *MPV17*-associated hepatocerebral MDS is generally mild or absent at disease onset, but progressive peripheral neuropathy and cerebellar degeneration appear later in those *MPV17* mutant patients who survive fatal, early-onset metabolic impairment, and liver failure. Although no cure is currently available for *MPV17*-related MDS, therapeutic interventions based on liver transplantation[13,14] or on frequent meals of a cornstarch-based diet[18] have been attempted, to delay disease progression or protect patients from fatal hypoglycemia. Liver transplantation has been carried out in 10 patients but five of them died early thereafter of multiorgan failure or sepsis.[14] Prompt-release carbohydrates, such as cornstarch, seem to be effective in preventing fatal hypoglycemic accidents, but the surviving patients invariably progress to hepatic, and eventually neurological, degeneration. Central and peripheral neuropathy is a predominant feature in

subjects affected by Navajo neurohepatopathy, a well-known disease of Navajo people from south-east US, recently shown to be caused by a specific mutation in the *MPV17* gene.19 Clinical features of Navajo neurohepatopathy/MPV17 syndrome include sensory motor neuropathy with ataxia, leukoencephalopathy, corneal ulcerations, acral mutilation, poor somatic development with sexual infantilism, serious systemic infections, and, of course, liver derangement.

The knockout mouse for *Mpv17* (*Mpv17*$^{-/-}$) is characterized by profound, early-onset mtDNA depletion in liver,[10] degeneration of the inner ear structures, particularly of the organ of Corti and stria vascularis, determining profound hearing loss,[20] and late-onset, fatal kidney dysfunction, dominated by proteinuria due to focal segmental glomerulosclerosis.[10] Although the molecular and biochemical features in the liver of *Mpv17*$^{-/-}$ mice closely resemble those of human patients, including severe mtDNA depletion, these animals show hardly any sign of hepatic dysfunction in standard captivity conditions and live well beyond the first year of life, with neither obvious neurological impairment nor neuro-pathological abnormalities. However, we show here that *Mpv17*$^{-/-}$ mice fed with a high-fat ketogenic diet (KD) rapidly develop liver cirrhosis and failure. Importantly, treatment with a liver-specific adenoassociated viral vector (serotype 2/8, AAV2/8) expressing human *MPV17* (*hMPV17*) restores mtDNA copy number and prevents liver degeneration. This effect is linked to the formation of the 600 kDa complex containing Mpv17, since Mpv17 variants that do not allow this

structure to be formed cannot rescue the liver phenotype *in vivo*.

Materials and Methods

Construction of AAV2/8 vectors.

AAV2/8-TBG-*h.MPV17* and AAV2/8-TBG-*h.MPV17HA* vectors were produced by the AAV Vector Core of the Telethon Institute of Genetics and Medicine (Naples, Italy) by triple transfection of 293 cells and purified by CsCl gradients.[34] Physical titers of the viral preparations (genome copies per ml) were determined by real-time PCR35 (Applied Biosystems, Foster City, CA) and dot-blot analysis.

Genomic DNA extraction, PCR, and quantitative PCR.

Total DNA was extracted from frozen tissues using the Maxwell apparatus (Promega, Madison, WI) following the instructions of the manufacturer. AAV-derived DNA was detected by standard PCR amplification using primer pairs specific to the *hMPV17* gene. SYBR-GREEN–based real-time quantitative PCR was carried out for mtDNA and AAV-copy number analysis as previously described10,22; the *RNAseP* gene was used as a reference. Total RNA was extracted from liquid nitrogen snap frozen liver by Total RNA Mini Kit (tissue), according to the manufacturer's instructions (Geneaid, Taipei, Taiwan). Of total RNA, 2 µg was treated with Rnase-free DNase and retrotranscribed using the GoTaq 2-Step RT-qPCR System (Promega). Approximately 25ng of cDNA was used for real-time

PCR assay using primers specific for amplifi- cation of several genes.36 Oligonucleotide sequences are available on request.

Biochemical analysis of MRC complexes.

Liver samples stored in liquid nitrogen were homogenized in 10 mmol/l phosphate buffer (pH 7.4), and the spectrophotometric activity of cI, cII, cIII, and cIV, as well as citrate synthase, was measured as described.37

Morphological analysis.

Histochemical analyses were performed as described.38 Hematoxylin and eosin and picrosirius red staining were performed according to standard protocols. Livers were formalin fixed and paraffin embedded. Consecutive sections (5–6 μm thick) were stained with hematoxylin and eosin and picrosirius red for histologic examination. Immunostaining with antiproliferating cell nuclear antigen monoclonal antibodies (Abcam, Cambridge, UK; dilution 1:6,000) was performed for quantitative evaluation of proliferating hepatocytes. Two-hundred cells per slide were manually counted in four high-power fields (original magnification: 40x), and the number of proliferating hepatocytes (in all cell cycle stages) was expressed as a ratio over the total cell number.

Immunoblotting.

Ten percent weight per volume homogenates in 10 mmol/l phosphate buffer pH 7.4 were prepared from liver and

centrifuged at 800*g* for 10 minutes to eliminate cellular debris. Total protein extracts were run through a 12% sodium dodecyl sulfate–polyacrylamide gel (40 µg/sample) and electroblotted onto nitrocellulose filters. The filters were immunostained with specific antibodies against MPV17 (Proteintech, Manchester, UK), Core1, and the 70kDa subunit of succinate dehydrogenase (Molecular Probes; Invitrogen, Paisley, UK), and protein bands were visualized using the ECL chemioluminscence kit (Amersham, Milan, Italy). Twenty microgram of proteins from isolated liver mitochondria39 were run on a 12% sodium dodecyl sulfate–polyacrylamide gel.

BNGE was performed in isolated liver mitochondria as described.40 Fifteen microliters of sample were run through a 5–13% nondenaturating gradient (1D-BNGE). For denaturing two-dimensional BNGE electrophoresis, the one-dimensional BNGE lane was excised, treated for 1 hour at room temperature (20 °C) with 1% sodium dodecyl sulfate and 1% β-mercaptoethanol and then run through a 16.5% tricine-sodium dodecyl sulfate–polyacrylamide gel using a 10% spacer gel.

Analysis of body fluids.

Aspartate aminotransferase and alanine amino- transferase were determined in blood samples by standard methods.

Experimental ethics policy.

Animal studies were approved by the Ethics Committee of the Foundation ‘Carlo Besta’ Neurological Institute, in accordance

with the guidelines of the Italian Ministry of Health. The use and care of animals followed the Italian Law D.L. 116/1992 and the EU directive 86/609/CEE. The mice were kept on a C57Bl6/129Sv mixed background, and wild-type littermates were used as controls. Standard food and water were given *ad libitum*. KD was administered for 2 months (SSNIFF, Germany) *ad libitum*. Body weight and food consumption were monitored twice a week.

Results

Mpv17 is part of a high molecular weight complex

In order to investigate the physical status of Mpv17 *in vivo*, we analyzed isolated mitochondria from *Mpv17*$^{+/-}$ and *Mpv17*$^{-/-}$ livers by 2-dimensional blue native gel electrophoresis (2D-BNGE) immunoblot, using an antibody specific against the mammalian Mpv17 protein (αMpv17). Although the antibody did not work in the (native) first dimension, in the (denaturing) second dimension, the αMpv17 was able to visualize Mpv17 cross-reacting material in the mitochondria of control, but not of knockout mice. Most of the 20kDa Mpv17 protein was in fact present in a spot corresponding to a complex of >600 kDa, as suggested by re-staining with an αCore1 antibody marking the mitochondrial complex III dimer (**Figure 1**). These findings are identical to those previously obtained on SYM1.[17]

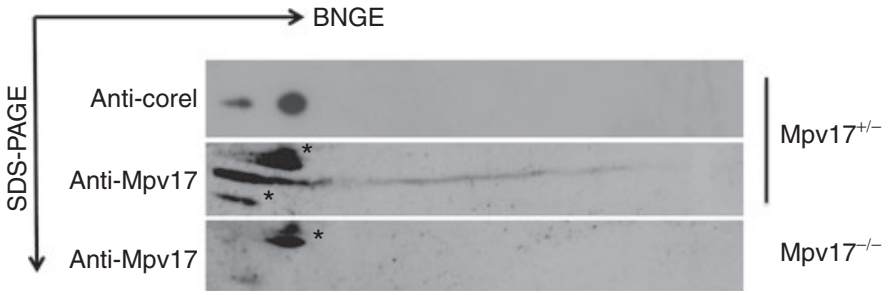

Figure 1 Characterization of the Mpv17-containing macromolecular complex. Liver mitochondria from (**a**) *Mpv17*$^{+/-}$ and (**b**) MPV17$^{-/-}$ were analyzed by 2D BNGE. The blots were immunostained with an MPV17 antibody;.The asterisks (*) mark unspecific bands. BNGE, blue native gel electrophoresis.

AAV2/8-mediated hMPV17 expression rescue the Mpv17−/− mouse liver phenotype

We constructed an AAV2/8 viral vector expressing the *hMPV17* cDNA to the liver, under the control of the liver-specific thyroxine-binding globulin (TBG) promoter. The hMPV17 protein is almost identical to the mouse (m)Mpv17 protein, displaying 14 changes, none of which was in highly conserved residues or was predicted to have deleterious consequences by SIFT analysis (**Supplementary Figure S1**).[21] AAV2/8-*hMPV17* was administered to groups of 2-month-old *Mpv17*$^{-/-}$ and *Mpv17*$^{+/-}$ mice (*n* = 4 each) by retro-orbital injection at a concentration of 4×10^{12} viral genomes (vg)/kg. The mice were sacrificed 3 weeks later. Blood samples drawn before AAV treatment and again just before the sacrifice showed that aspartate aminotransferase and alanine aminotransferase enzymes, two markers of hepatocyte leakage, were high before

AAV administration in *Mpv17*$^{-/-}$ mice, whereas they were normalized after AAV administration (**Figure 2a**), suggesting correction of liver damage. No change was observed in control animals upon AAV injection, suggesting that AAV has no hepatotoxicity *per se*. Viral DNA was detected by polymerase chain reaction (PCR) in liver, but not in kidney, skeletal muscle, heart, and brain (data not shown), confirming the specific hepatotropism of AAV2/8[22]; similar amounts of viral DNA per cell were found in *Mpv17*$^{+/-}$ and *Mpv17*$^{-/-}$ livers (0.9 ± 0.3 versus 1.2 ± 0.5; **Figure 2b**). Next, we measured *MPV17* mRNA expression by real-time (RT)-qPCR. Since human and mouse *MPV17* sequences are almost identical, we were unable to design primers suitable to distinguish endogenous from AAV-mediated expression. However, in both AAV-treated *Mpv17*$^{-/-}$ and *Mpv17*$^{+/-}$ mice, *Mpv17* mRNA levels were much higher than the levels found in untreated *Mpv17*$^{+/-}$ mice (**Figure 2f**). Accordingly, western blot immunovisualization with αMpv17 showed that the amount of Mpv17-crossreacting material in AAV-treated *Mpv17*$^{-/-}$ liver homogenates (data not shown) and isolated mitochondria (**Figure 2d**) were much higher than that found in control mice. Analysis by 2D-BNGE immunoblotting demonstrated that hMPV17 was integrated into a high molecular weight complex similar to that detected in control mitochondria (**Figure 2e**). The mtDNA copy number was markedly increased in livers from AAV-treated *Mpv17*$^{-/-}$ mice (1282 ± 372 copies/cell) compared to untreated *Mpv17*$^{-/-}$ littermates (95 ± 34 copies/cell; Whitney–Mann test: $P <$

0.0001), and similar to that of untreated wild-type livers (1402 ± 192; *P* = 0.90; **Figure 2c**). Intriguingly, the AAV-treated *Mpv17*$^{+/-}$ mice had slightly increased levels of mtDNA as well (1857±144) compared to untreated litter- mates (*P* < 0.0001; **Figure 2c**). Notably, an AAV expressing *hMPV17* tagged with a HA epitope, was neither able to enter the complex (**Supplementary Figure S2a**) nor to complement the mtDNA depletion (**Supplementary Figure S2b**) in spite of high viral content in liver (**Supplementary Figure S2c**), suggesting that the HA epitope hampers the function of MPV17, possibly by interfering with the formation of the supramolecular complex, which appears as necessary for mtDNA maintenance. As expected, the mtDNA copy number in skeletal muscle was similar in treated versus untreated *Mpv17*$^{-/-}$ individuals (data not shown). The increase in mtDNA copy number in AAV-treated versus untreated *Mpv17*$^{-/-}$ livers, was paralleled by an increase in mtDNA-encoded transcripts (COI, COII, ND5, ND6, and CYTB), and in the enzymatic activities of complexes I, III, and IV (**Figure 2f**,**g**). Mitochondrial respiratory chain (MRC) activities were not increased in mice treated with *hMPV17-HA*-recombinant AAV vectors (**Supplementary Figure S2d**), and in fact transaminase levels were as high as those found in untreated naive *Mpv17*$^{-/-}$ littermates (**Supplementary Figure S2e**).

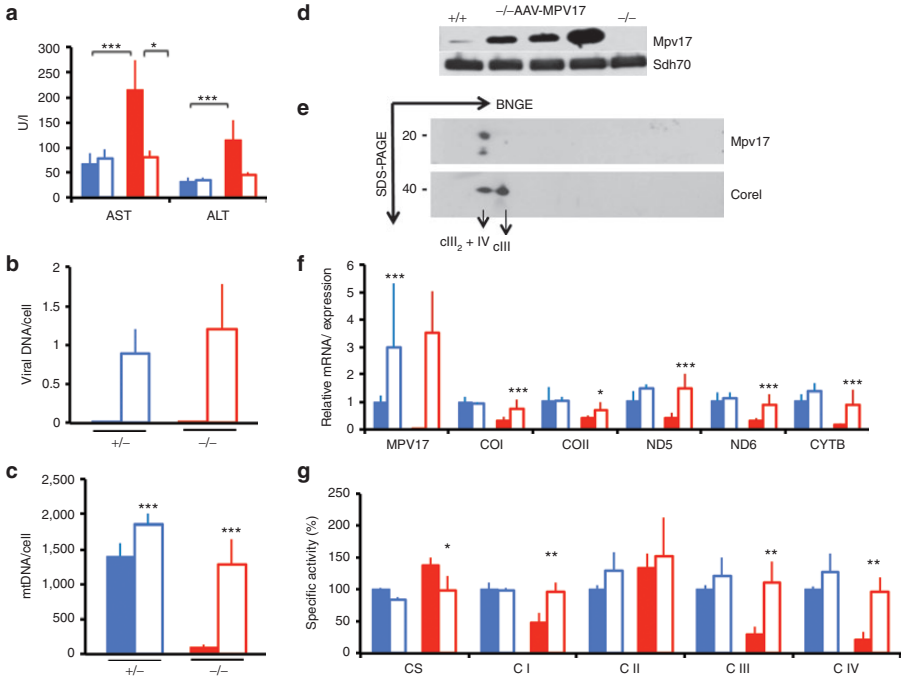

Figure 2 Molecular and clinical characterization of AAV2/8-TBG-*h.MPV17*-treated mice. A single retro-orbital injection of $4x10^{12}$ vg/Kg was performed in two months old $Mpv17^{+/-}$ and $Mpv17^{-/-}$ mice.
A) Analysis of AST and ALT plasma levels in mice before and after AAV-administration. The asterisks represent the significance levels calculated by paired Student's two-tailed t test: *p < 0.05.
B) Viral DNA content in livers from $Mpv17^{+/-}$ and $Mpv17^{-/-}$ mice. No amplification was obtained in AAV-untreated mice.
C) MtDNA content in livers from AAV-treated and untreated $Mpv17^{+/-}$ and $Mpv17^{-/-}$ mice.
D) Western blot analysis of h.MPV17 protein
E) 2D-BNGE on liver mitochondria from AAV-treated $Mpv17^{-/-}$ mice.
F) mRNA expression analysis. All values are normalized to the untreated control.
G) MRC activities in treated vs. untreated $Mpv17^{+/-}$ and $Mpv17^{-/-}$ mice. CI, CIII, and CIV. The asterisks represent the significance levels calculated by unpaired Student's two-tailed t test: *p < 0.05; **p < 0.01; ***p < 0.001.*Color codes: Solid blue:* untreated $Mpv17^{+/-}$ mice; *blue outline:* AAV-treated $Mpv17^{+/-}$ mice; *solid red:* $Mpv17^{-/-}$ mice; *red outline:* AAV- treated $Mpv17^{-/-}$ mice. The bars represent the standard deviation (SD).

Ketogenic diet induces severe cirrhosis in Mpv17$^{-/-}$ mice

Ketogenic diet (KD) supplies ≈80% of the energy from fat. Although KD has been suggested to induce mitochondrial biogenesis in skeletal muscle (Ahola-Erkkila et al 2010), it seems to act detrimentally in OXPHOS defective mouse models unable to consume the excess of NADH derived from fat metabolism (Wenz et al., 2009). We investigated the effects of KD administered for two months to two-month old groups of Mpv17$^{-/-}$ and Mpv17$^{+/-}$ mice (n. 4 individuals each). Both Mpv17$^{-/-}$ and Mpv17$^{+/-}$ KD-treated animals showed initial weight loss, which was progressively recovered by Mpv17$^{+/-}$ but not Mpv17$^{-/-}$ individuals (Supporting Information Fig S3A). After 2 months, KD-treated mice showed marked increase of plasma ALT and AST levels, which was much higher in the Mpv17$^{-/-}$ than in the Mpv17$^{+/-}$ group (Supporting Information Fig S3B). At necroscopy, the Mpv17$^{-/-}$ livers were markedly enlarged and yellowish (Supporting Information Fig S3C). Histologic examination revealed diffuse micro and macro-vacuolar steatosis, hepatocellular necrosis with inflammatory infiltrates, lipogranulomas and nodules of regenerating hepatocytes surrounded by fibrous septa, consistent with cirrhosis (Fig 3A,B). Contrariwise, Mpv17$^{+/-}$ livers displayed only a mild, albeit variable, micro- and macrovacuolar steatosis and peri-sinusoidal collagen deposition (Fig 3C,D), as expected by prolonged exposure to a high-fat diet. The mtDNA content was unchanged in both KD-fed genotypes compared to standard diet (SD)-fed littermates, indicating that KD failed to induce

mitochondrial biogenesis in liver (Supporting Information Fig S4A), as confirmed by histochemical staining for COX (Supporting Information Fig S4B). Indeed, transcript analysis showed a reduction of some MRC subunits in KD- vs. SD-fed mice (Supporting Information Fig S4C,D). Massive steatosis prevented us to perform spectrophotometric assays of MRC activities in liver homogenates.

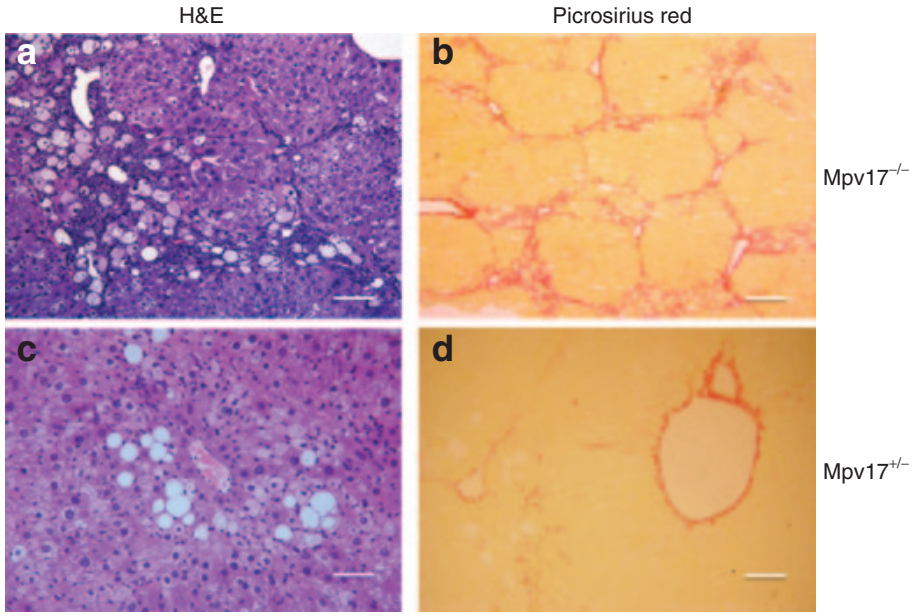

Figure 3. Histological analysis of livers from KD-fed mice.
Ematoxilin-eosin (A and C), and picrosirius red (B and D) staining in KD-fed vs. SD-fed Mpv17$^{-/-}$ and Mpv17$^{+/-}$ livers. *See text for details*. Scale bars: 150 μm (A-C); 300 μm (B-D).

AAV-mediated Mpv17 expression corrects liver damage of ketogenic diet

We next investigated whether treatment by AAV2/8-*hMpv17* was able to (i) prevent and/or (ii) correct the severe liver derangement induced in Mpv17$^{-/-}$ mice by KD.

In a first protocol, aiming at preventing damage, KD administration for two months was started three weeks after the injection of 4x10^{12} (n=4) or 4x10^{13} (n=3) vg/Kg AAV2/8-*hMpv17* into 2 month old Mpv17$^{+/-}$ and Mpv17$^{-/-}$ mice. Here we show data referred to the higher viral dose, but similar results were also obtained using the lower dose (Supporting Information Fig S5). Body weights were monitored throughout the experiment and hepatic enzyme levels were measured at the end of the treatment. As mentioned before, untreated Mpv17$^{-/-}$ mice showed progressive loss of body weight, whereas AAV-treated Mpv17$^{-/-}$ individuals recovered their starting weight after initial loss, and gained weight over time with a trend similar to that of AAV-treated and untreated Mpv17$^{+/-}$ animals (Supporting Information Fig S6A). In contrast to untreated KD-fed Mpv17$^{-/-}$ mice, AAV-treated KD-fed Mpv17$^{-/-}$ mice showed plasmatic levels of hepatic enzymes similar to those of control littermates in KD (Supporting Information Fig S6B). Livers from KD-fed AAV-treated Mpv17$^{-/-}$ animals were significantly less enlarged (9.9±2.6 vs. 7.0±1.0; Student's t test $p<0.05$; Supporting Information Fig S6C), and remarkably less damaged upon histological examination than those from untreated Mpv17$^{-/-}$ littermates (Fig 4). Eventually, whilst AAV-untreated Mpv17$^{-/-}$

individuals invariably developed overt cirrhosis and necrosis by two months of KD, AAV-treated Mpv17$^{-/-}$ animals showed only variable degrees of steatosis and some inflammatory infiltrates, comparable to those of control animals exposed to the same diet (Fig 4). These results clearly indicate that AAV2/8-*hMpv17* treatment prevents KD-induced liver damage in Mpv17$^{-/-}$ mice.

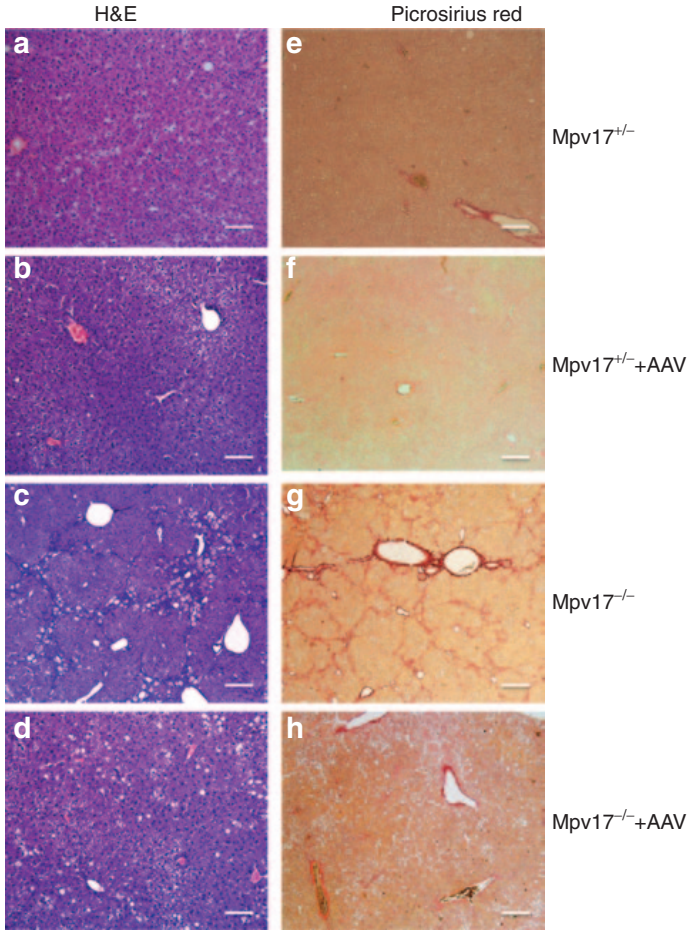

Figure 4. Histological analysis of livers from KD-fed mice pre-treated with AAV.
A single retro-orbital injection of 4x10^{13} vg/Kg was performed in two months old Mpv17$^{+/-}$ and Mpv17$^{-/-}$ mice. KD was started three weeks later. Ematoxilin-eosin (A-D); picrosirius red (E-H) staining. Scale bars: A-D: 150 μm, E-H: 300 μm.

We observed that the viral DNA content was much lower in KD-fed than in SD-fed livers (1.2±0.2 vs. 12.8±2.3 in Mpv17$^{+/-}$, p=0.0024; 0.4±0.3 vs. 14.8±1.0 copies/cell in Mpv17$^{-/-}$, p<0.005) (Fig 5A), suggesting that KD induced strong dilution of viral DNA. Since the DNA of recombinant AAV vectors remains episomal (Nakai et al, 2001) and is replication-defective, a possible explanation for this phenomenon is increased cell proliferation. To confirm this hypothesis, we performed quantitative analysis of proliferating vs. non-proliferating hepatocytes by measuring proliferating cell nuclear antigen (PCNA), a marker of cell proliferation (Pritchard et al, 2011). The nuclear staining index for PCNA was 18.2±13.6% in SD vs. 74.2±7.7% in KD in Mpv17$^{+/-}$ and 20.9±15.1% in SD vs. 81.7±12.5 in KD in Mpv17$^{-/-}$ mice (Student t test: p<0.005 for both groups; Supporting Information Fig S7A). Similar results were obtained in mice treated with AAV (Supporting Information Fig S7B). This result highlights the effect of KD in promoting hepatocyte proliferation in mouse liver, and may explain the observed decrease of viral content during the KD treatment. Nevertheless, the mtDNA content increased from 49±8 copies/cell in naïve Mpv17$^{-/-}$ to 576±211 copies/cell in AAV-treated Mpv17$^{-/-}$ littermates (Fig5B). This increase was paralleled by robust expression of mtDNA transcripts, becoming quantitatively comparable to that of untreated KD-fed Mpv17$^{+/-}$ littermates (Fig 5C), and led to significant recovery of COX histochemical activity (Fig 5D).

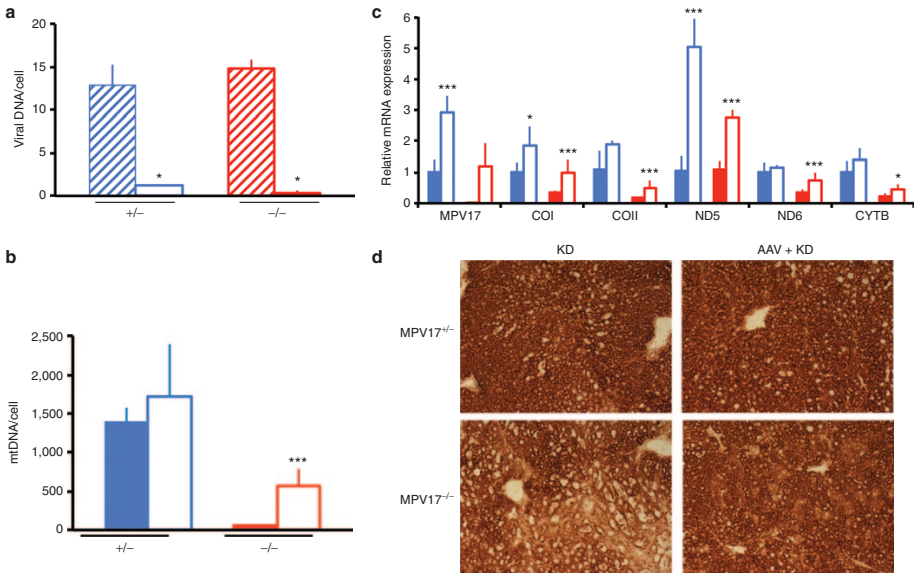

Figure 5. Molecular and biochemical characterization of KD-fed mice pre-treated with AAV

A) Viral DNA content in livers from AAV-treated Mpv17$^{+/-}$ and Mpv17$^{-/-}$ mice in SD vs. KD. *Blue stripes:* AAV-treated Mpv17$^{+/-}$ mice in SD; *blue outline:* AAV- treated Mpv17$^{+/-}$ mice in KD; *red stripes:* AAV-treated Mpv17$^{-/-}$ mice in SD; *red outline:* AAV-treated Mpv17$^{-/-}$ mice in KD. The bars represent the standard deviation (SD).

B) MtDNA analysis in AAV-treated vs. untreated, KD-fed mice.

C) Mitochondrial transcripts analysis in AAV-treated vs. untreated, KD-fed mice. All values are normalized to the KD-fed untreated controls.

D) COX histochemical staining.

In B and C, the asterisks represent the significance levels calculated by unpaired Student's two-tailed t test: *p < 0.05; **p < 0.01; ***p < 0.001. Color codes*: Solid blue:* untreated Mpv17$^{+/-}$ mice; *blue outline:* AAV-treated Mpv17$^{+/-}$ mice; *solid red:* Mpv17$^{-/-}$ mice; *red outline:* AAV-treated Mpv17$^{-/-}$ mice. The bars represent the standard deviation (SD).

In a second protocol, aiming at correcting damage, we tested whether AAV-based *hMPV17* gene replacement therapy can stop or reverse an already ongoing liver derangement, as typically found in patients. We first KD-fed for one month two groups of Mpv17$^{-/-}$ and Mpv17$^{+/-}$ two-month old mice. This

treatment caused liver damage, as clearly indicated by increased hepatic-enzyme levels in plasma of both groups (Supporting Information Fig S8A). We then administered $4x10^{13}$ vg/Kg of AAV-*hMpv17* to both groups of animals, while KD was continued for one additional month before sacrifice, so that this group of mice was overall exposed to KD as long as the first group. Livers from Mpv17$^{-/-}$ animals showed a statistically non-significant trend towards reduced hepatomegaly compared to untreated littermates, whereas livers from Mpv17$^{+/-}$ mice were unaffected (Supporting Information Fig S8B).

Again, the livers from Mpv17$^{-/-}$ mice were protected from developing extensive KD-induced liver damage, showing moderate hepatocyte steatosis, in absence of necrosis and fibrosis (Fig 6A,B), while livers from Mpv17$^{+/-}$ exposed to this protocol displayed only mild and focal steatosis (Fig 6C,D).

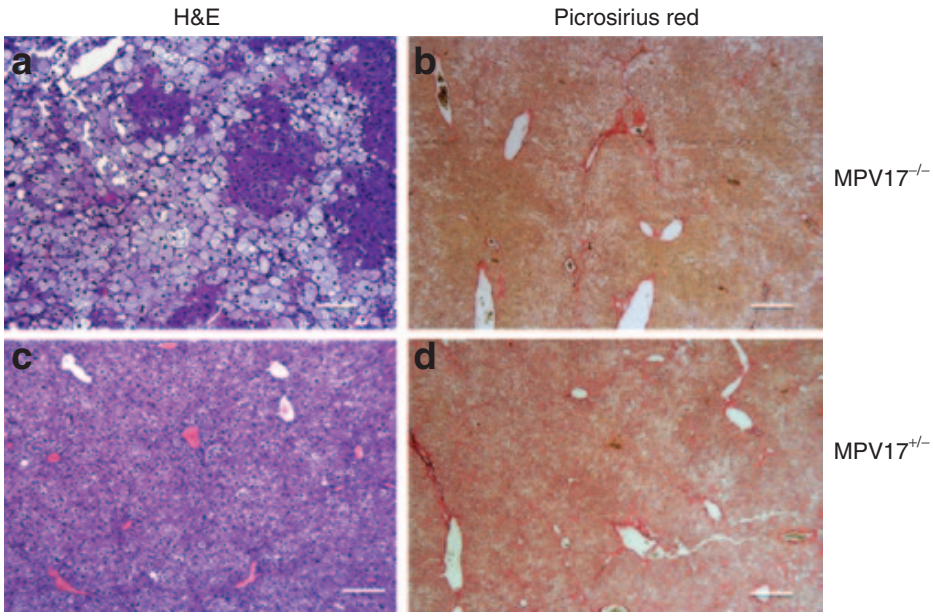

Figure 6. Histological analysis of livers from AAV post-treated, KD-fed mice.
A single retro-orbital injection of $4x10^{13}$ vg/Kg was performed in two months old $Mpv17^{+/-}$ and $Mpv17^{-/-}$ mice one month after starting KD. Haematoxilin-Eosin (A and C), and Picrosirius red (B and D) staining in AAV post-treated $Mpv17^{-/-}$ and $Mpv17^{+/-}$ livers. Scale bars: A-C: 150 μm, B-D: 300 μm.

Viral DNA quantification showed 5.6±3.1 vg/cell in $Mpv17^{-/-}$ and 5.0±2.5 vg/cell in $Mpv17^{+/-}$ mice (Fig 7A), leading to high levels of MPV17 mRNA in both $Mpv17^{-/-}$ and $Mpv17^{+/-}$ livers (Fig 7B). The mtDNA copy number was significantly increased in AAV-treated vs. untreated $Mpv17^{-/-}$ (501±263 vs. 49±8, $p<0.01$) although remained lower than in treated (1387±331 copies/cell) and untreated (1384±194 copies/cell) $Mpv17^{+/-}$ littermates (Fig 7C). In parallel, mitochondrial transcripts were significantly increased in the $Mpv17^{-/-}$ livers, up to levels comparable to KD-fed control littermates (Fig 7B), and COX histochemical activity was increased as well (Fig 7D). Nevertheless, the overall clinical conditions were clearly worse in post-KD AAV-treated

than in pre-KD AAV treated Mpv17$^{-/-}$ mice. The hepatic enzyme levels increased, whereas the body-weight decreased (Supporting Information Fig S8C,D), suggesting that our "late" AAV treatment can possibly slow the evolution of pre-existing liver damage, but is unable to reverse the downhill clinical progression of the disease.

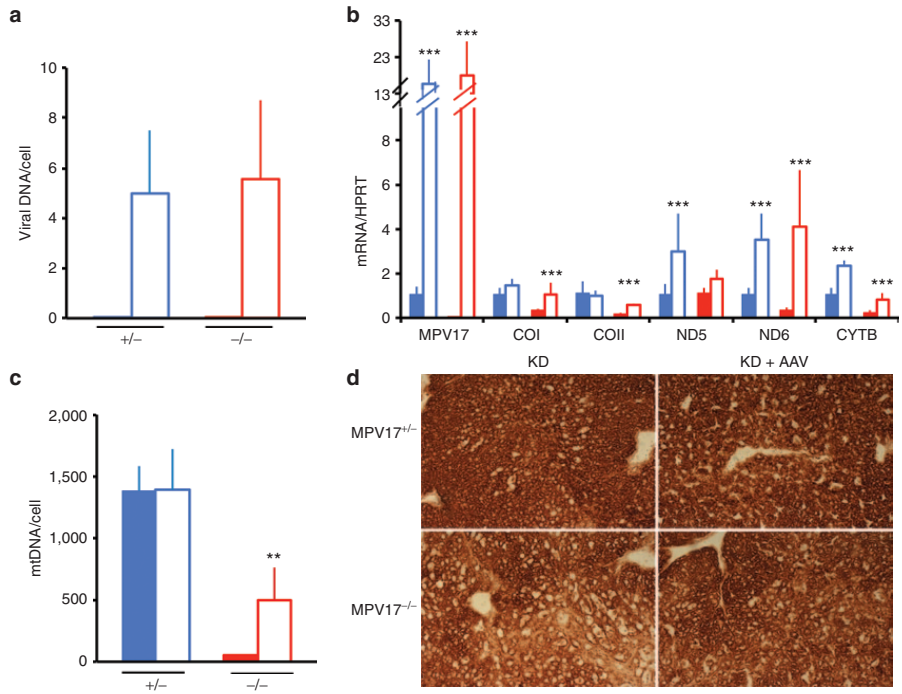

Figure 7. Molecular and biochemical characterization of livers from AAV post-treated, KD-fed mice

A) Viral DNA content in livers.
B) MtDNA analysis.
C) Mitochondrial transcripts analysis.
D) COX histochemical staining.
The asterisks represent the significance levels calculated by unpaired Student's two-tailed t test: *p < 0.05; **p < 0.01; ***p < 0.001.
Color codes: *solid blue:* untreated Mpv17$^{+/-}$ mice; *blue outline:* AAV-treated Mpv17$^{+/-}$ mice; *solid red:* Mpv17$^{-/-}$ mice; *red outline:* AAV-treated Mpv17$^{-/-}$ mice. The bars represent the standard deviation (SD)

Discussion

We provide here novel information on the connection between MPV17 and mtDNA maintenance, although the complete elucidation of the physiological role of this elusive, medically relevant and biologically intriguing protein is still missing. First, we have demonstrated that, like the yeast ortholog SYM1, mammalian MPV17 forms a high molecular weight complex in both cell cultures and mouse tissues. By reconstitution into lipid bilayers, Sym1 has recently been shown to aggregate as a high molecular complex to form a functional pore (Reinhold et al, 2012) possibly a cation channel. Similar to mitochondrial carrier proteins, both Mpv17 and SYM1 are imported into the inner mitochondrial membrane via the TIM23 complex without cleavage of a leader peptide. A channel activity has not been (yet) demonstrated for the mammalian Mpv17, but we have shown here that Mpv17 participates in a high molecular weight complex necessary for its function, since MPV17 variants that fail to be incorporated do not rescue the liver phenotype of $Mpv17^{-/-}$ mice, including mtDNA depletion.

A second goal of our work consisted in the development of therapeutic strategies for liver-specific MDS. Although many mitochondrial abnormalities cause multisystem disorders, some affect only or predominantly a single organ, being thus amenable to treatment by tissue-specific gene replacement. Most of the MPV17 mutant cases are characterized by early onset, often fatal liver failure, associated with profound tissue-specific whereas other tissues are relatively (e.g. skeletal

muscle), or completely (e.g. heart) spared. We used recombinant AAV vectors to target the therapeutic gene to the liver, because this approach is relatively safe, non invasive and translatable to humans We clearly showed that AAV-mediated expression of human MPV17 in Mpv17$^{-/-}$ mouse livers can correct the molecular phenotype, i.e. severe mtDNA depletion, in standard conditions, thus normalizing the MRC defects. We then showed that ketogenic diet (KD) cause Mpv17$^{-/-}$ mice to rapidly develop severe hepatomegaly and macrovacuolar steatosis, which evolves into cirrhosis and overt liver failure within two months. By contrast, Mpv17$^{+/-}$ littermates exposed to the same diet displayed only mild steatosis, mostly of the microvacuolar type. Administration of AAV2/8-hMPV17 before starting KD effectively protected Mpv17$^{-/-}$ mice from liver derangement.

Partial protection from KD-induced liver failure was also obtained in mice exposed to KD before AAV treatment, that is when liver damage was already ongoing, as indicated by elevated plasma levels of hepatic enzymes. However, in this case AAV-treatment was able to halt the progression of the disease, but not to revert already established liver damage. This result is in agreement with the evidence that AAV1 serotype is able to efficiently transduce both normal and cirrhotic livers (Sobrevals et al, 2012), with no significant dilution of the viral load over time.

We propose AAV2/8-based therapy as a realistic strategy to prevent liver failure in patients with mutations in *MPV17* and

eventually in other forms of liver MDS. AAV2/8 serotype can remain for a long time in the liver of mice (Tessitore et al, 2008; Chandler & Venditti, 2010; Moscioni et al, 2006), cats (Cotugno et al, 2011), and humans (Nathwani et al, 2012), with no significant side effects. Whilst targeting of AAV-mediated therapeutic protein is still challenging for large-size tissues such as skeletal muscle, or impermeable organs such as the brain, this approach is becoming a realistic option for gene conditions affecting a single, compliant organ, such as the liver in case of hepatic MDS, for proteins that are secreted by a targetable organ, such as the liver again for factor IX, the circulating enzyme missing in Haemophilia B (Nathwani et al, 2012), or in disorders that can be effectively cured by using liver to clear the bloodstream from toxic substances by making liver competent for clearing the bloodstream from toxic compounds. The latter strategy has proven successful for Ethylmalonic Encephalopathy, a mitochondrial disease due to the accumulation of toxic free sulphide (Di Meo et al, 2012), and can in principle be applied to mitochondrial neuro-gastro-intestinal encephalomyopathy MNGIE, due to accumulation of thymidine to toxic levels in plasma and tissues.

Acknowledgements

This work was supported by the Pierfranco and Luisa Mariani Foundation Italy, Telethon-Italy GPP10005 and GGP11011 (to MZ), Cariplo 2011-0526 (to MZ), and GR-2010-2306-756 (to CV). We wish to thank dr Daniele Ghezzi for helpful discussion.

Authors contribution

EB performed the in vivo experiments and the transcriptional analysis; CG and GdA performed the histological analysis and shared expertise; GC prepared the AAV vectors; IDM performed the AAV injections and the western blot analysis; AA shared expertise and provided the AAV vectors and viruses; EC performed the analysis of serum samples; SM and CL performed the histochemical analysis, CV and MZ designed the study and wrote the manuscript.

References

Ahola-Erkkilä S, Carroll CJ, Peltola-Mjösund K, Tulkki V, Mattila I, Seppänen-Laakso T, Oresic M, Tyynismaa H, Suomalainen A (2010) Ketogenic diet slows down mitochondrial myopathy progression in mice. Hum Mol Genet 19: 1974-1984

AlSaman A, Tomoum H, Invernizzi F, Zeviani M (2012) Hepatocerebral form of mitochondrial DNA depletion syndrome due to mutation in MPV17 gene. Saudi J Gastroenterol 18: 285-289

Bourdon A, Minai L, Serre V, Jais JP, Sarzi E, Aubert S, Chretien D, de Lonlay P, Paquis-Flucklinger V, Arakawa H et al (2007) Mutation of RRM2B, encoding p53-controlled ribonucleotide reductase (p53R2), causes severe mitochondrial DNA depletion. Nat Genet 39: 776-780

Chandler RJ, Venditti CP (2010) Long-term rescue of a lethal murine model of methylmalonic acidemia using adeno-associated viral gene therapy. Mol Ther. 1: 11-16

Cotugno G, Annunziata P, Tessitore A, O'Malley T, Capalbo A, Faella A, Bartolomeo R, O'Donnell P, Wang P, Russo F, *et al* (2011) Long-term amelioration of feline Mucopolysaccharidosis VI after AAV-mediated liver gene transfer. Mol Ther 19: 461-469

Dallabona C, Marsano RM, Arzuffi P, Ghezzi D, Mancini P, Zeviani M, Ferrero I, Donnini C (2010) Sym1, the yeast ortholog of the MPV17 human disease protein, is a stress-induced bioenergetic and morphogenetic mitochondrial modulator. Hum Mol Genet 19: 1098-1107

Di Meo I, Auricchio A, Lamperti C, Burlina A, Viscomi C, Zeviani M (2012) Effective AAV-mediated gene therapy in a mouse model of ethylmalonic encephalopathy. EMBO Mol Med 4:1008-1014

El-Hattab AW, Li FY, Schmitt E, Zhang S, Craigen WJ, Wong LJ (2010) MPV17-associated hepatocerebral mitochondrial DNA depletion syndrome: new patients and novel mutations. Mol Genet Metab 99: 300-308

Ferrari G, Lamantea E, Donati A, Filosto M, Briem E, Carrara F, Parini R, Limonati A, Santer R, Zeviani M. (2005) Infantile hepatocerebral syndromes associated with mutations in the mitochondrial DNA polymerase-gammaA. Brain 128: 723-731

Gao G, Qu G, Burnham MS, Huang J, Chirmule N, Joshi B, Yu QC, Marsh JA, Conceicao CM, Wilson JM (2000) Purification of recombinant adeno-associated virus vectors by column chromatography and its performance in vivo. Hum Gene Ther 11: 2079-2091

Hakonen AH, Isohanni P, Paetau A, Herva R, Suomalainen A and Lonnqvist T. (2007) Recessive Twinkle mutations in early onset encephalopathy with mtDNA depletion. Brain 130: 3032-3040

Karadimas CL, Vu TH, Holve SA, Chronopoulou P, Quinzii C, Johnsen SD, Kurth J, Eggers E, Palenzuela L, Tanji K *et al* (2006) Navajo neurohepatopathy is caused by a mutation in the MPV17 gene. Am J Hum Genet 79: 544-548

Mandel H, Szargel R, Labay V, Elpeleg O, Saada A, Shalata A, Anbinder Y, Berkowitz D, Hartman C, Barak M. *et al* (2001) The deoxyguanosine kinase gene is mutated in individuals with depleted hepatocerebral mitochondrial DNA. Nat Genet 29: 337-341

Meyer zum Gottesberge AM, Reuter A, Weiher H. (1996) Inner ear defect similar to Alport's syndrome in the glomerulosclerosis mouse model Mpv17. Eur Arch Otorhinolaryngol 253: 470-474

Moscioni D, Morizono H, McCarter RJ, Stern A, Cabrera-Luque J, Hoang A, Sanmiguel J, Wu D, Bell P, Gao GP, *et al*. (2006) Long-term correction of ammonia metabolism and prolonged survival in ornithine transcarbamylase-deficient mice following liver-directed treatment with adeno-associated viral vectors. Mol Ther 14: 25-33

Nakai H, Yant SR, Storm TA, Fuess S, Meuse L, Kay MA (2001) Extrachromosomal recombinant adeno-associated virus vector genomes are primarily responsible for stable liver transduction in vivo. J Virol 75: 6969-6976

Nathwani AC, Tuddenham EG, Rangarajan S, Rosales C, McIntosh J, Linch DC, Chowdary P, Riddell A, Pie AJ, Harrington C *et al*. (2011) Adenovirus-associated virus vector-mediated gene transfer in hemophilia B. N Engl J Med. 365: 2357-2365

Navarro-Sastre A, Martin-Hernandez E, Campos Y, Quintana E, Medina E, de Las Heras RS, Lluch M, Munoz, A, del Hoyo, P, Martin, R *et al* (2008) Lethal hepatopathy and leukodystrophy caused by a novel mutation in MPV17 gene: description of an alternative MPV17 spliced form. Mol Genet Metab 94: 234-239

Ng PC, Henikoff S (2003) SIFT: Predicting amino acid changes that affect protein function. Nucleic Acids Res 31: 3812-3814

Nishino I, Spinazzola A, Hirano M. (1999) Thymidine phosphorylase gene mutations in MNGIE, a human mitochondrial disorder. Science 283: 689-692

Nogueira C, de Souza CF, Husny A, Derks TG, Santorelli FM, Vilarinho L (2012) MPV17: fatal hepatocerebral presentation in a Brazilian infant. Mol Genet Metab 107: 764

Parini R, Furlan F, Notarangelo L, Spinazzola A, Uziel G, Strisciuglio P, Concolino D, Corbetta C, Nebbia G, Menni F, Rossi G, Maggioni M, Zeviani M (2009) Glucose metabolism and diet-based prevention of liver dysfunction in MPV17 mutant patients. J Hepatol 50: 215-21

Pritchard MT, Malinak RN, Nagy LE (2011) Early growth response (EGR)-1 is required for timely cell-cycle entry and progression in hepatocytes after acute carbon tetrachloride exposure in mice. Am J

Physiol Gastrointest Liver Physiol 300: 1124-1131
Saada A, Shaag A, Mandel H, Nevo Y, Eriksson S, Elpeleg, O (2001) Mutant mitochondrial thymidine kinase in mitochondrial DNA depletion myopathy. Nat Genet 29: 342-344
Schägger H, von Jagow G (1987) Tricine-sodium dodecyl sulfate-polyacrylamide gel electrophoresis for the separation of proteins in the range from 1 to 100 kDa. Anal Biochem 166: 368-379
Sciacco M, Bonilla E (1996) Cytochemistry and immunocytochemistry of mitochondria in tissue sections. Methods Enzymol 264:509-521
Sobrevals L, Enguita M, Rodriguez C, Gonzalez-Rojas J, Alzaguren P, Razquin N, Prieto J, Fortes P (2012) AAV vectors transduce hepatocytes in vivo as efficiently in cirrhotic as in healthy rat livers. Gene Ther 19: 411-417
Spinazzola A, Viscomi C, Fernandez-Vizarra E, Carrara F, D'Adamo P, Calvo S, Marsano RM, Donnini C, Weiher H, Strisciuglio P *et al* (2006) MPV17 encodes an inner mitochondrial membrane protein and is mutated in infantile hepatic mitochondrial DNA depletion. Nat Genet, 38: 570-575
Spinazzola A, Zeviani M (2007) Disorders of nuclear-mitochondrial intergenomic communication. Biosci Rep 27: 39-51
Spinazzola A, Santer R, Akman OH, Tsiakas K, Schaefer H, Ding X, Karadimas CL, Shanske S, Ganesh J, Di Mauro S *et al* (2008) Hepatocerebral form of mitochondrial DNA depletion syndrome. Arch Neurol 65: 1-6
Tessitore A, Faella A, O'Malley T, Cotugno G, Doria M, Kunieda T, Matarese G, Haskins M, Auricchio A (2008) Biochemical, pathological, and skeletal improvement of mucopolysaccharidosis VI after gene transfer to liver but not to muscle. Mol Ther 16: 30-37
Viscomi C, Spinazzola A, Maggioni M, Fernandez-Vizarra E, Massa V, Pagano C, Vettor R, Mora M, Zeviani M. (2009) Early-onset liver mtDNA depletion and late-onset proteinuric nephropathy in Mpv17 knockout mice. Hum Mol Genet 18:12-26
Wenz T, Luca C, Torraco A, Moraes CT (2009) mTERF2 regulates oxidative phosphorylation by modulating mtDNA transcription. Cell Metab 9: 499-511
Wong LJ, Brunetti-Pierri N, Zhang Q, Yazigi N, Bove KE, Dahms BB, Puchowicz MA, Gonzalez-Gomez I, Schmitt ES, Truong CK *et al* (2007) Mutations in the MPV17 gene are responsible for rapidly progressive liver failure in infancy. Hepatology 46: 1218-1227
Xiao W, Chirmule N, Berta SC, McCullough B, Gao G, Wilson JM (1999) Gene therapy vectors based on adeno-associated virus type 1. J Virol 73: 3994- 400

Supplemental information

Supplemental Figure 1

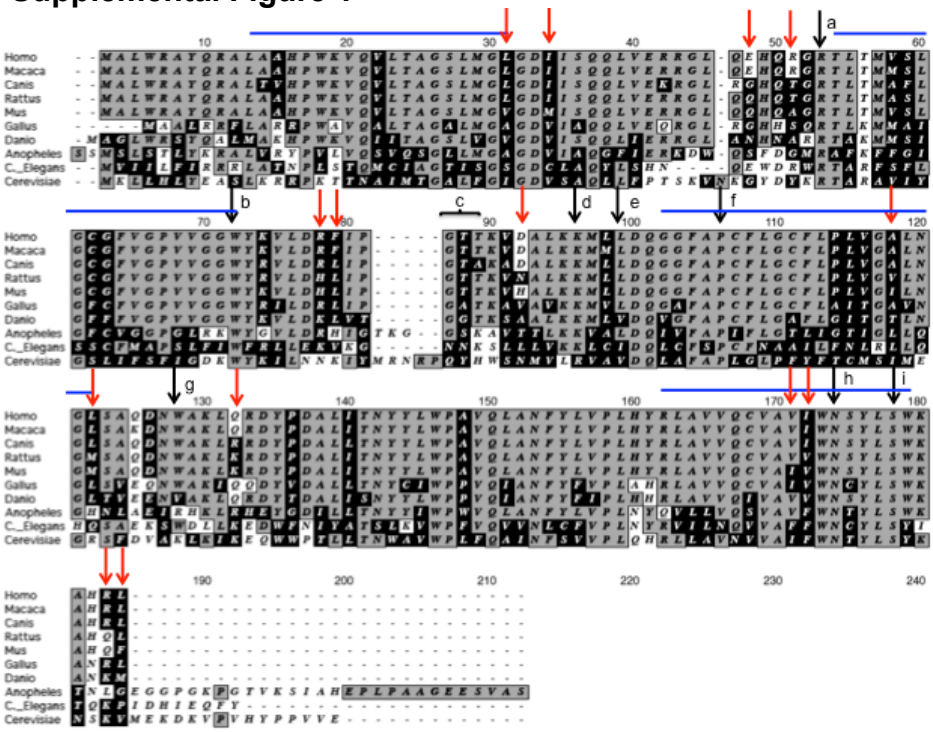

Alignment of eukaryotic Mpv17 orthologues. The blue lines indicate the transmembrane domains predicted with TMpred (Hofman and Stofel, 1993). *Shaded grey*: identities; *letters on black background*: similarities; *letters on white background*: mismatches. Note that none of the mismatches between humans and mice was predicted to be deleterious in humans, suggesting preservation of protein function. The *red arrows* show the differences between human and murine proteins. The black arrows and the bracket show the position of residues mutated in patients (note that the numbers in the alignment are NOT referred to the position in humans):

230. a) R50Q8
231. b) W69X: Wong et al, 2007
232. c) G79_T81Del10
233. d) K88E; K88Del13
234. e) L91Del13
235. f) P98L13
236. g) W120X8
237. h) N166K8

Supplemental Figure 2

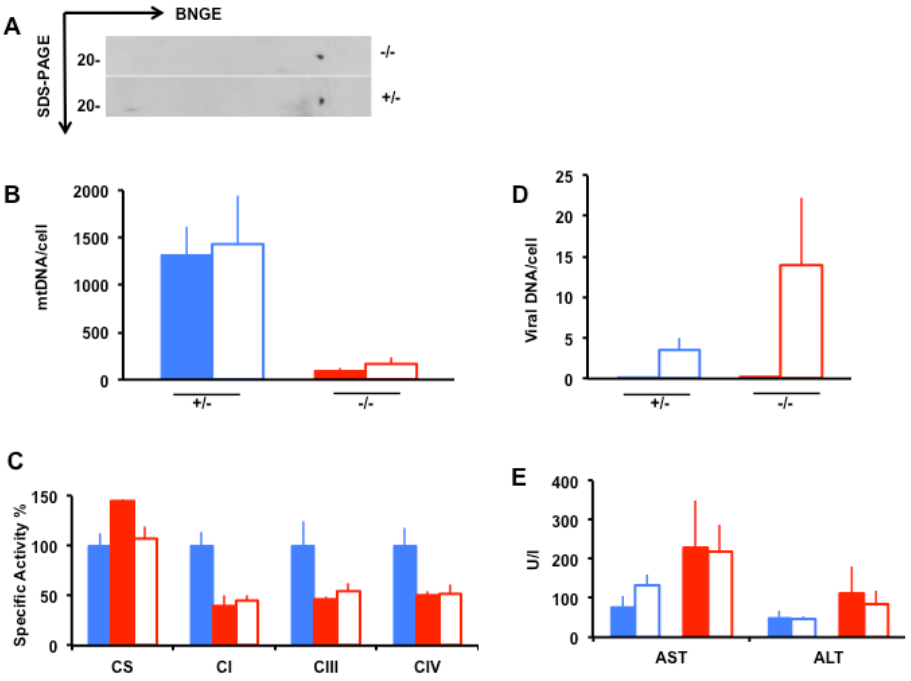

AAV-mediated expression of hMPV17-HA in *Mpv17*$^{-/-}$ mice.
A) 2D-BNGE using anti-HA in *Mpv17*$^{-/-}$ and *Mpv17*$^{+/-}$ mice
B) mtDNA analysis. Note that there is no significant difference between AAV- *h.MPV17-HA* treated vs. untreated samples.
C) Biochemical analysis
D) Viral DNA content
E) AST and ALT transaminases levels in plasma Colour codes: *solid blue:* untreated *Mpv17*$^{+/-}$ mice; *blue outline:* AAV-treated *Mpv17*$^{+/-}$ mice; *solid red:* untreated *Mpv17*$^{-/-}$ mice; *red outline:* AAV-treated *Mpv17*$^{-/-}$ mice. Bars indicate the standard deviation (SD).

Supplemental Figure 3

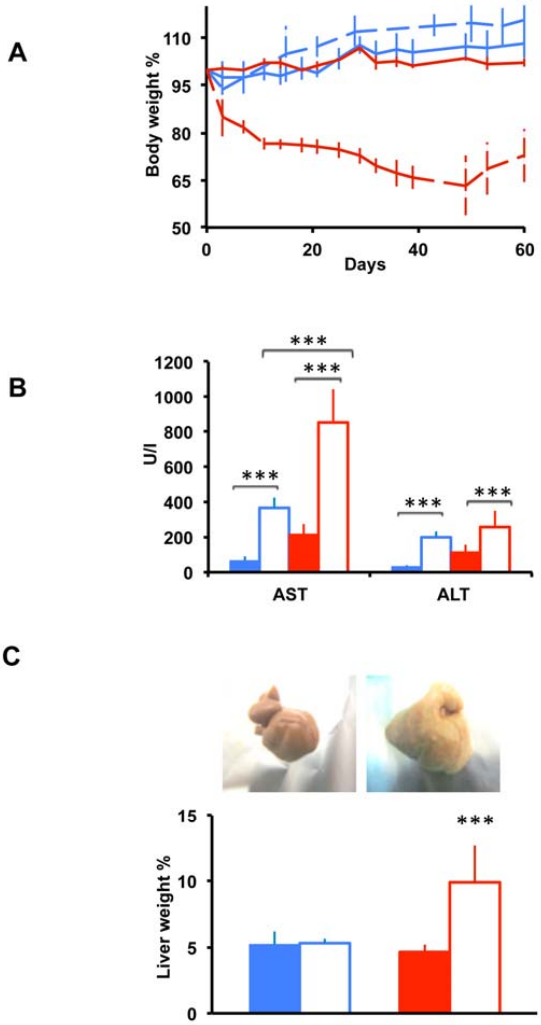

Effects of KD on *Mpv17-/-* and control littermates.
A) Body weight changes during 2-months of SD and KD. *Solid blue*: SD-fed Mpv17$^{+/-}$; *dashed blue*: KD-fed Mpv17$^{+/-}$; *solid red*: SD-fed Mpv17$^{-/-}$; *dashed red*: KD-fed Mpv17$^{-/-}$.
B) AST and ALT transaminases levels in plasma
C) Liver weight (as a percentage of body weight). Colour codes: *solid blue:* SD-fed *Mpv17*$^{+/-}$ mice; *blue outline:* KD-fed *Mpv17*$^{+/-}$ mice; *solid red:* SD-fed *Mpv17*$^{-/-}$ mice; *red outline:* KD-fed *Mpv17*$^{-/-}$ mice.

Supplemental Figure 4

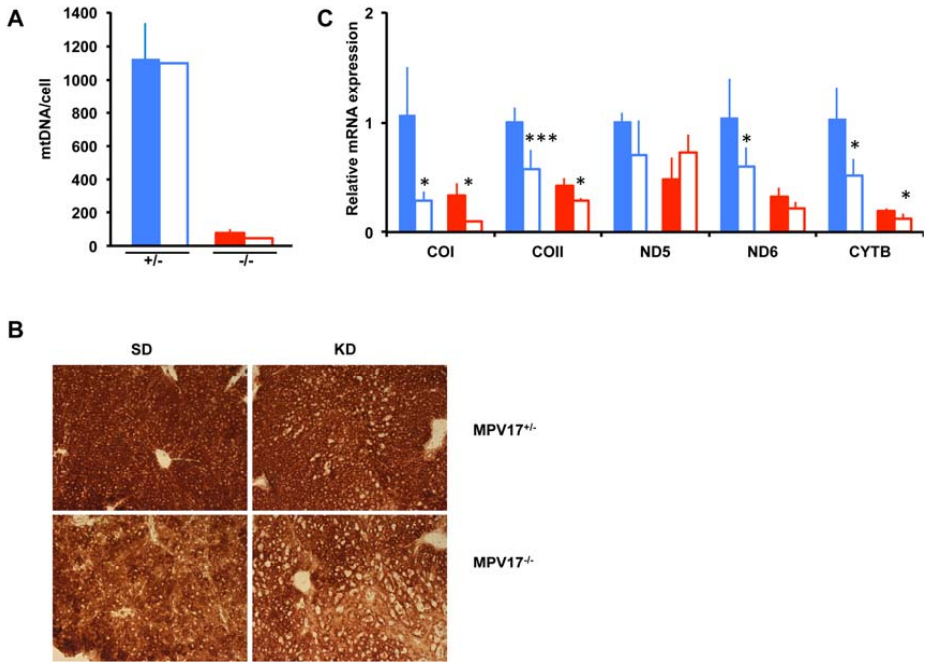

KD does not induce mitochondrial biogenesis in liver

A) MtDNA content analysis in SD- and KD-fed *Mpv17*$^{+/-}$ and *Mpv17*$^{-/-}$ mice.

B) COX histochemical staining. Note that COX activity is as much reduced in KD- as in SD-fed animals.

C) mRNA transcription analysis. Note that some of the mitochondrial transcripts are significantly reduced in both control and knockout KD-fed mice. Asterisks indicate significance (p) calculated by Mann-Whitney test for unpaired samples: *p < 0.05; ***p < 0.0001 Colour codes*: solid blue:* SD-fed *Mpv17*$^{+/-}$ mice; *blue outline:* KD-fed *Mpv17*$^{+/-}$ mice; *solid red:* SD-fed *Mpv17*$^{-/-}$ mice; *red outline:* KD-fed *Mpv17*$^{-/-}$ mice. Bars indicate the standard deviation (SD).

Supplemental Figure 5

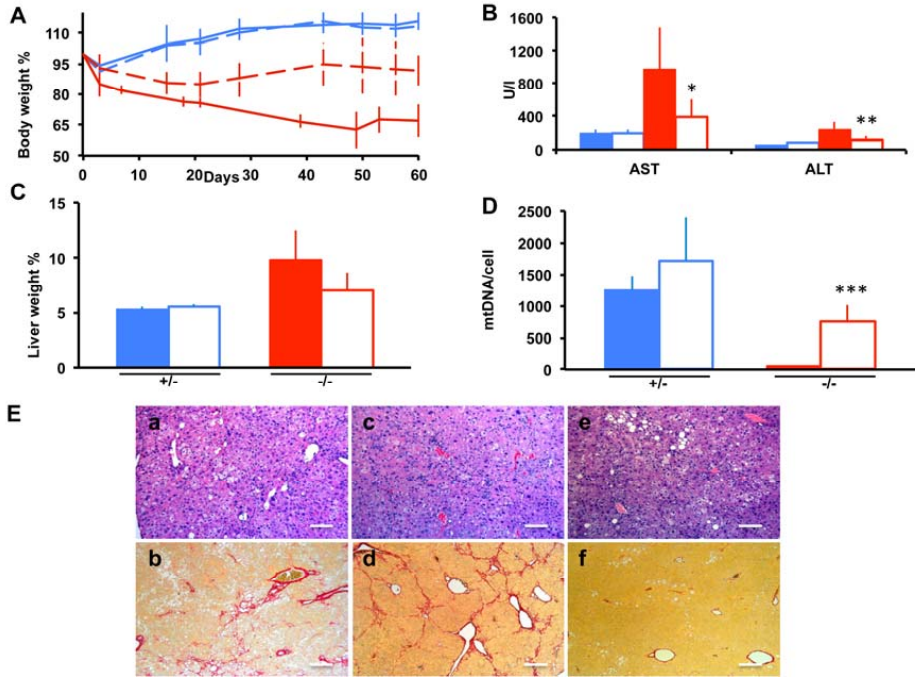

AAV2/8-h*MPV17* 4 x 10^{12} vg/Kg partially rescues KD-induced liver damage in *Mpv17*$^{-/-}$ mice. A single retro-orbital injection of 4x10^{12} vg/Kg was performed in two-month old *Mpv17*$^{+/-}$ and *Mpv17*$^{-/-}$ mice. KD was started three weeks later.

A) Body weight changes during 2 months of KD in AAV-treated and untreated mice. *Solid blue*: untreated *Mpv17*$^{-/-}$; *dashed blue*: AAV-treated *Mpv17*$^{+/-}$; *solid red*: untreated *Mpv17*$^{-/-}$; *dashed red*: AAV-treated *Mpv17*$^{-/-}$.

B) AST and ALT transaminases levels in plasma.

C) Liver weight (% of body weight).

D) MtDNA analysis.

Colour codes: *solid blue:* SD-fed *Mpv17*$^{+/-}$ mice; *blue outline:* KD-fed *Mpv17*$^{+/-}$ mice; *solid red:* SD-fed *Mpv17*$^{-/-}$ mice; *red outline:* KD-fed *Mpv17*$^{-/-}$ mice. Bars indicate the standard deviation (SD). E) Histological features on hematoxylin-eosin (a, c, e); picrosirius red (b, d, f) staining. **a,b**: AAV-treated *Mpv17*$^{-/-}$ show liver steatosis and focal inflammatory infiltrates. There is only a mild increase in fibrosis, without overt cirrhosis. **c,d**: untreated *Mpv17*$^{-/-}$ with liver steatosis, moderate inflammatory infiltrates and cirrhosis. **e,f**:

Supplemental Figure 6

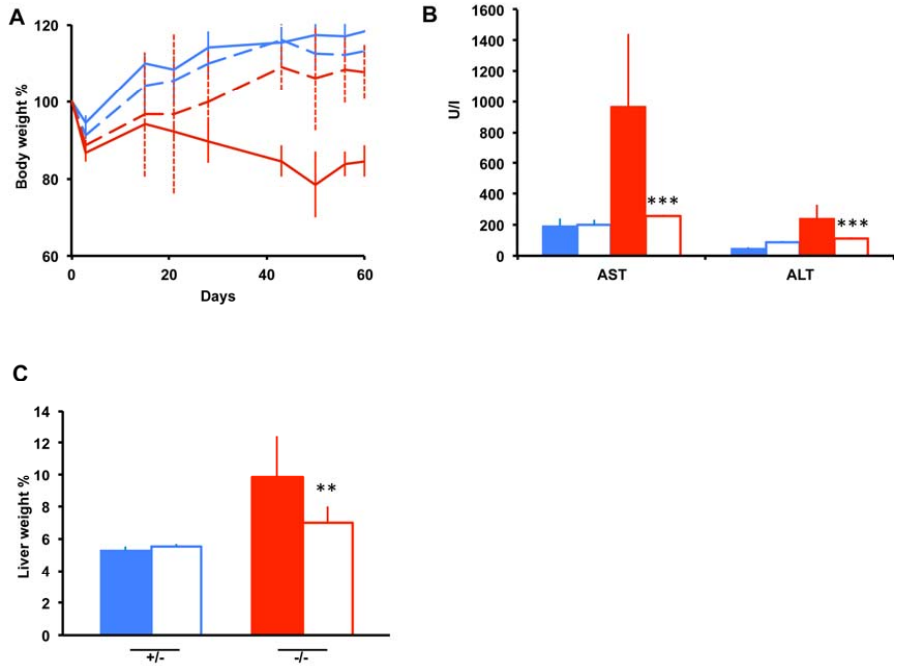

AAV2/8-h*MPV17* 4 x 10^{13} vg/Kg rescues KD-induced liver damage in *Mpv17*$^{-/-}$ mice A single retro-orbital injection of 4x10^{13} vg/Kg was performed in two months old *Mpv17*$^{+/-}$ and *Mpv17*$^{-/-}$ mice. KD was started three weeks later.

A) Body weight changes during 2-months of KD in AAV-treated and untreated mice. *Solid blue*: untreated *Mpv17*$^{+/-}$; *dashed blue*: AAV-treated *Mpv17*$^{+/-}$; *solid red*: untreated *Mpv17*$^{-/}$; *dashed red*: AAV-treated *Mpv17*$^{-/-}$. B) AST and ALT levels in plasma in AAV-treated and untreated groups.

C) Liver weight (% of body weight.

Colour codes: *solid blue:* untreated *Mpv17*$^{+/-}$; *blue outline:* AAV-treated *Mpv17*$^{+/-}$; *solid red:* untreated *Mpv17*$^{-/-}$; *red outline:* AAV-treated *Mpv17*$^{-/-}$.

Supplemental Figure 7

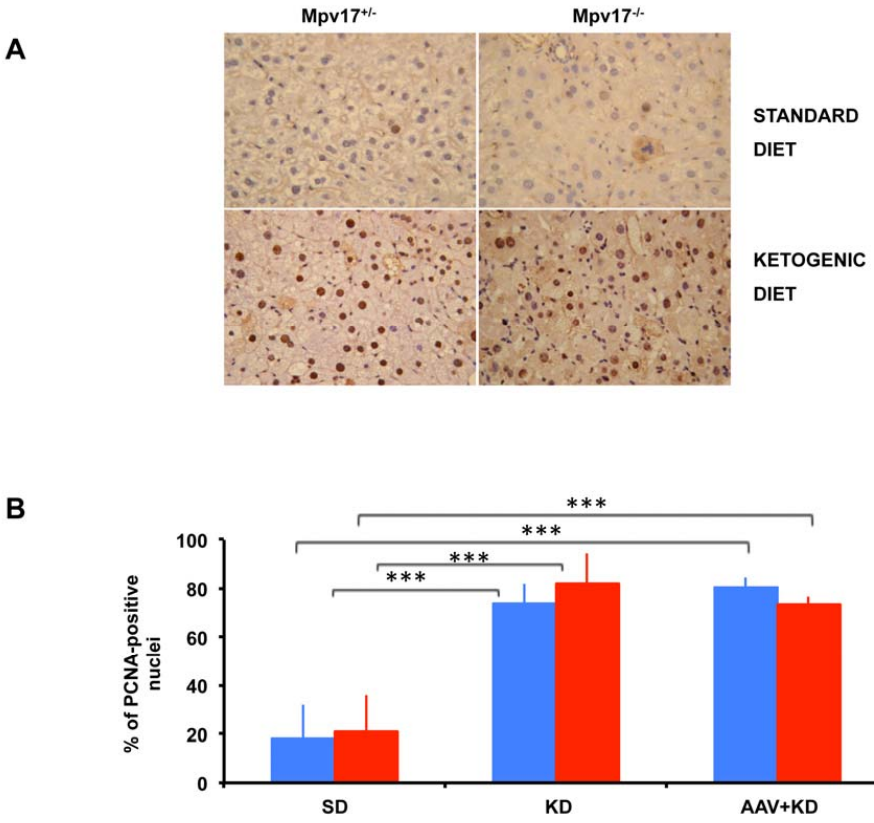

Effect of KD on hepatocytes proliferation
A) PCNA immuno-histochemical staining of SD and KD fed livers
B) quantitation of PCNA-positive nuclei. Colour codes*: Solid blue:* *Mpv17*$^{+/-}$ mice; *solid red: Mpv17*$^{-/-}$ mice.

Supplemental Figure 8

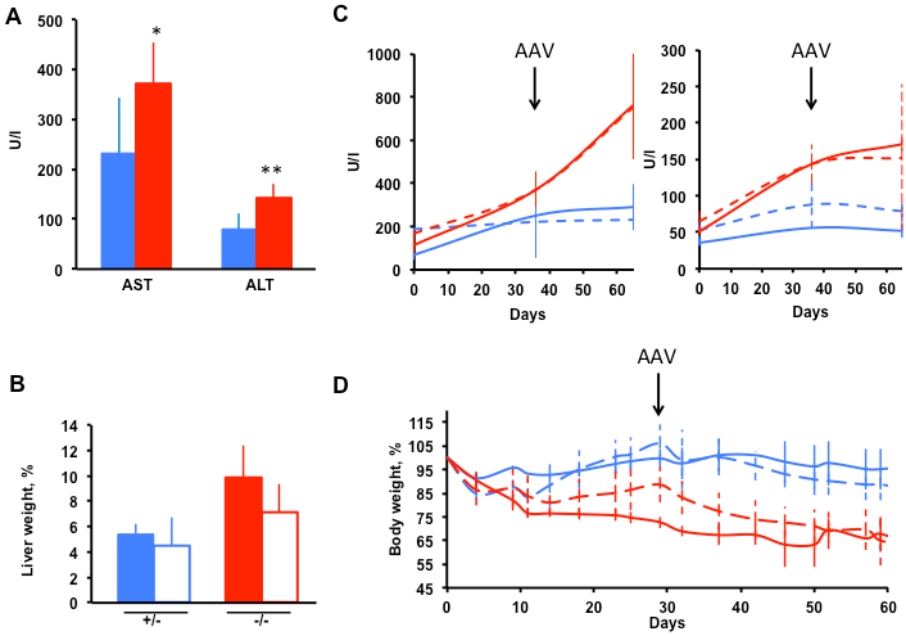

Effects of administration of AAV-*hMPV17* in mice pre-treated with KD

A) AST and ALT levels in plasma of *Mpv17*$^{+/-}$ and *Mpv17*$^{-/-}$ animals after one month of KD, just before AAV administration..

B) Liver weight (% of body weight). *Solid blue*: untreated *Mpv17*$^{+/-}$, *blue outline*: AAV-treated *Mpv17*$^{+/-}$, *solid red*: untreated *Mpv17*$^{-/-}$, *red outline*: AAV-treated *Mpv17*$^{-/-}$.

C) AST (*left*) and ALT (*right*) trend during the experimental protocol. The arrow indicates the time point of AAV administration.

D) Body weight changes during 2-months of KD in AAV-treated and untreated mice. The arrow indicates the time point of AAV administration. *Solid blue*: untreated *Mpv17*$^{+/-}$; *dashed blue*: AAV-treated *Mpv17*$^{+/-}$; *solid red*: untreated *Mpv17*$^{-/-}$; *dashed red*: AAV-treated *Mpv17*$^{-/-}$.

Chapter 5

Summary, conclusions and future perspectives

Summary

During my PhD program I have been involved in a project aimed to find effective therapies for the treatment of primary mitochondrial diseases.

In order to achieve this aim I initially focused on the molecular, biochemical and clinical characterization of the skeletal muscle-specific *Cox15* knockout mouse model (*Cox15*$^{sm/sm}$) generated in my lab. The phenotype of this mouse consists of a severe myopathy which correlates to reduced motor performance and profound COX deficiency restricted to skeletal muscle,. As these features resemble those observed in skeletal muscle of *COX15* mutant patients, this mouse is a suitable model for therapeutic trials. The *Cox15*$^{sm/sm}$, along with a Surf1 constitutive knockout (Surf1$^{-/-}$) and a Sco2 constitutive knockout/knockin (Sco2$^{KO/KI}$) mouse models, has been employed for pharmacological treatments aimed to promote mitochondrial biogenesis via PPARs and PGC-1α activation. Our experiments did not evidence any induction of OXPHOS activity in mice after exposure to the pan-PPAR agonist bezafibrate. Therefore we re-addressed our study to PGC-1α activation following a double strategy: transgenic overexpression of PGC-1α and pharmacological treatment with the AMPK agonist AICAR. Both attempts resulted in the activation of mitochondrial biogenesis and partial correction of COX deficiency, combined to amelioration of the mitochondrial

ultrastructure observed in the most severe mouse model, *Cox15*$^{sm/sm}$. These data indicate that activation of the AMPK/PGC-1α axis effectively can be pharmacologically modulated in order to enhance the mitochondrial respiratory chain activity and limit the deleterious effects of energy fault caused by genetic defects of the OXPHOS machinery.

Mitochondrial diseases may affect specific tissues or organs, requiring the development of specific targeted therapies. An example is mtDNA depletion syndrome caused by *MPV17* mutations. In humans this disease involves mostly the liver, leading to cirrhosis and premature death. The *Mpv17* knockout mouse model reproduces the profound depletion of mtDNA but hardly any clinical phenotype related to a liver dysfunction is evidenced in normal conditions. In order to target the therapeutic gene to the liver, we constructed an AAV2/8 viral vector expressing the human *MPV17 c*DNA under the control of a liver specific (TBG) promoter and introduced it in *Mpv17*$^{-/-}$ mice (and WT littermates) by systemic I.V. injection. Interestingly, viral DNA was detected only in the liver of treated animals. Accordingly, the expression and function of the protein were completely rescued in Mpv17$^{-/-}$ mice, leading to the normalization of the mtDNA copy number in liver and transaminase levels in blood, without any adverse effect on WT littermates. In addition we observed that, if exposed to a fat rich ketogenic diet, *Mpv17*$^{-/-}$ mice develop lethal hepatic cirrhosis, likely due to decreased MRC activity and inability to catabolize fat for energy supply through respiration On the basis of this

observation we exposed mice to ketogenic diet after AAV administration and found that AAV treated , *Mpv17*$^{-/-}$ mice were fully protected from liver failure induced by ketogenic diet. This was accompanied by histological improvement of liver, restoration of normal mtDNA copy number and normalization of OXPHOS biochemical proficiency. We also investigated the potential ability of this therapy to correct liver damage rather than prevent it. Mice underwent ketogenic diet and, once the hepatic damage was established, they were treated with AAV2/8-hMPV17 injection, as in the first protocol. Although liver in these mice appeared already compromised, expression of the WT gene was able to block the fatal progress of the disease even though we did not observe a complete regression of liver abnormalities. Taken together these observations suggest that the AAV based therapy is a promising strategy to combat mitochondrial diseases affecting specific, targetable organs.

Among the possible targets for therapy of mitochondrial diseases, we then focused on Opa1, an essential protein operating in mitochondrial dynamics and cristae shaping, and also involved in several cellular stress responses included apoptosis and autophagy. These multitasking activities make Opa1 an attractive target to increase protection mechanisms in vivo against cell damage related to mitochondrial dysfunction. As proof of principle, our collaborators showed that moderate overexpression of OPA1 has a protective role in various models of *in vivo* induced cell damage, including denervation-driven skeletal muscle atrophy, brain and heart necrosis/apoptosis

caused by ischemia-reperfusion, and liver failure caused by Fas-ligand induced apoptosis. Since mitochondrial metabolism and dysfunction are directly involved in these conditions and *Opa1* overexpression seems is protective, we adopted the same strategy to study the consequence of OPA1 overexpression on mouse models of mitochondrial disease. In particular CI and CIV deficient mouse models (*Ndus4*$^{-/-}$ and *Cox15*$^{sm/sm}$ respectively) were crossed with *OPA1*^{tg} mouse model that moderately overexpresses Opa1. Both *Ndufs4*$^{-/-}$*::Opa1*^{tg} and *Cox15*$^{sm/sm}$*::Opa1*^{tg} mice displayed improvement of both clinical phenotype and survival probability compared to their respective controls. These data are supported by behavioural experiments that show partial rescue of motor coordination in the *Ndufs4*$^{-/-}$*::Opa1*^{tg} mice (mainly affected in the central nervous system), and endurance motor performance in the *Cox15*$^{sm/sm}$*::Opa1*^{tg} (characterized by a mitochondrial myopathy). Clinical recovery was associated with enhancement of the MRC efficiency including single enzyme activities, respiratory rate, and stabilization of respiratory chain complexes. Light and electron microscopy analysis performed on the *Cox15*$^{sm/sm}$*::Opa1*^{tg} showed a dramatic amelioration of the mitochondrial ultrastructure, connecting the overall biochemical improvement to morphological correction. These results suggest that overexpression of OPA1 has great therapeutic potential and open doors to the development of OPA1-mimetic drugs as a suitable target to correct mitochondrial diseases.

Conclusions

The complexity of mitochondrial metabolism and related disorders associated with their dysfunction stands as a formidable challenge for the development of effective treatments. Despite remarkable advances in the identification of the molecular mechanisms of primary mitochondrial diseases their treatment options remain limited to supportive therapies rather than correction of the underlying deficiencies. Furthermore, it has become clear in the last decade that progresses in understanding and treating primary mitochondrial diseases will be potentially beneficial for understanding and managing a large spectrum of degenerative conditions known to have mitochondrial dysfunction as a significant component of their pathogenic mechanisms (secondary mitochondrial diseases). These conditions include disorders of high social impact such as Alzheimer's disease, Parkinson's disease, diabetes, ALS, autistic spectrum disorders, and many others[1]. Given the extreme clinical, biochemical and genetic heterogeneity of mitochondrial disease, it is unlikely that a universal cure able to correct all of them will be found. Rather, it is more realistic to expect that different interventions will be effective in different subgroups of diseases.

In this thesis I have evaluated the effects of three different therapeutic approaches on mouse models of mitochondrial failure determined by different gene defects and pathogenic mechanisms. These approaches are either aimed at correcting several dysfunctions or tailored to specific defects. Treatments

aimed at increasing mitochondrial biogenesis and modulating mitochondrial shape/dynamics belong to the first category, while AAV-based gene therapy is an example of the second. Both approaches were highly effective in correcting the underlying biochemical and molecular defect.

As for the first approach, increasing mitobiogenesis, although AICAR, a compound known for a very long time, was very effective in vivo, no clinical trial has been implemented for any human pathology, because of its low bioavailability upon oral administration and cardiotoxicity[2]. Nevertheless, my results suggest that this approach could significantly delay or stop at least some mitochondrial diseases. Other compounds activating PGC-1α can be used to stimulate mitochondrial biogenesis, such as those acting on Sirt1, such as NAD^+ precursors (e.g. nicotinic acid or nicotinamide riboside) or inhibitors of NAD+-consuming enzymes (e.g. PARP inhibitors).

The modulation of mitochondrial shape is a very innovative approach, but at the moment it stands as a genetic proof of principle, which warrants future development of specific drugs. Importantly, this approach seems to be able to significantly change the course of very severe diseases such as those associated to profopund cI- or cIV- defects, while the previous approach seemed to be less effective on very severe phenotypes.

Finally, liver-specific AAV-based gene therapy ihas been successfully tested in several preclinical models[3-6] and a number of clinical trials are ongoing (www.clinicaltrial.org).

However, mitochondrial diseases exquisitely affecting the liver are a minority, and serotypes to efficiently target different organs are still under development. In particular, the availability of AAV vectors able to cross the blood-brain barrier will be a major advance towards therapy of mitochondrial encephalopathies.

Future perspectives

Mitochondria play a key role in cellular physiology and, consequently, mitochondrial dysfunction has been implicated in a wide range of diseases, encompassing all areas of modern medicine. The last 20 years witnessed a huge increase in our understanding of the molecular mechanisms underlying these conditions. The development of animal models that faithfully mimic human mitochondrial disease mutations is also essential to understand the physiological significance of these pathways, to unravel the molecular basis of tissue specificity, and to develop therapeutic strategies. The identification of novel drugs targeting the signaling cascades controlling mitochondrial biogenesis and mitochondrial dynamics warrant the development and trial of new therapeutic agents. For instance, OPA1 activity has been shown to be modulated by SIRT3[7], which in turn can be regulated by different compounds, such as resveratrol, already used in some pre-clinical studies[8,9], and oroxylin A, a component of the plant *Scutellaria baicalensis Georgi*[10]. Since OPA1 is involved in mitochondria dynamics and quality control, it will be interesting to explore more deeply the

therapeutic potential of these partially unheeded pathways. Recent studies showed that enhancing mitochondrial fusion could alleviate the consequences of mutant mtDNA load by promoting intra-organellar complementation,. On the other hand, priomoting fission could allow the elimination of mitochondria with high mtDNA mutation load via autophagy[11]. Thus, the development of pharmacological agents able to manipulate organellar dynamics is a promising therapeutic strategy. The recent discovery of specific activators of mitochondrial fusion (M-hydrazone) and inhibitors of fission (MDIVI-1 and P110) may provide new therapeutic options for these disorders[12-14]. However, preclinical studies are first needed to investigate efficacy and possible adverse effects.

References

1. Moraes CT, Anderson V, Mohan C, Workshop p. Translational research in primary mitochondrial diseases: challenges and opportunities. Mitochondrion 2013;13:945-52.
2. Goodyear LJ. The exercise pill--too good to be true? The New England journal of medicine 2008;359:1842-4.
3. Di Meo I, Auricchio A, Lamperti C, Burlina A, Viscomi C, Zeviani M. Effective AAV-mediated gene therapy in a mouse model of ethylmalonic encephalopathy. EMBO molecular medicine 2012;4:1008-14.
4. Flierl A, Jackson C, Cottrell B, Murdock D, Seibel P, Wallace DC. Targeted delivery of DNA to the mitochondrial compartment via import sequence-conjugated peptide nucleic acid. Molecular therapy : the journal of the American Society of Gene Therapy 2003;7:550-7.
5. Guy J, Qi X, Koilkonda RD, et al. Efficiency and safety of AAV-mediated gene delivery of the human ND4 complex I subunit in the mouse visual system. Investigative ophthalmology & visual science 2009;50:4205-14.
6. Torres-Torronteras J, Viscomi C, Cabrera-Perez R, et al. Gene Therapy Using a Liver-targeted AAV Vector Restores Nucleoside and Nucleotide Homeostasis in a Murine Model of MNGIE. Molecular therapy : the journal of the American Society of Gene Therapy 2014;22:901-7.
7. Samant SA, Zhang HJ, Hong Z, et al. SIRT3 deacetylates and activates OPA1 to regulate mitochondrial dynamics during stress. Molecular and cellular biology 2014;34:807-19.
8. Hofer A, Noe N, Tischner C, et al. Defining the action spectrum of potential PGC-1alpha activators on a mitochondrial and cellular level in vivo. Human molecular genetics 2014;23:2400-15.
9. Lopes Costa A, Le Bachelier C, Mathieu L, et al. Beneficial effects of resveratrol on respiratory chain defects in patients' fibroblasts involve estrogen receptor and estrogen-related receptor alpha signaling. Human molecular genetics 2014;23:2106-19.
10. Wei L, Zhou Y, Dai Q, et al. Oroxylin A induces dissociation of hexokinase II from the mitochondria and inhibits

glycolysis by SIRT3-mediated deacetylation of cyclophilin D in breast carcinoma. Cell death & disease 2013;4:e601.
11. Wikstrom JD, Twig G, Shirihai OS. What can mitochondrial heterogeneity tell us about mitochondrial dynamics and autophagy? The international journal of biochemistry & cell biology 2009;41:1914-27.
12. Andreux PA, Houtkooper RH, Auwerx J. Pharmacological approaches to restore mitochondrial function. Nat Rev Drug Discov 2013;12:465-83.
13. Cassidy-Stone A, Chipuk JE, Ingerman E, et al. Chemical inhibition of the mitochondrial division dynamin reveals its role in Bax/Bak-dependent mitochondrial outer membrane permeabilization. Developmental cell 2008;14:193-204
14. Wang D, Wang J, Bonamy GM, et al. A small molecule promotes mitochondrial fusion in mammalian cells. Angewandte Chemie 2012;51:9302-5.

The research presented in this thesis was performed at the Unit of Molecular Neurogenetics, of the Foundation IRCCS Neurological Institute Carlo Besta, Milan, Italy and at the MRC Mitochondrial Biology Unit, Cambridge, United Kingdom since November 2011 until November 2014.

I want to thank Prof. Massimo Zeviani for giving me the opportunity to pursue a PhD in his lab, for his experience and precious advice; dr. Carlo Viscomi for having followed me throughout the period of PhD research and all my colleagues

This work was supported by the Pierfranco and Luisa Mariani Foundation Italy, Telethon-Italy, Cariplo, Italian Ministry of health, Fondazione Tomasello and Associazione Mitocon